The influence of selected genetic and environmental factors on white matter pathway structure measured with diffusion tensor imaging

Raquel Fenoll Sanguino

Brain and Behavior

Open Access

Airborne copper exposure in school environments associated with poorer motor performance and altered basal ganglia

Jesus Pujol[1,2], Raquel Fenoll[1], Dídac Macià[1], Gerard Martínez-Vilavella[1], Mar Alvarez-Pedrerol[3,4,5], Ioar Rivas[3,4,5,6], Joan Forns[3,4,5], Joan Deus[1,7], Laura Blanco-Hinojo[1], Xavier Querol[6] & Jordi Sunyer[3,4,5,8]

[1]MRI Research Unit, Hospital del Mar, Barcelona, Spain
[2]Centro Investigación Biomédica en Red de Salud Mental, CIBERSAM G21, Barcelona, Spain
[3]Centre for Research in Environmental Epidemiology (CREAL), Barcelona, Catalonia, Spain
[4]Pompeu Fabra University, Barcelona, Catalonia, Spain
[5]Ciber on Epidemiology and Public Health (CIBERESP), Barcelona, Spain
[6]Institute of Environmental Assessment and Water Research (IDAEA-CSIC), Barcelona, Catalonia, Spain
[7]Department of Clinical and Health Psychology, Autonomous University of Barcelona, Barcelona, Spain
[8]IMIM (Hospital del Mar Medical Research Institute), Barcelona, Catalonia, Spain

Keywords
Air pollution, brain development, copper, diffusion tensor imaging, fMRI, neurodegenerative disorders

Correspondence
Jesus Pujol, MRI Department, Hospital del Mar, Passeig Marítim 25-29. 08003, Barcelona, Spain. Tel: +34932212180; Fax: +34932212181; E-mail: 21404jpn@comb.cat

Funding Information
This work was supported by the European Research Council under the ERC (grant number 268479)—the BREATHE project. The Agency of University and Research Funding Management of the Catalonia Government participated in the context of Research Group SGR2014-1673.

Received: 4 August 2015; Revised: 2 March 2016; Accepted: 9 March 2016

***Brain and Behavior*, 2016; 0(0), e00467, doi: 10.1002/brb3.467**

Abstract

Introduction: Children are more vulnerable to the effects of environmental elements. A variety of air pollutants are among the identified factors causing neural damage at toxic concentrations. It is not obvious, however, to what extent the tolerated high levels of air pollutants are able to alter brain development. We have specifically investigated the neurotoxic effects of airborne copper exposure in school environments. **Methods:** Speed and consistency of motor response were assessed in 2836 children aged from 8 to 12 years. Anatomical MRI, diffusion tensor imaging, and functional MRI were used to directly test the brain repercussions in a subgroup of 263 children. **Results:** Higher copper exposure was associated with poorer motor performance and altered structure of the basal ganglia. Specifically, the architecture of the caudate nucleus region was less complete in terms of both tissue composition and neural track water diffusion. Functional MRI consistently showed a reciprocal connectivity reduction between the caudate nucleus and the frontal cortex**. Conclusions:** The results establish an association between environmental copper exposure in children and alterations of basal ganglia structure and function.

Introduction

Brain development is extraordinarily complex and extends into adulthood to achieve maximum effectiveness in cognition and skills (Pujol et al. 1993; Paus 2005). Nonetheless, both the complexity and duration of such a process expose developing children to the potentially harmful effects of environmental elements. A variety of air pollutants are among the identified factors causing neural damage at toxic concentrations (Grandjean and Landrigan 2014). It is not obvious, however, to what extent the tolerated high levels of urban air pollutants are able to generate subtle, subclinical alterations in the developing brain in school-age children.

Copper is an air pollutant that may potentially interfere with brain development. Although this element is necessary for cellular metabolism, abnormal copper levels lead to relevant brain impairment (Scheiber et al. 2014). The deleterious effect of an excess of copper is well-known from Wilson's disease, an inherited metabolic disorder affecting the basal ganglia with symptoms usually evident from preadolescence onward and mainly in the form of deficient motor control (Bandmann et al. 2015).

We have tested the potential harmful effects of copper as an air pollutant in children aged from 8 to 12 years using specific motor testing and brain structural and functional imaging. Exposure to airborne copper at school was estimated for 2836 children in the city of Barcelona. Both the speed and consistency of motor response were measured to test the integrity of motor function in the whole sample. High-resolution 3D MRI, DTI (diffusion tensor imaging), and functional MRI were used to directly test the potential repercussion on brain anatomy, architecture, and function in a subgroup of 263 children.

Methods

Participants

This study was developed in the context of the BREATHE project (The European Commission: FP7-ERC-2010-AdG, ID 268479) aimed at assessing the impact of long-term exposure to traffic-related air pollutants on school children. A total of 2897 children participated in the whole survey from 39 representative schools of the city of Barcelona (Sunyer et al. 2015). A group of 2836 children completed the behavioral testing (mean age at the study end, 9.4 years; SD 0.9; and range 7.9–12.1 years) and served to test the effect of copper on motor function. From this sample, 1564 families were invited to participate in the MRI study via post, e-mail, or telephone, and 810 of them gave an initial positive response. The recruitment of this group was consecutive with the aim of including children from all participating schools. Parents of 491 children were directly contacted. Consent to participate was finally not obtained in 165 cases, 27 children were lost before the assessment and 21 children were not eligible because of dental braces. The finally selected MRI group included 278 participants, 263 of whom completed the imaging protocol (mean age of 9.7 years, SD 0.9 and range, 8.0–12.1 years) and served to test direct effects of copper on brain. Study design and participant selection is fully described in Sunyer et al. (2015). Table 1 reports the characteristics of the study samples.

All parents or tutors signed the informed consent form approved by the Research Ethical Committee (No. 2010/41221/I) of the IMIM-Parc de Salut MAR, Barcelona, Spain, and the FP7-ERC-2010-AdG Ethics Review Committee (268479-22022011).

Copper exposure

Each school was measured twice during 1-week periods separated by 6 months, in the warm (year 2012) and cold

Table 1. Characteristics of study samples.

	Whole sample (n = 2836)	MRI sample (n = 263)
Gender	49.5% girls 50.5% boys	48.3% girls 51.7% boys
Age, years, mean ± SD (range)	9.4 ± 0.9 (7.9–12.1)	9.7 ± 0.9 (8.0–12.1)
Overall school achievement, 5-point scale	3.5 ± 1.1 (1–5)	3.7 ± 1.0 (1–5)
Difficulties score (SDQ), range 0–40	8.4 ± 5.2 (0–32)	8.8 ± 5.3 (0–25)
Obesity: Normal	72.1%	71.4%
Overweight, BMI ≥ 25–29.9 kg/m^2	18.5%	18.4%
Obesity, BMI ≥ 30 kg/m^2	9.4%	10.2%
Mother education (5-point scale, 5 = University)	4.4 ± 0.8 (1–5)	4.5 ± 0.8 (1–5)
Father education (5-point scale, 5 = University)	4.4 ± 0.8 (1–5)	4.4 ± 0.8 (1–5)
Vulnerability index[1]–Home	0.45 ± 0.21 (0.06–1.0)	0.43 ± 0.21 (0.06–0.90)
Vulnerability index[1]–School	0.42 ± 0.21 (0.13–0.84)	0.43 ± 0.22 (0.13–0.84)
Public/Nonpublic school	36% vs. 64%	43% vs. 57%
Task performance		
Reaction time (mean of medians, msec)	671.5 ± 124.6 (389–1277)	650.6 ± 119.9 (431–1091)
Reaction time standard deviation (msec)	235.7 ± 91.1 (60.6–598.6)	222.9 ± 91.2 (77.5–571.6)
Commission errors (number)	4.0 (3.1%) ± 4.2 (0–50)	4.3 (3.4%) ± 5–0 (0–49)
Omission errors (number)	1.4 (1.1%) ± 3.6 (0–94)	1.6 (1.3%) ± 3.9 (0–44)

BMI, body mass index; SDQ, Strengths and Difficulties Questionnaire.
[1]Neighborhood socioeconomic status vulnerability index based on the level of education, unemployment, and occupation at the census tract (Atlas de vulnerabilidad urbana de España, 2012).

(year 2012/2013) periods. Indoor air in a single classroom and outdoor air in the courtyard were measured simultaneously. Several pollutants were measured during class time (Amato et al. 2014; Rivas et al. 2014; Sunyer et al. 2015). Copper specifically was measured during 8 h (09:00–17:00 h) in particulate matter with an aerodynamic diameter <2.5 μm (PM2.5) collected on filters with high-volume samplers (MCV SA, Spain). After acid digestion of the filter, copper concentrations were determined via ICP-MS (inductively coupled plasma mass spectrometry). Yearly school air pollution levels were obtained by averaging the two 1-week measurements. This study was focused on outdoor (courtyard) copper measurements, as they are more directly related to urban pollution, which is the primary interest of this project. All children had been in the school for more than 18 months (and 98% more than 2 years) at imaging assessment, which was carried out after the pollution measurement campaigns.

Behavioral measurements

Behavioral assessment was focused on testing speed and consistency of motor responses. We used the computerized "Attentional Network Test," child version (Child ANT) (Rueda et al. 2004), which was developed to specifically assess children's motor speed during attentional challenge. Among the ANT measurements, we used the overall "reaction time" to measure speed and "reaction time standard deviation" to measure trial-to-trial consistency of motor responses. A higher reaction time standard deviation indicates higher reaction time variability, which increases with reduced executive and attentional resources depending on the integrity of frontal-basal ganglia circuits (Bellgrove et al. 2004; MacDonald et al. 2006; Langner and Eickhoff 2013). Normal children become efficient in sustained motor responses during the preadolescent age period contemplated in our study (MacDonald et al. 2006).

The procedure used to administer the task is fully described in a previous report (Forns et al. 2014). The Child ANT takes approximately 20 min to complete. Groups of 10–20 children were assessed together wearing ear protectors and were supervised by one trained examiner per 3–4 children. The task required to respond to a target (yellow-colored fishes) presented on a computer screen by pressing a key. The whole task contains cues to test different attentional aspects, but outcome measurements for the current study were limited to median reaction time and standard deviation expressed in milliseconds from the correct responses obtained across the 128 trials of the task (four separate blocks of 32 trials each). Commission and omission errors were also registered. Cases with more than 30% commission or omission errors were excluded from further analyses (total nine cases in the whole sample and two cases in the MRI sample).

Contextual behavioral assessment

Sociodemographic factors were measured using a neighborhood socioeconomic status vulnerability index (based on the level of education, unemployment, and occupation at the census tract) (Atlas de Vulnerabilidad Urbana de España, 2012; http://www.fomento.gob.es/. . ./AtlasVulnerabilidadUrbana/) according to both school and home address. Parental education was registered for both parents using a 5-point scale (1 illiterate/2 less than/3 primary/4 secondary/5 university). Standard measurements of height and weight were performed to define overweight and obesity (de Onis et al. 2009). Parents completed the SDQ (Strengths and Difficulties Questionnaire) on child behavioral problems (Goodman 2001). A "difficulties" score ranging from 0 to 40 was generated. Overall school achievement was rated by teachers using a 5-point scale (from the worse = 1 to the best = 5).

MRI acquisition

A 1.5-Tesla Signa Excite system (General Electric, Milwaukee, WI) equipped with an eight-channel phased-array head coil and single-shot EPI (echoplanar imaging) software was used. The imaging protocol included high-resolution T1-weighted 3D anatomical images, DTI, and a functional MRI sequence acquired in the resting state.

High-resolution 3D anatomical images were obtained using an axial T1-weighted three-dimensional fast spoiled gradient inversion recovery prepared sequence. A total of 134 contiguous slices were acquired with repetition time 11.9 msec, echo time 4.2 msec, flip angle 15°, field of view 30 cm, 256 × 256 pixel matrix, and slice thickness 1.2 mm.

Diffusion tensor imaging was obtained using spin-echo single-shot echo-planar sequences of 25 directions with a B-factor of 1000 sec/mm^2. Twenty-six slices were acquired with repetition time 8300 msec, echo time 94 msec, thickness 5 mm, no gap, pulse angle 90°, field of view 26 cm, and 128 × 128 acquisition matrix reconstructed into a 256 × 256 matrix.

The functional MRI sequence consisted of gradient recalled acquisition in the steady state with repetition time 2000 msec, echo time 50 msec, pulse angle 90°, field of view 24 cm, 64 × 64-pixel matrix, and slice thickness 4 mm (interslice gap, 1.5 mm). Twenty-two interleaved slices were prescribed parallel to the anterior–posterior commissure line covering the whole brain. A 6-min

continuous resting-state scan was acquired for each participant. Children were instructed to relax, stay awake, and lie still without moving, while keeping their eyes closed throughout. This scan generated 180 whole-brain EPI volumes. The first four (additional) images in each run were discarded to allow magnetization to reach equilibrium.

Image preprocessing

Anatomical 3D

All the anatomical images were visually inspected before analysis by a trained operator to detect any motion effect. A total of 10 children were discarded as a result of poor quality images and thus the final sample for the 3D anatomical analysis included 253 children. Anatomical 3D data were processed in two separate analyses assessing different anatomical characteristics.

Gray and white matter tissue concentration and volume at a voxel level were measured using Statistical Parametric Mapping (SPM8) (http://www.fil.ion.ucl.ac.uk/spm, Wellcome Department of Cognitive Neurology, London, UK, 2008). SPM VBM (voxel-based morphometry) algorithms with DARTEL registration were used with the following processing steps: segmentation of anatomical images into gray and white matter tissue probability maps in their native space; estimation of the deformations that best align the images together by iteratively registering the segmented images with their average; finally, generating spatially normalized and smoothed segmentations ($5 \times 5 \times 5$ FWHM) using the deformations estimated in the previous step. The analyses were performed with scaling by Jacobian determinants (estimates of volume change during the normalization) to consider tissue volume and without Jacobian scaling to assess the relative concentration of gray matter and white matter. Normalized images were finally transformed to the standard SPM template, resliced to 1.5 mm resolution in MNI (Montreal Neurological Institute) space.

Cortical thickness measurements across the whole cortex were obtained using FREESURFER tools (http://surfer.nmr.mgh.harvard.edu/). Processing steps included removal of nonbrain tissue, segmentation of the subcortical white matter and deep gray matter volumetric structures, tessellation of the gray and white matter boundary, registration to a spherical atlas which is based on the individual cortical folding patterns to match cortical geometry across subjects, and creation of a variety of surface-based data. Cortical thickness is calculated as the closest distance from the gray/white boundary to the gray/CSF boundary at each vertex on the tessellated surface (Fischl et al. 1999).

Diffusion tensor imaging

Diffusion tensor imaging was processed using FMRIB (functional MRI of the brain) Software Library 5.0 (FSL), developed by the Analysis Group at the Oxford Centre for FMRIB (Smith et al. 2004). Diffusion-weighted images were corrected for motion and eddy current distortions ("Eddy Current Correction" option in the FMRIB Diffusion Toolbox [FDT] version 2.0 in FSL), and a whole-brain mask was applied using the FSL Brain Extracting Tool. A further rigorous image quality control was carried out to identify potential residual effects of head motion, which involved the visual inspection of each DTI slice for all 25 DTI volumes in all participants. Volumes with slices with signal loss (greater than ~ 10%) or residual artifacts were identified by an expert researcher. DTI full examinations showing one or more degraded images in more than five volumes were discarded. A total of 76 children were removed from the DTI analysis on the basis of this criterion (in addition to 10 cases showing gross image degradation). The final DTI sample involved 177 children showing a mean $\pm$ SD of 23.5 (94%) $\pm$ 1.9 optimal quality volumes. Subsequently, we estimated FA (fractional anisotropy) maps using FDT in FSL after local fitting of the diffusion tensor model at each voxel ("dtifit"). Next, diffusion data were processed using tract-based spatial statistics (Smith et al. 2006). Each FA dataset was resliced to a 1 mm $\times$ 1 mm $\times$ 1 mm anatomical resolution and normalized to standard MNI space via the FMRIB58_FA template using the FMRIB's nonlinear registration tool.

To complement the analysis and assist interpretation of the FA results, we carried out a directional analysis of water diffusion along each (x, y, z) axis separately. We used the diffusion tensor estimated by FSL "dtifit" algorithm to determine diffusion strengths. Geometrically, the procedure involved determining the radius of the arbitrarily oriented ellipsoid along the spatially fixed x, y, and z axes using basic 3D quadratic geometry. As the eigenvectors and eigenvalues were previously normalized to MNI space in all subjects, we were able to carry out group-level voxel-wise analyses.

Functional MRI

Preprocessing was carried out using SPM8 and involved motion correction, spatial normalization, and smoothing using a Gaussian filter (full-width half-maximum, 8 mm). Data were normalized to the standard SPM-EPI template and resliced to 2-mm isotropic resolution in MNI space.

The following procedures were adopted to control for potential head motion effects: (1) Conventional SPM time-series alignment to the first image volume in each

subject. (2) Exclusion of 24 children with large head motion (boxplot-defined outliers) (Pujol et al. 2014b). The finally analyzed sample therefore included 239 children. (3) Both motion-related regressors and estimates of global brain signal fluctuations were included as confounding variables in first-level (single-subject) analyses. (4) Within-subject, censoring-based MRI signal artifact removal (Power et al. 2014) (scrubbing) was used to discard motion-affected volumes. For each subject, interframe motion measurements (Pujol et al. 2014b) served as an index of data quality to flag volumes of suspect quality across the run. At points with interframe motion >0.2 mm, that corresponding volume, the immediately preceding and the succeeding two volumes were discarded. Using this procedure, a mean ± SD of 11.2 (6.2%) ± 13.8 volumes of the 180 fMRI sequence volumes were removed in the analyzed sample. (5) Potential motion effects were further removed using a summary measurement for each participant (mean interframe motion across the fMRI run) as a regressor in the second-level (group) analyses in SPM (Pujol et al. 2014b).

Functional connectivity maps were generated using procedures detailed in previous reports (Harrison et al. 2013; Pujol et al. 2014a). Maps representative of frontal lobe functional connectivity were obtained by locating seed regions at the medial-dorsal, lateral (right and left), and medial-anterior aspects of the frontal cortex using coordinates taken from previous literature (Fox et al. 2005) converted to MNI: medial-dorsal ($x = -2$, $y = -2$, $z = 55$), right lateral ($x = 45$, $y = 3$, $z = 15$), left lateral ($x = -45$, $y = 5$, $z = 9$), and medial-anterior ($x = 1$, $y = 54$, $z = 26$). Additional maps were generated from the results obtained in the structural (anatomical and DTI) analyses. The seed regions were centered at the left caudate nucleus at three anterior–posterior levels covering the part of the head of the caudate nucleus showing significant copper effects on its structure (MNI coordinates [$x = -12$, $y = 20$, $z = 4$], [$x = -12$, $y = 14$, $z = 9$], and [$x = -12$, $y = 8$, $z = 12$]).

For each of the striatal locations, the seed region was defined as a 3.5-mm radial sphere (sampling ~ 25 voxels in 2 mm isotropic space). This was performed using MarsBaR ROI (region of interest) toolbox in MNI stereotaxic space (Brett et al. 2003). Signals of interest were then extracted for each seed region, respectively, by calculating the mean ROI value at each time point across the time series. To generate the seed maps, the signal time course of a selected seed region was used as a regressor to be correlated with the signal time course of every voxel in the brain in order to generate first-level (single-subject) voxel-wise statistical parametric maps (contrast images). The maps were estimated for each seed separately. A high-pass filter set at 128 sec was used to remove low-frequency drifts below ~0.008 Hz. In addition, we derived estimates of white matter, CSF, and global brain signal fluctuations to include in the regression analyses as nuisance variables.

Statistical analysis

A multiple linear regression was used to estimate the source of copper and the relative contributions were given as standardized β values. A linear regression was used to estimate the association of copper measurements with motor performance. β values are reported as time increments (msec) for each copper measurement unit (ng/m^3).

Imaging data were analyzed using SPM. Individual anatomical (Jacobian-modulated and nonmodulated white and gray matter and cortical thickness), DTI, and functional connectivity maps were included in second-level (group) analyses to map voxel-wise the correlation across-subjects between individual brain measurements and individual copper exposure (the measurements obtained in the school of each participant). Results were considered significant with clusters of 1.032 mL (e.g., 129 voxels with a resolution of 2 × 2 × 2 mm) at a height threshold of $P < 0.005$, which satisfied the FWE (family-wise error) rate correction of $P_{FWE} < 0.05$ according to recent Monte Carlo simulations (Pujol et al. 2014c). Maps in figures are displayed at $t > 2.3$.

Results

Copper as an air pollutant

Copper measured in fine particles ($PM_{2.5}$) from school playgrounds showed a mean of 8.7 ng/m^3 (SD, 3.0; range 3.7–13.8). According to the correlation with specific tracers, the main source of copper was road traffic, but a significant contribution was the result of industrial activity. An additional third source was identified in relation to the close proximity (mean ± SD, 90 ± 58 m) of seven schools to busy overhead-wire railway lines. For instance, a multiple regression accounted for 70% variance of copper measurements including elemental carbon as a single road traffic tracer (Amato et al. 2014) (standardized $\beta = 0.66$, $P < 0.00001$), zinc as a single industry tracer (Amato et al. 2014) (standardized $\beta = 0.31$, $P = 0.002$), and train proximity (standardized $\beta = 0.20$, $P = 0.037$).

Relationship of copper exposure with children's performance

Higher copper exposure was associated with poorer motor performance in children. Although in terms of the whole sample ($n = 2827$ after nine exclusions), the

association was significant for motor response speed (reaction time, $\beta = 2.2$ and $P = 0.006$), the effect was more robust on motor response consistency (reaction time standard deviation, $\beta = 2.9$ and $P < 0.00001$). Such a negative relationship with reaction time variability was significant in the group of children receiving MRI ($n = 261$ after two exclusions; $\beta = 4.2$ and $P = 0.026$). Table 1 shows descriptive statistics.

Neuroimaging results

Three-dimensional anatomical (T1-weighted) MRI and DTI were used to assess the potential association of copper exposure with alteration in the fine brain structure. Copper was associated with higher gray matter concentration (i.e., a higher proportion of gray matter in the tissue) in the striatum, specifically in the caudate nucleus (Fig. 1 and Table 2), with no effect on tissue volume. This finding potentially expresses a relative reduction of striatum white matter (i.e., of white matter "striae" that actually give the corpus striatum its anatomical name). No other significant alterations were identified with 3D anatomical MRI with the exception of an area of increased cortical thickness in the supplementary motor area of the left hemisphere (data not shown).

Results from the DTI analysis were highly consistent with the anatomical results (Fig. 2, Table 2). Copper was associated with an increase of neural tissue FA. This DTI measurement may express the extent to which an anatomical structure is composed of white matter tracts showing one dominant direction. In brain regions containing tracts with a single direction, FA increases as a result of brain maturation. Nevertheless, in complex structures with tracts crossing in different directions, higher FA may denote less mature or less structured tissue (Douaud et al. 2011; Jones et al. 2013). In our analysis, higher copper levels were associated with higher FA in white matter close to the caudate nucleus and in the caudate nucleus itself. This region is anatomically characterized as showing superior–inferior, posterior–anterior, and lateral–medial crossing white matter tracts (see Fig. 3 and Kotz et al. 2013). Within this scenario, a less mature structure will show higher FA (the effect of copper in our study).

A voxel-wise correlation analysis with behavior measurements helped to establish the nature of the identified changes associated with copper exposure. Reaction time and, mostly, reaction time variability showed significant positive correlation with FA of white matter adjacent to the caudate nucleus (Fig. 2). Thus, in the direction of copper exposure findings, slower children and the children with less consistent motor response exhibited higher FA in this region.

To investigate copper effects on the neural track architecture in the caudate nucleus region, we analyzed tissue diffusion along the three orthogonal (x, y, z) directions separately. Higher copper exposure was associated with a complex combination of diffusion changes in the caudate nucleus region, with distinct sectors showing reduced diffusion in one or more directions (Fig. 4). In other words, copper was related to changes in the complex architecture of neural tissue diffusion, further supporting the notion that white matter pathways in the caudate nucleus region may be affected by copper exposure.

The functional significance of the identified basal ganglia changes was further investigated by assessing functional connectivity in the basal ganglia network. Functional connectivity MRI maps representative of frontal-basal ganglia circuits were generated using coordinates taken from previous works and from the current anatomical and DTI results centered at the caudate nucleus (see Methods). The most relevant finding was the association of higher copper exposure to a reciprocal reduction of functional connectivity between the caudate nucleus and the frontal lobe operculum bilaterally (Fig. 5). This association was consistent with the anatomical and DTI results and notably specific in terms of functional anatomy. Remarkably, reduced caudate-to-frontal operculum connectivity was the only significant finding in three functional connectivity maps (see Table 2).

The effect of potential confounders was tested for each significant finding including age, sex, academic achieve-

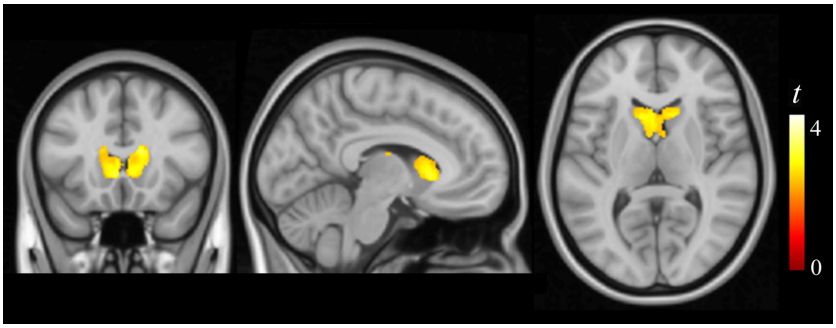

Figure 1. Correlation of copper measurements with brain tissue composition. Higher copper levels correlated with higher gray matter (presumably expressing lower white matter) concentration in the caudate nucleus bilaterally. The right hemisphere corresponds to the right side of axial and coronal views.

Table 2. MRI correlation results.

	Cluster size, mL	*x*, *y*, *z*	*t*
Copper versus gray matter concentration			
R Caudate nucleus-positive correlation	4.09	8, 19, 3	3.12
L Caudate nucleus-positive correlation	4.09 (same cluster)	−3, 16, 6	3.12
Copper versus fractional anisotropy			
R Caudate nucleus-positive correlation	1.40	11, 9, 9	3.8
L Caudate nucleus-positive correlation	9.23	−8, 9, 10	3.9
L Supracaudate white matter-positive correlation	9.23 (same cluster)	−17, 20, 25	3.6
L Suprathalamic white matter-positive correlation	9.23 (same cluster)	−20, −17, 28	3.4
R Corpus callosum-positive correlation	1.90	17, −40, 13	3.8
Reaction time versus fractional anisotropy			
L Supracaudate white matter-positive correlation	1.46	−15, 11, 21	3.6
Reaction time SD versus fractional anisotropy			
L Supracaudate white matter-positive correlation	4.29	−17, 10, 19	3.9
R Supracaudate white matter-positive correlation	3.60	19, 15, 20	4.1
Copper versus functional connectivity			
Left caudate nucleus seed map			
R Frontal operculum-negative correlation	5.85	48, 2, 16	4.2
L Frontal operculum-negative correlation	3.30	−38, 14, 12	3.9
Right frontal operculum seed map			
L Caudate nucleus-negative correlation	2.35	−14, 22, 8	3.9
R Caudate nucleus-negative correlation	1.39	16, 22, 10	3.1
Left frontal operculum seed map			
L Caudate nucleus-negative correlation	1.30	−16, 24, 6	4.4
Frontal medial seed map			
L Frontal operculum-positive correlation	3.29	−44, 32, −2	3.2
L Auditory cortex-positive correlation	1.72	−50, −18, 2	3.5
L Medial frontal cortex-positive correlation	1.42	−12, 22, 44	3.9
R Visual cortex-negative correlation	12.81	14, −54, 2	3.8
Supplementary motor area seed map			
L Supramarginal gyrus-positive correlation	1.08	−56, −34, 24	3.6

SD, standard deviation.

x, *y*, *z* coordinates given in MNI (Montreal Neurological Institute) space. Statistics at corrected threshold $P_{FWE} < 0.05$ estimated using Monte Carlo simulations.

ment, academic difficulties score, obesity, parental education, home and school vulnerability index, and public/nonpublic school category as covariates. No single confounder or combination showed a significant effect. That is, decreases in β estimates after the inclusion of confounders in a regression model were very small with no variables affecting the primary results with β reductions >10%. Finally, potential alterations associated with Mn (manganese) were also investigated, as this element may be associated with basal ganglia alterations. We did not, however, find any significant finding associated with manganese. Moreover, the effect of copper had a tendency to be more robust when adjusted by Mn (e.g., the primary correlation between copper and motor response consistency showing $\beta = 2.9$ in the whole sample, showed $\beta = 3.3$ after entering Mn measurements as a covariate). Similarly, the effect of copper remained (no β decrease > 10%) after additionally adjusting by other representative elements (Table 3, i.e., C, Pb, Fe, and Sb).

Discussion

Airborne copper was significantly associated with poorer motor performance and detectable brain damage in developing children. The alterations are highly consistent with the known consequences of copper excess on the brain with basal ganglia as the main target. The associations were demonstrated with copper levels common in urban environments, thus suggesting a risk to large populations with potentially significant implications for public health. Children may be particularly vulnerable to copper as an agent capable of interfering with brain development during critical developmental stages. Consistent with our results, a recent study has reported a significant association between high copper levels in blood and poorer cognitive performance in normal school children (Zhou et al. 2015).

The β weights reported in Table 4 may help in determining the biological relevance of behavior and imaging

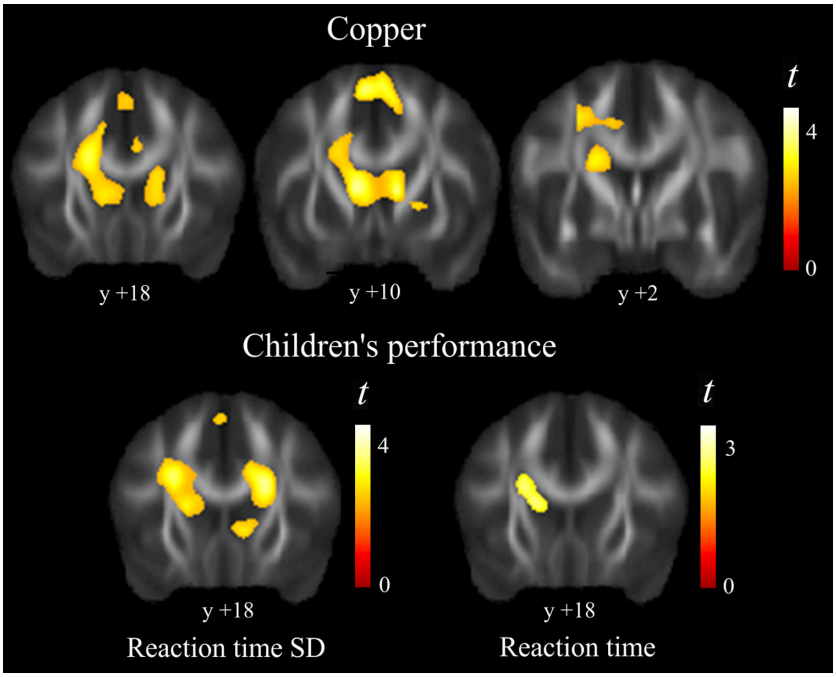

Figure 2. Diffusion tensor imaging results. Higher copper levels correlated with higher FA (fractional anisotropy) predominantly in caudate nucleus region (top panel). The correlation with motor performance (bottom panel) showed both slower reaction time and larger reaction time standard deviation associated with higher FA in white matter adjacent to the caudate nucleus. The right hemisphere corresponds to the right side. *Y* denotes "*y*" MNI coordinates.

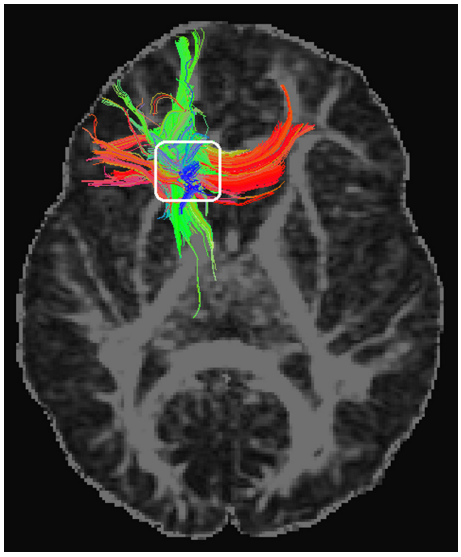

Figure 3. Diffusion tensor imaging tractographic display of a representative participant. The colors are coded to show diffusion-defined left–right tracts in red, anterior–posterior tracts in green, and superior–inferior tracts in blue. Note convergence of the three directions in our region of interest (white rectangle).

changes associated with air copper in our study. While the change related to reaction time was small, the effect on motor response consistency (measured as reaction time standard deviation) was more important. For instance, the increase in one unit (ng/m^3) of air copper predicts an increase of 2.9 msec in reaction time standard deviation. Therefore, if the range of copper measurements is 10 units, from the least (3.7 ng/m^3) to the most polluted school (13.8 ng/m^3), the potential variation predicted is 29 msec, which is approximately one third of the standard deviation of this motor performance measurement (SD, 91 msec). The magnitude of the effect on the caudate nucleus structure and function was of the same order. Overall, our conclusion is that the effect of copper is subtle, but biologically meaningful.

In the current study, we have identified copper as one road traffic-related pollutant. Traffic-related copper is thought to be mostly released from brake pads (Hulskotte et al. 2007) and it was the main source in our study. A significant proportion of copper, however, comes from industrial activity and a third source seems to be the result of railway traffic. This is consistent with reports indicating that the air in busy train stations contains large amounts of copper generated by overhead train wire supplying electrical power (Kim et al. 2010; Loxham et al. 2013).

Although a normal oral diet contains a considerable amount (~1 mg) of copper (Morris et al. 2006), our data suggest that relatively lower levels are neurotoxic in chronic airborne exposures. Ingested copper is mostly incorporated into ceruloplasmin (safe copper) and any excess is removed by excretion into the bile (Madsen and Gitlin 2007). There is evidence indicating that the "toxic copper" is actually the circulating free (i.e., nonceruloplasmin bound) copper (Squitti 2014c; Pal and Prasad 2015), which is the only fraction capable of penetrating the brain parenchyma (Zheng and Monnot 2012). Inhaled copper

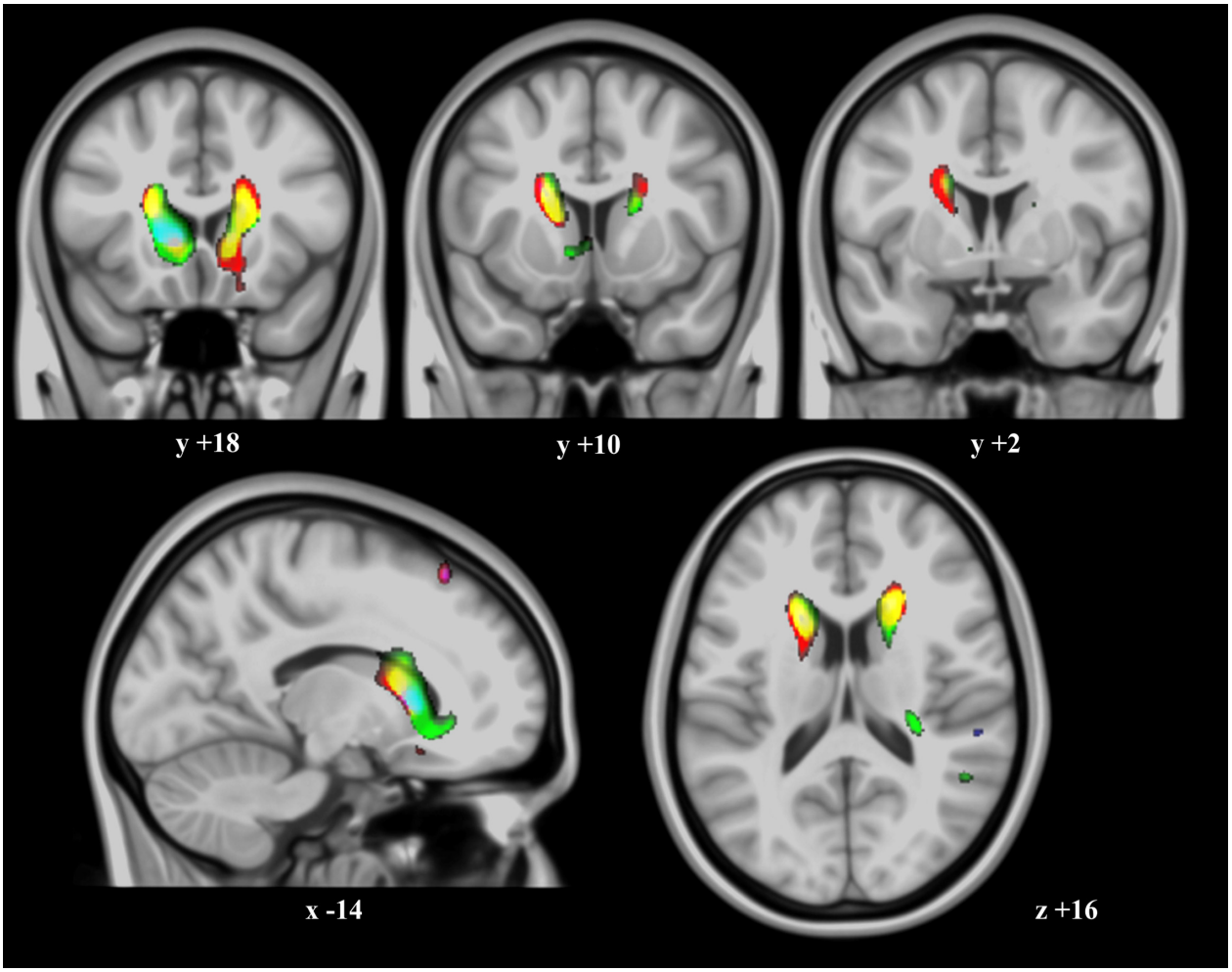

Figure 4. Water diffusion direction changes related to copper. Correlation of copper measurements with water diffusion along the three (*x*, *y*, *z*) axes separately and superimposed in a single RGB color display (thresholded at $P = 0.001$ in MRIcron®). Color regions express sites where higher copper levels were associated with reduced diffusion for one or more directions. The most evident changes were along the right–left (red), anterior–posterior (green) directions, or both (yellow) (note that regions with mixed effects show RGB composite colors). The right hemisphere corresponds to the right side of axial and coronal views. *X*, *Y*, *Z*, denote MNI coordinates.

may notably circumvent the liver regulation and safe binding to ceruloplasmin. So, nonceruloplasmin-bound copper absorbed in the respiratory tract can more easily enter the brain and achieve higher tissue concentrations.

Environmental copper has been proposed as a risk factor for neurodegenerative disease (Morris et al. 2006; Caudle 2015; Pal and Prasad 2015). The highest exposures occur through the inhalation of fumes generated from welding, as well as metal mining and smelting activities. Long-term (20 years) occupational copper exposure has been shown associated with 2.5-fold increase in risk for Parkinson's disease (Gorell et al. 2004; Caudle 2015) and with a younger age at onset (46 years) (Racette et al. 2001). However, manifest neurological disease seems not to be a necessary outcome in occupational copper exposure, which suggests different susceptibilities among individuals and the potential interaction between a genetic predisposition and copper availability. This is obvious in the paradigmatic Wilson disease where a similar genetic alteration may correspond to a range of clinical severity and, on the other hand, the neurological disorder may be not expressed if copper intake is properly controlled (Bandmann et al. 2015). Also, there is a possibility that the toxic capacity of environmental copper excess saturates at relatively lower copper levels (i.e., high environmental copper concentrations and very high concentrations could generate similar brain damage if the assumption is correct).

The neurotoxic action of copper via oxidative stress and mitochondrial injury (Eskici and Axelse 2012; Bandmann

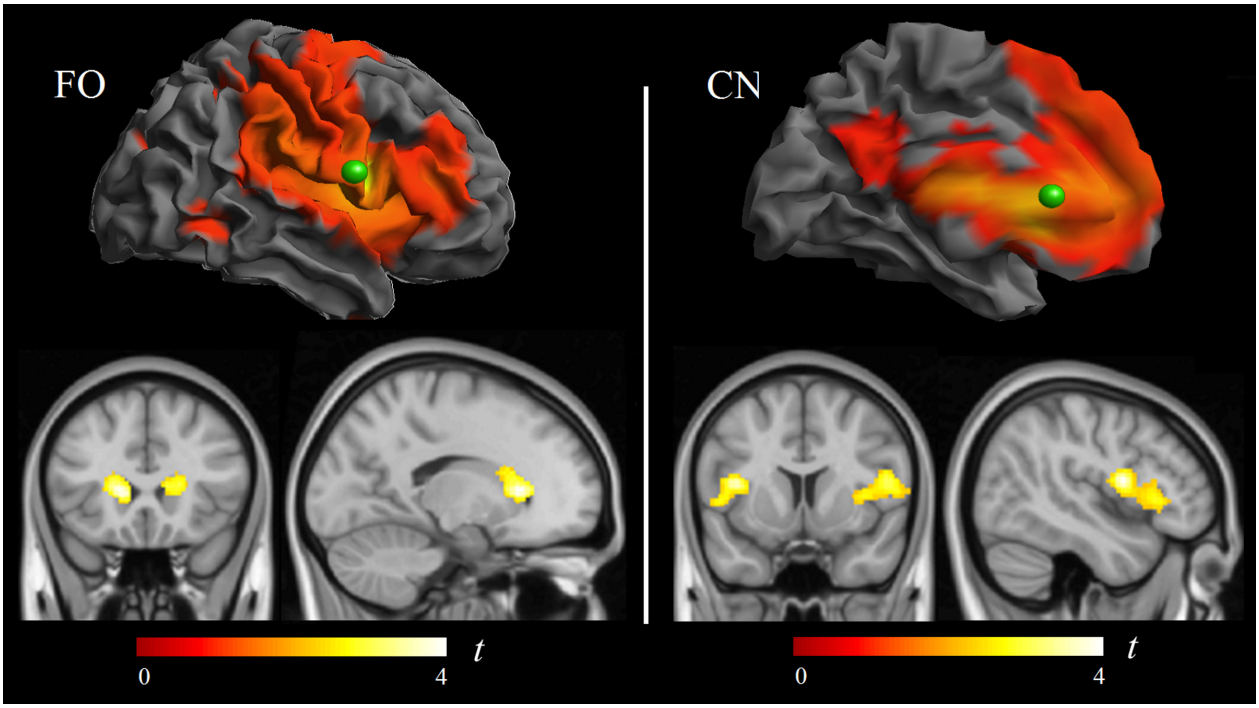

Figure 5. Correlation of copper measurements with functional connectivity MRI. Within the frontal operculum functional connectivity map (left panel), copper was associated with a connectivity reduction between the frontal (seed) region of interest (green sphere) and the caudate nuclei. Reciprocally, within the caudate nucleus functional connectivity map (right panel), copper was associated with a connectivity reduction between the caudate nucleus seed region (green sphere) and the frontal lobe opercula.

Table 3. Potentially relevant airborne elements and their correlation with Cu.

Measures from 39 schools	Mean ± SD	Range	Corr, with Cu *r* values	Shared variance (adjusted $r^2 \times 100$)
Carbon (C), $\mu g/m^3$	1.5 ± 0.7	0.6–3.9	0.41	15%
Manganese (Mn), ng/m^3	15.3 ± 13.8	3.7–64.8	0.22	2%
Lead (Pb), ng/m^3	8.1 ± 2.8	4.3–16.8	0.46	19%
Iron (Fe), $\mu g/m^3$	0.6 ± 0.6	0.1–3.0	0.15	0.4%
Antimony (Sb), ng/m^3	1.1 ± 0.4	0.4–2.4	0.75	55%

Cu, copper; SD, standard deviation.

et al. 2015) may also depend on tissue energy consumption rates. In children, the highly energetic basal ganglia appear to be the main target. This occurs in our study and in Wilson's disease, in which the lenticular nucleus (putamen and globus pallidus) was originally described with the most dramatic pathological changes (Compston 2009), although the caudate nucleus may show the most severe reduction in glucose consumption (Hermann 2014). By contrast, a more persistent subtle excess of copper throughout life could be responsible for protracted but widespread brain damage. In this context, an increasing amount of evidence indicates that copper may play a causal role in late-onset neurodegenerative disorders (Bush 2003; Bandmann et al. 2015). For example, nonceruloplasmin-bound copper levels are higher than normal reference values in up to 60% of Alzheimer's disease patients (Squitti 2014c; Squitti et al. 2014b). Also, high-nonceruloplasmin-bound copper concentrations were associated with an increased rate of mild cognitive impairment conversion to full Alzheimer's disease (Squitti et al. 2014a). A prospective study revealed an association between a diet simultaneously high in copper and saturated fats and cognitive decline (Morris et al. 2006). In a variety of experimental animal studies, oral copper intake resulted in significant amyloid β deposition and performance decline (Alzheimer's disease-like pathology), even at low concentrations (Pal and Prasad 2015).

Table 4. Behavior and imaging changes associated with air copper (copper range, 3.7–13.8 ng/m^3).

Whole sample (n = 2827)	Mean ± SD	β Coefficient (adjusted β)[2]	95% CI (adjusted 95% CI)	t	P
Motor speed (reaction time)	671 ± 124 msec	2.2 (4.7) ms/(ng/m^3)	0.6 to 3.7 (1.8 to 7.5) ms/(ng/m^3)	2.7	0.006
Motor response consistency (reaction time SD)	235 ± 91 msec	2.9 (3.4) ms/(ng/m^3)	1.7 to 4.0 (1.4 to 5.5) ms/(ng/m^3)	4.9	8e-7
MRI sample (n = 261)[1]					
Motor response consistency (reaction time SD)	224 ± 91 msec	4.2 (9.6) ms/(ng/m^3)	0.5 to 7.9 (1.7 to 17.6) ms/(ng/m^3)	2.2	0.026
Gray matter concentration L caudate nucleus	14.2 ± 3.9 GMc	0.3 (0.3) GMc/(ng/m^3)	0.1 to 0.4 (0.1 to 0.5) GMc/(ng/m^3)	3.1	0.001
Fractional anisotropy DTI L caudate nucleus	16 ± 1 FAi	0.1 (0.1) FAi/(ng/m^3)	0.06 to 0.2 (0.05 to 0.2) FAi/(ng/m^3)	3.9	0.0001
Functional connectivity L frontal cortex to L caudate	0.3 ± 1.1 FCi	−0.1 (−0.1) FCi/(ng/m^3)	−0.14 to −0.05 (−0.2 to −0.1) FCi/(ng/m^3)	−4.4	0.00001

SD, standard deviation; β, β coefficients from the regressions with copper as the predictor factor; GMc, percentage of gray matter concentration; FAi, anisotropy index expressed in the range of 0–100 units; FCi, strength of functional connectivity expressed in arbitrary units.
[1]n varied in each imaging modality (see Methods section).
[2]Socioeconomic status, a general indicator of traffic pollution (elemental carbon) and other potentially toxic agents (Pb, Mn, Sb, and Fe) were used in the adjusted model.

In the broader context of traffic-related pollution, the effect of air pollutants may be more dramatic when the exposure involves earlier developmental periods. Indeed, Peterson et al. (2015) have provided evidence of brain structural alterations in later childhood associated with prenatal pollutant exposure affecting large areas of the left-hemisphere white matter, and a less severe effect associated with postnatal exposures at age 5 years. On the other hand, recent studies have revealed that long-term ambient air pollution exposure may ultimately affect brain tissue volume in older people (Chen et al. 2015; Wilker et al. 2015).

A general limitation when assessing children with MRI is the potential effect of head movements on image quality, particularly on functional MRI and DTI acquisitions. We have considered this issue carefully and adopted several means to rigorously control the effects of motion on functional MRI (see Methods). In the case of DTI, we decided to exclude cases with detectable image degradation, as no correction procedure is wholly efficient. A post hoc analysis on DTI using less rigorous exclusion criteria (n = 242) showed similar but weakened DTI results, indicating that the data obtained in the more selective sample (n = 177) were most probably not the result of motion effects. Also, a higher MRI signal may be obtained using a higher magnetic field (i.e., 3-Tesla magnets). Although we did have the 3-Tesla option, the present study was developed using a 1.5-Tesla magnet following the recommendations of the FP7-ERC Ethics Review Committee to limit magnetic field strength in children.

Conclusions

Our study has revealed that apparently safe school environments may indeed to expose developing children to the harmful effects of air pollutants. Tolerated amounts of airborne copper were associated with poorer motor performance in children in the city of Barcelona. The effect on motor performance was directly associated with changes in the structure and function of the basal ganglia, suggesting underdevelopment of the caudate nucleus complex neural connections.

Acknowledgments

This work was supported by the European Research Council under the ERC (grant number 268479) —the BREATHE project. The Agency of University and Research Funding Management of the Catalonia Government participated in the context of Research Group SGR2014-1673. We acknowledge C. Persavento, J. González, L. Bouso, M. López, and P. Figueras their contribution to the field work. We also acknowledge all the families and schools participating in the study.

Conflict of Interest

We have no competing interests.

References

Amato, F., I. Rivas, M. Viana, T. Moreno, L. Bouso, C. Reche, et al. 2014. Sources of indoor and outdoor PM2.5 concentrations in primary schools. Sci. Total Environ. 490:757–765.

Bandmann, O., K. H. Weiss, and S. G. Kaler. 2015. Wilson's disease and other neurological copper disorders. Lancet Neurol. 14:103–113.

Bellgrove, M. A., R. Hester, and H. Garavan. 2004. The functional neuroanatomical correlates of response variability: Evidence from a response inhibition task. Neuropsychologia 42:1910–1916.

Brett, M., R. Valabregue, and J. Poline. 2003. Region of interest analysis using an SPM toolbox. Neuroimage 16: S497.

Bush, A. I. 2003. The metallobiology of Alzheimer's disease. Trends Neurosci. 26:207–214.

Caudle, W. M. 2015. Occupational exposures and parkinsonism. Handb. Clin. Neurol. 131:225–239.

Chen, J. C., X. Wang, G. A. Wellenius, M. L. Serre, I. Driscoll, R. Casanova, et al. 2015. Ambient air pollution and neurotoxicity on brain structure: evidence from Women's Health Initiative Memory Study. Ann. Neurol. 78:466–476.

Compston, A. 2009. "Progressive lenticular degeneration: a familial nervous disease associated with cirrhosis of the liver, by S. A. Kinnier Wilson, (From the National Hospital, and the Laboratory of the National Hospital, Queen Square, London) Brain 1912: 34; 295–509.". Brain 132:1997–2001.

Douaud, G., S. Jbabdi, T. E. Behrens, R. A. Menke, A. Gass, A. U. Monsch, et al. 2011. DTI measures in crossing-fibre areas: increased diffusion anisotropy reveals early white matter alteration in MCI and mild Alzheimer's disease. NeuroImage 55:880–890.

Eskici, G., and P. H. Axelse. 2012. Copper and oxidative stress in the pathogenesis of Alzheimer's disease. Biochemistry 51:6289–6311.

Fischl, B., M. I. Sereno, and A. M. Dale. 1999. Cortical surface-based analysis. II: inflation, flattening, and a surface-based coordinate system. NeuroImage 9:195–207.

Forns, J., M. Esnaola, M. López-Vicente, E. Suades-González, M. Alvarez-Pedrerol, J. Julvez, et al. 2014. The n-back test and the attentional network task as measures of child neuropsychological development in epidemiological studies. Neuropsychology 28:519–529.

Fox, M. D., A. Z. Snyder, J. L. Vincent, M. Corbetta, D. C. Van Essen, and M. E. Raichle. 2005. The human brain is intrinsically organized into dynamic, anticorrelated functional networks. Proc. Natl Acad. Sci. USA 102:9673–9678.

Goodman, R. 2001. Psychometric properties of the strengths and difficulties questionnaire. J. Am. Acad. Child Adol. Psychiatry 40:1337–1345.

Gorell, J. M., E. L. Peterson, B. A. Rybicki, and C. C. Johnson. 2004. Multiple risk factors for Parkinson's disease. J. Neurol. Sci. 217:169–174.

Grandjean, P., and P. J. Landrigan. 2014. Neurobehavioural effects of developmental toxicity. Lancet Neurol. 13:330–338.

Harrison, B. J., J. Pujol, N. Cardoner, J. Deus, P. Alonso, M. López-Solà, et al. 2013. Brain corticostriatal systems and the major clinical symptom dimensions of obsessive-compulsive disorder. Biol. Psychiatry 73:321–328.

Hermann, W. 2014. Morphological and functional imaging in neurological and non-neurological Wilson's patients. Ann. N. Y. Acad. Sci. 1315:24–29.

Hulskotte, J. H., H. A. van der Gon, A. J. Visschedijk, and M. Schaap. 2007. Brake wear from vehicles as an important source of diffuse copper pollution. Water Sci. Technol. 56:223–231.

Jones, D. K., T. R. Knösche, and R. Turner. 2013. White matter integrity, fiber count, and other fallacies: the do's and don'ts of diffusion MRI. NeuroImage 73:239–254.

Kim, C. H., D. C. Yoo, Y. M. Kwon, W. S. Han, G. S. Kim, M. J. Park, et al. 2010. A study on characteristics of atmospheric heavy metals in subway station. Toxicol. Res. 26:157–162.

Kotz, S. A., A. Anwander, H. Axer, and T. R. Knösche. 2013. Beyond cytoarchitectonics: the internal and external connectivity structure of the caudate nucleus. PLoS One 8: e70141.

Langner, R., and S. B. Eickhoff. 2013. Sustaining attention to simple tasks: a meta-analytic review of the neural mechanisms of vigilant attention. Psychol. Bull. 39:870–900.

Loxham, M., M. J. Cooper, M. E. Gerlofs-Nijland, F. R. Cassee, D. E. Davies, M. R. Palmer, et al. 2013. Physicochemical characterization of airborne particulate matter at a mainline underground railway station. Environ. Sci. Technol. 47:3614–3622.

MacDonald, S. W., L. Nyberg, and L. Bäckman. 2006. Intra-individual variability in behavior: links to brain structure, neurotransmission and neuronal activity. Trends Neurosci. 29:474–480.

Madsen, E., and J. D. Gitlin. 2007. Copper and iron disorders of the brain. Annu. Rev. Neurosci. 30:317–337.

Morris, M. C., D. A. Evans, C. C. Tangney, J. L. Bienias, J. A. Schneider, R. S. Wilson, et al. 2006. Dietary copper and high saturated and trans fat intakes associated with cognitive decline. Arch. Neurol. 63:1085–1088.

de Onis, M., C. Garza, A. W. Onyango, and M. F. Rolland-Cachera. 2009. WHO development standards for infants and young children. Arch. Pediatr. 16:47–53.

Pal, A., and R. Prasad. 2015. An overview of various mammalian models to study chronic copper intoxication

associated Alzheimer's disease like pathology. Biometals 28:1–9.

Paus, T. 2005. Mapping brain maturation and cognitive development during adolescence. Trends Cogn. Sci. 9:60–68.

Peterson, B. S., V. A. Rauh, R. Bansal, X. Hao, Z. Toth, G. Nati, et al. 2015. Effects of prenatal exposure to air pollutants (polycyclic aromatic hydrocarbons) on the development of brain white matter, cognition, and behavior in later childhood. JAMA Psychiatry 72:531–540.

Power, J. D., A. Mitra, T. O. Laumann, A. Z. Snyder, B. L. Schlaggar, and S. E. Petersen. 2014. Methods to detect, characterize, and remove motion artifact in resting state fMRI. NeuroImage 84:320–341.

Pujol, J., P. Vendrell, C. Junqué, J. L. Martí-Vilalta, and A. Capdevila. 1993. When does human brain development end? Evidence of corpus callosum growth up to adulthood. Ann. Neurol. 34:71–75.

Pujol, J., L. Del Hoyo, L. Blanco-Hinojo, S. de Sola, D. Macià, G. Martínez-Vilavella, et al. 2014a. Anomalous brain functional connectivity contributing to poor adaptive behavior in Down syndrome. Cortex 64C:148–156.

Pujol, J., D. Macià, L. Blanco-Hinojo, G. Martínez-Vilavella, J. Sunyer, R. de la Torre, et al. 2014b. Does motion-related brain functional connectivity reflect both artifacts and genuine neural activity? NeuroImage 101:87–95.

Pujol, J., D. Macià, A. Garcia-Fontanals, L. Blanco-Hinojo, M. López-Solà, S. Garcia-Blanco, et al. 2014c. The contribution of sensory system functional connectivity reduction to clinical pain in fibromyalgia. Pain 155:1492–1503.

Racette, B. A., L. McGee-Minnich, S. M. Moerlein, J. W. Mink, T. O. Videen, and J. S. Perlmutter. 2001. Welding-related parkinsonism: clinical features, treatment, and pathophysiology. Neurology 6:8–13.

Rivas, I., M. Viana, T. Moreno, M. Pandolfi, F. Amato, C. Reche, et al. 2014. Child exposure to indoor and outdoor air pollutants in schools in Barcelona, Spain. Environ. Int. 69:200–212.

Rueda, M. R., J. Fan, B. D. McCandliss, J. D. Halparin, D. B. Gruber, L. P. Lercari, et al. 2004. Development of attentional networks in childhood. Neuropsychologia 42:1029–1040.

Scheiber, I. F., J. F. Mercer, and R. Dringen. 2014. Metabolism and functions of copper in brain. Prog. Neurobiol. 116:33–57.

Smith, S. M., M. Jenkinson, M. W. Woolrich, C. F. Beckmann, T. E. Behrens, H. Johansen-Berg, et al. 2004. Advances in functional and structural MR image analysis and implementation as FSL. NeuroImage 23(Suppl 1):S208–S219.

Smith, S. M., M. Jenkinson, H. Johansen-Berg, D. Rueckert, T. E. Nichols, C. E. Mackay, et al. 2006. Tract-based spatial statistics: voxelwise analysis of multi-subject diffusion data. NeuroImage 31:1487–1505.

Squitti, R. 2014c. Copper subtype of Alzheimer's disease (AD): meta-analyses, genetic studies and predictive value of non-ceruloplasmim copper in mild cognitive impairment conversion to full AD. J. Trace Elem. Med Biol. 28:482–485.

Squitti, R., R. Ghidoni, M. Siotto, M. Ventriglia, L. Benussi, A. Paterlini, et al. 2014a. Value of serum nonceruloplasmin copper for prediction of mild cognitive impairment conversion to Alzheimer disease. Ann. Neurol. 75:574–580.

Squitti, R., I. Simonelli, M. Ventriglia, M. Siotto, P. Pasqualetti, A. Rembach, et al. 2014b. Meta-analysis of serum non-ceruloplasmin copper in Alzheimer's disease. J. Alzheimers Dis. 38:809–822.

Sunyer, J., M. Esnaola, M. Alvarez-Pedrerol, J. Forns, I. Rivas, M. López-Vicente, et al. 2015. Association between traffic-related air pollution in schools and cognitive development in primary school children: a prospective cohort study. PLoS Med. 12:e1001792.

Wilker, E. H., S. R. Preis, A. S. Beiser, P. A. Wolf, R. Au, I. Kloog, et al. 2015. Long-term exposure to fine particulate matter, residential proximity to major roads and measures of brain structure. Stroke 46:1161–1166.

Zheng, W., and A. D. Monnot. 2012. Regulation of brain iron and copper homeostasis by brain barrier systems: implication in neurodegenerative diseases. Pharmacol. Ther. 133:177–188.

Zhou, G., X. Ji, N. Cui, S. Cao, C. Liu, and J. Liu. 2015. Association between serum copper status and working memory in schoolchildren. Nutrients 7:7185–7196.

NeuroImage 129 (2016) 175–184

Contents lists available at ScienceDirect

NeuroImage

journal homepage: www.elsevier.com/locate/ynimg

Traffic pollution exposure is associated with altered brain connectivity in school children

Jesus Pujol [a,b,*], Gerard Martínez-Vilavella [a], Dídac Macià [a], Raquel Fenoll [a], Mar Alvarez-Pedrerol [c,d,e], Ioar Rivas [c,d,e,f], Joan Forns [c,d,e], Laura Blanco-Hinojo [a], Jaume Capellades [g], Xavier Querol [f], Joan Deus [a,h,i], Jordi Sunyer [c,d,e,j]

[a] MRI Research Unit, Hospital del Mar, Barcelona, Spain
[b] Centro Investigación Biomédica en Red de Salud Mental, CIBERSAM G21, Barcelona, Spain
[c] Centre for Research in Environmental Epidemiology (CREAL), Barcelona, Catalonia, Spain
[d] Pompeu Fabra University, Barcelona, Catalonia, Spain
[e] Ciber on Epidemiology and Public Health (CIBERESP), Spain
[f] Institute of Environmental Assessment and Water Research (IDAEA-CSIC), Barcelona, Catalonia, Spain
[g] Radiology Department, Hospital del Mar, Barcelona, Spain
[h] Department of Clinical and Health Psychology, Autonomous University of Barcelona, Spain
[i] Instituto Universitario de Neurorrehabilitación Guttmann, Badalona, Spain
[j] IMIM (Hospital del Mar Medical Research Institute), Barcelona, Catalonia, Spain

ARTICLE INFO

Article history:
Received 22 September 2015
Accepted 14 January 2016
Available online 26 January 2016

Keywords:
Brain development
Air pollution
Functional MRI
Functional connectivity

ABSTRACT

Children are more vulnerable to the effects of environmental elements due to their active developmental processes. Exposure to urban air pollution has been associated with poorer cognitive performance, which is thought to be a result of direct interference with brain maturation. We aimed to assess the extent of such potential effects of urban pollution on child brain maturation using general indicators of vehicle exhaust measured in the school environment and a comprehensive imaging evaluation. A group of 263 children, aged 8 to 12 years, underwent MRI to quantify regional brain volumes, tissue composition, myelination, cortical thickness, neural tract architecture, membrane metabolites, functional connectivity in major neural networks and activation/deactivation dynamics during a sensory task. A combined measurement of elemental carbon and NO_2 was used as a putative marker of vehicle exhaust. Air pollution exposure was associated with brain changes of a functional nature, with no evident effect on brain anatomy, structure or membrane metabolites. Specifically, a higher content of pollutants was associated with lower functional integration and segregation in key brain networks relevant to both inner mental processes (the default mode network) and stimulus-driven mental operations. Age and performance (motor response speed) both showed the opposite effect to that of pollution, thus indicating that higher exposure is associated with slower brain maturation. In conclusion, urban air pollution appears to adversely affect brain maturation in a critical age with changes specifically concerning the functional domain.

Introduction

Common to living beings, the brain development cycle is characterized by primary growth and subsequent maturation. Maturation changes implicate structure and function with anatomical shaping, progressive myelination of neural tracks and fine-tuning of functional brain networks (Menon, 2013; Pujol et al., 2006; Toga et al., 2006). The highest-order events procure the integration of brain areas into functional systems and the segregation of distinct but interconnected large-scale networks (Uddin et al., 2010; Vogel et al., 2010: Dwyer et al., 2014; Di Martino et al., 2014).

Developing children are at risk due to the potentially hazardous effects of environmental factors (Paus, 2010). Long-term exposure to traffic-related air pollution has been associated with alterations in children's cognition (Perera et al., 2009; Suglia et al., 2008; Wang et al., 2009). We have recently identified a significant association between general markers of road traffic pollution and slower cognitive growth in a large group of children (Sunyer et al., 2015).

Epidemiological studies, therefore, indicate that high levels of urban air pollution may be dangerous to children, as they presumably interfere with brain maturation processes. This hypothesis is largely supported by a set of studies in both animals and humans showing significant associations of pollutant exposure with

* Corresponding author at: MRI Department, Hospital del Mar, Passeig Marítim 25-29, 08003, Barcelona, Spain. Fax: +34 932212181.
E-mail address: 21404jpn@comb.cat (J. Pujol).

http://dx.doi.org/10.1016/j.neuroimage.2016.01.036
1053-8119/

inflammatory and degenerative brain pathology (Block and Calderón-Garcidueñas, 2009; Calderón-Garcidueñas, 2012). However, such an interference effect on brain development has not been thoroughly investigated. We aimed to assess the extent of potential repercussions of traffic pollution exposure on child brain maturation using a variety of imaging measurements ranging from basic anatomy to high-order functional integration. A group of 263 children, aged 8 to 12 years, recruited from a large study assessing the impact of long-term exposure to urban pollution in Barcelona city school environments (Sunyer et al., 2015) completed the protocol.

Our hypothesis was that the potential brain effects of air pollution will be more evident on the more detectable anatomical and functional maturation processes. Whereas developmental changes in gray matter volume are less evident in this age period, active myelination implicates increases of relative white matter volumes, elevated choline compounds and water diffusion changes within white matter tracts (Blüml et al., 2013; Toga et al., 2006; Yoshida et al., 2013). At the functional domain, preadolescence is critical to the optimal assembling of large-scale functional networks (Menon, 2013). Accordingly, the imaging protocol included a high resolution 3D anatomical acquisition to measure regional volumes, brain tissue composition, myelination levels and cortical thickness. Diffusion tensor imaging (DTI) measurements of fractional anisotropy served to explore white matter tract architecture. In vivo spectroscopy was used to grossly estimate precursors of membrane components in white matter. Finally, functional MRI was used to test the integrity of relevant networks using both resting-state functional connectivity and a task activation/deactivation paradigm.

Selected cognitive assessment was also conducted to determine to what extent potential repercussions were also detectable on children's performance in the current study sample.

Table 1
Characteristics of the study sample (n = 263).

Gender	48.3% girls 51.7% boys
Age, years, mean ± SD (range)	9.7 ± 0.9 (8.0–12.1)
Overall school achievement—5-point scale	3.7 ± 1.0 (1–5)
Difficulties Score (SDQ), range 0–40	8.8 ± 5.3 (0–25)
Obesity: normal	71.4%
Overweight, BMI 85–94	18.4%
Obesity, BMI >94	10.2%
Mother education (5-point scale. 5 = university)	4.5 ± 0.8 (1–5)
Father education (5-point scale. 5 = university)	4.4 ± 0.8 (1–5)
Vulnerability index[a]—home	0.43 ± 0.21 (0.06–0.90)
Vulnerability index[a]—school	0.43 ± 0.22 (0.13–0.84)
Public/non-public school	43% *vs* 57%
Task performance, N-back	
Working memory, 2-back (detectability)	2.5 ± 1.3 (−0.6–3.9)
Working memory, 3-back (detectability)	1.5 ± 1.1 (−1.4–3.9)
Task performance, attentional network test	
Reaction time (ms)	650.6 ± 119.9 (431–1091)
Reaction time standard deviation (ms)	222.9 ± 91.2 (77.5–571.6)
Commission errors (number)	4.3 (3.4%) ± 5.0 (0–49)
Omission errors (number)	1.6 (1.3%) ± 3.9 (0–44)
Alerting (ms)	53.1 ± 55.5 (−138–270)
Orienting (ms)	24.4 ± 56.8 (−204–191)
Interference (ms)	39.4 ± 35.5 (−91–170)
Air pollution measurements[b]	
Outdoor elemental carbon (EC) year average (μg/m^3)	1.4 ± 0.6 (0.6–3.99)
Outdoor NO_2 year average (μg/m^3)	46.8 ± 12.0 (25.9–84.6)
Indoor elemental carbon (EC) year average (μg/m^3)	1.2 ± 0.5 (0.4–2.7)
Indoor NO_2 year average (μg/m^3)	29.4 ± 11.7 (11.5–65.6)
Overall air pollution indicator (EC + NO_2 weighted average)	0.92 ± 0.30 (0.42–1.92)

BMI, body mass index. SDQ, Strengths and Difficulties Questionnaire.
[a] Neighborhood socioeconomic status vulnerability index based on level of education, unemployment, and occupation at the census tract (Atlas de vulnerabilidad urbana de España, 2012).
[b] After excluding 3 children with outlier measurements.

Methods

Participant selection

This study was developed in the context of the BREATHE project (The European Commission: FP7-ERC-2010-AdG, ID 268479). The general project design is fully described in Sunyer et al. (2015). A total of 1564 families, from 39 schools in the city of Barcelona, were invited to participate in the MRI study via post, email or telephone, and 810 of them gave an initial positive response. The study sample was consecutively recruited from this group with the aim of including children from all participating schools. Parents of 491 children were directly contacted. Consent to participate was finally not obtained in 165 cases, 27 children were lost before the assessment and 21 children were not eligible because of dental braces. The finally selected study group included 278 cases. A total of 263 children completed the imaging protocol (mean age of 9.7 years, SD 0.9 and range, 8.0 to 12.1 years). Table 1 reports the characteristics of these participants. Additional cases were excluded on the basis of image quality criteria in each specific MRI analysis (see further).

All parents or tutors signed the informed consent form approved by the Research Ethical Committee (No. 2010/41221/I) of the IMIM-Parc de Salut Mar., Barcelona, Spain and the FP7-ERC-2010-AdG Ethics Review Committee (268479-22022011).

Pollutant exposure

Each school was measured twice during one-week periods separated by 6 months, in the warm (year 2012) and cold (year 2012/2013) seasons. Indoor air in a single classroom and outdoor air in the playground were measured simultaneously. Pollutants were measured during class-time using methods previously described (Amato et al., 2014; Rivas et al., 2014; Sunyer et al., 2015).

Elemental carbon was measured during 8 h (09:00 to 17:00 h) in particulate matter with an aerodynamic diameter < 2.5 μm (PM2.5) collected on filters with High-Volume samplers (MCV SA, Spain) using a Thermo Optical Transmission method (Sunset Laboratories Inc.). We carefully followed the EUSAAR-2 protocol, TOT Sunset Laboratories measurements, with a detection limit of 0.1 μg/m^3 and an uncertainty of ±5%. The air cleaning effect of High-Volume samplers may underestimate absolute measurements of elemental carbon in poorly ventilated indoors. In our study, however, elemental carbon penetration was almost 1(indoor/outdoor ratio 94.1% [95% CI 85.7%–102.4%]), which suggests a permanent ventilation of the measured classrooms. Elemental carbon was additionally measured in each classroom using the MicroAeth AE51 (AethLabs). The correlation between elemental carbon measured through High-Volume samplers and with the aethalometer was 0.95, supporting that High-Volume sampler measurements may be adequate estimations of classroom elemental carbon.

Nitrogen dioxide (NO_2) was measured with passive dosimeters (Gradko). The dosimeter was exposed during a period of 96 h (4 days) from Monday to Thursday in each school in both the warm and cold campaigns. Weekly data from both seasons were averaged to obtain a single measurement. Prior to the campaigns, we tested Gradko NO_2 passive dosimeters in our urban background monitoring station Palau Reial (with relatively low NO_2 concentrations) by measuring during 4 days and comparing the results with simultaneous chemiluminescence NO_2 online data. The results showed that sampling periods of 4 days were enough for ensuring a good precision. Also, during the whole sampling campaign, NO_2 was measured each week (from Monday to Thursday) with both the Gradko passive dosimeter and conventional chemiluminiscence analyzers in this reference station. We obtained a correlation of Gradko =

0.85 × chemiluminescence + 3.6 (R2 = 0.7) for a mean of 37 $\mu gNO_2/m^3$, and an uncertainty of ±17%.

We operationally selected elemental carbon and NO_2 to compute a general traffic pollution indicator given their relation to vehicle exhaust emissions in the city of Barcelona (Amato et al., 2014). Our interest here was not to identify specific neurotoxic agents directly responsible for neuronal damage, but it was merely to use a measurement globally representing exposure to this sort of air contamination. NO_2 is highly correlated with elemental carbon in Barcelona and shows the two typical rush hour peaks (Reche et al., 2011). Barcelona has a diesel dominated vehicle fleet (with very high NO_x emissions and a high NO_2/NO_x rate) with a primary NO_2 driven daily pattern (Reche et al., 2011). In Barcelona, 80% of the NO_x emissions arise from road traffic (Catalonian Government Emission Inventory, 2011–2015 Air Quality. http://airuse.eu/wp-content/uploads/2012/10/Kick-off_Generalitat.pdf), and even if a fraction of NO_2 is secondary, this is arising in a large proportion from NO emitted from road traffic as well (Grice et al., 2009). We did not use in this study levels of ultrafine particles, which may be more directly related to the potential neural damage, because in high insolation cities such as Barcelona, levels of ultrafine particles are highly influenced by photochemical nucleation usually occurring at midday. This effect prevents a high correlation of ultrafine particle levels with other traffic tracers (Brines et al., 2015; Reche et al., 2011).

To obtain more representative measurements, elemental carbon and NO_2 were adjusted for temporal variability using whole-year data from a background monitoring station in Barcelona (Sunyer et al., 2015). A single traffic-related pollutant indicator was computed using the weighted average of elemental carbon and NO_2 [(EC/group median) + (NO_2/group median) / 2] of pooled indoor and outdoor measurements from both cold and warm seasons. All children had been in the school for more than 18 months (and 98% more than two years) at imaging assessment, which was carried out after the pollution measurement campaigns.

Cognitive performance measurements

General cognitive assessment included working memory, motor response speed and attention. Working memory was assessed using a computerized version of the N-Back task (Anderson, 2002). Children's correct detections on 2-back and 3-back loads for number items were used. Specifically, the n-back parameter analyzed was "detectability", a measure of detection subtracting the normalized false alarm rate from the hit rate (Z hit rate − Z false alarm rate). A higher detectability indicates more accurate test performance. Attention and speed of motor responses were assessed using the computerized "Attentional Network Test", child version (Child ANT) (Rueda et al., 2004). We used the overall "reaction time" to measure speed of motor responses and reaction time standard deviation to measure trial-to-trial variability. A higher reaction time standard deviation indicates lower executive and general attentional resources (Langner and Eickhoff, 2013). The ANT task also uses a set of cued and congruent/incongruent conditions to measure specific attention features such as "alerting", "orienting" and "interference". Details for administering both ANT and N-Back tasks are fully described in a previous report (Forns et al., 2014).

Additional contextual assessments

Socio-demographic factors were measured using a neighborhood socioeconomic status vulnerability index (based on level of education, unemployment and occupation at the census tract) (Atlas de Vulnerabilidad Urbana de España, 2012. http://www.fomento.gob.es/.../Atlas Vulnerabilidad Urbana/) according to both school and home address. Distance from home to school was estimated based at the geocoded postal address of each participant and school. Parental education was registered for both parents using a 5-point scale (1 illiterate/2 less than/3 primary/4 secondary/5 university). Standard measurements of height and weight were performed to define overweight and obesity (de Onis et al., 2009). Parents completed the Strengths and Difficulties Questionnaire (SDQ) on child behavioral problems (Goodman, 2001). A "difficulties" score ranging from 0 to 40 was generated. Overall school achievement was rated by teachers using a 5-point scale (from the worse = 1 to the best = 5).

MRI and MR spectroscopy acquisition

A 1.5 Tesla Signa Excite system (General Electric, Milwaukee, WI, USA) equipped with an eight-channel phased-array head coil and single-shot echoplanar imaging (EPI) software was used. The imaging protocol involved an anatomical T1-weighted 3D sequence, diffusion tensor imaging (DTI), MR proton spectroscopy and functional MRI.

High-resolution 3D anatomical images

High-resolution 3D anatomical images were obtained using an axial T1-weighted three-dimensional fast spoiled gradient inversion recovery-prepared sequence. A total of 134 contiguous slices were acquired with inversion time 400 ms; repetition time 11.9 ms; echo time 4.2 ms; flip angle 15°; field of view 30 cm; 256 × 256 pixel matrix; slice thickness 1.2 mm.

Diffusion tensor imaging (DTI)

Diffusion tensor imaging (DTI) was obtained using spin-echo single-shot echo-planar sequences of 25 directions with a B-factor of 1000 s/mm^2. Twenty-six slices were acquired with repetition time 8300 ms; echo time 94 ms; thickness 5 mm, no gap; pulse angle 90°; field of view 26 cm; 128 × 128 acquisition matrix reconstructed into a 256 × 256 matrix.

Magnetic resonance spectroscopy

Proton (1 H) spectroscopy was performed using the fully automated Proton Brain Exam-Single Voxel (PROBE-SV) software package (GE Medical Systems, Milwaukee, WI) and a Stimulated Echo Acquisition Mode (STEAM) pulse sequence with TR/TE = 2000/30 ms and 128 signal averages. Total acquisition time was 5 m 4 s. The voxel showed a dimension of 23 × 14 × 14 mm and was always placed in the left frontal white matter with the aid of high-resolution 3-D images. Orthogonal projections in the three planes assisted the placement of the voxel. The major axis (23 mm) was aligned along the anterior–posterior direction in the frontal white matter. Care was taken to minimally include gray matter and to place the voxel just above the caudate nucleus between the cingulate cortex and the frontal cortex at the level of the precentral sulcus.

The functional MRI sequences

The functional MRI sequences consisted of gradient recalled acquisition in the steady state with repetition time 2000 ms; echo time 50 ms; pulse angle 90°; field of view 24 cm; 64 × 64-pixel matrix; slice thickness 4 mm (inter-slice gap, 1.5 mm). Twenty-two interleaved slices were prescribed parallel to the anterior–posterior commissure line covering the brain. Two fMRI sequences were acquired for each participant including a 6-min continuous resting-state scan generating 180 whole-brain EPI volumes, and a 4-min sensory task generating 120 whole-brain EPI volumes. The first four (additional) images in each fMRI run were discarded to allow magnetization to reach equilibrium.

During the resting-state functional MRI, children were instructed to relax, stay awake and lie still without moving, while keeping their eyes closed throughout. The task-activation paradigm involved an ABABABAB block design alternating four 30-s periods of rest (visual fixation to a cross) with four 30-s periods of visual–auditory stimulation delivered using MRI compatible goggles and headphones (VisuaStim Digital, Resonance Technology, USA). Subjects were passively confronted with a set of facial images expressing happiness and with music showing a rapid tempo (Beethoven Symphony No. 6 "Pastorale").

Image/spectra processing

3D anatomical images

All the anatomical images were visually inspected before analysis by a trained operator to detect any motion effect. A total of 10 children were discarded as a result of poor quality images and thus the final sample for the 3D anatomical analysis included 253 children. Anatomical 3D data were processed in two separate analyses assessing different anatomical characteristics:

Gray and white matter tissue concentration and volume at a voxel level was measured using Statistical Parametric Mapping (SPM8) (http://www.fil.ion.ucl.ac.uk /spm, Wellcome Department of Cognitive Neurology, London, UK, 2008). SPM voxel-based morphometry (VBM) algorithms with DARTEL registration were used with the following processing steps: segmentation of anatomical images into gray and white matter tissue probability maps in their native space; estimation of the deformations that best align the images together by iteratively registering the segmented images with their average; finally, generating spatially normalized and smoothed segmentations ($5 \times 5 \times 5$ FWHM) using the deformations estimated in the previous step. The analyses were performed with scaling by Jacobian determinants (estimates of volume change during the normalization) to consider tissue volume and without Jacobian scaling to assess the relative concentration of gray matter and white matter. Normalized images were finally transformed to the standard SPM template, re-sliced to 1.5 mm resolution in Montreal Neurological Institute (MNI) space.

Cortical thickness measurements across the whole cortex were obtained using FreeSurfer tools (http://surfer.nmr.mgh.harvard.edu/). Processing steps included removal of non-brain tissue, segmentation of the subcortical white matter and deep gray matter volumetric structures, tessellation of the gray and white matter boundary, registration to a spherical atlas which is based on individual cortical folding patterns to match cortical geometry across subjects and creation of a variety of surface based data. Cortical thickness is calculated as the closest distance from the gray/white boundary to the gray/CSF boundary at each vertex on the tessellated surface (Fischl et al., 1999).

Diffusion tensor imaging (DTI)

DTI was processed using Functional MRI of the Brain (FMRIB) Software Library 5.0 (FSL), developed by the Analysis Group at the Oxford Centre for FMRIB (Smith et al., 2004). Diffusion-weighted images were corrected for motion and eddy current distortions ("Eddy Current Correction" option in the FMRIB Diffusion Toolbox [FDT] version 2.0 in FSL), and a whole-brain mask was applied using the FSL Brain Extracting Tool. A further rigorous image quality control was carried out to identify potential residual effects of head motion, which involved the visual inspection of each DTI slice for all 25 DTI volumes in all participants. Volumes with slices with signal loss (greater than ~10%) or residual artifacts were identified by an expert researcher. DTI full examinations showing one or more degraded images in more than 5 volumes were discarded. A total of 76 children were removed from the DTI analysis on the basis of this criterion (in addition to 10 cases showing gross image degradation). The final DTI sample involved 177 children showing a mean ± SD of 23.5 (94%) ± 1.9 optimal-quality volumes. Subsequently, we estimated fractional anisotropy (FA) maps using FDT in FSL after local fitting of the diffusion tensor model at each voxel ("dtifit"). Next, diffusion data were processed using Tract-Based Spatial Statistics (Smith et al., 2006). Each FA data set was re-sliced to a 1 mm × 1 mm × 1 mm anatomical resolution and normalized to standard MNI space via the FMRIB58_FA template using the FMRIB's Nonlinear Registration Tool.

Magnetic resonance spectroscopy

Metabolite relative measurements were performed on the Advantage Windows, v. 4.2, workstation using the PROBE-SV software package, which includes automatic processing of the raw data that permits immediate display and evaluation of spectra. Measurements of choline-containing compounds (choline-to-total creatine ratio) were

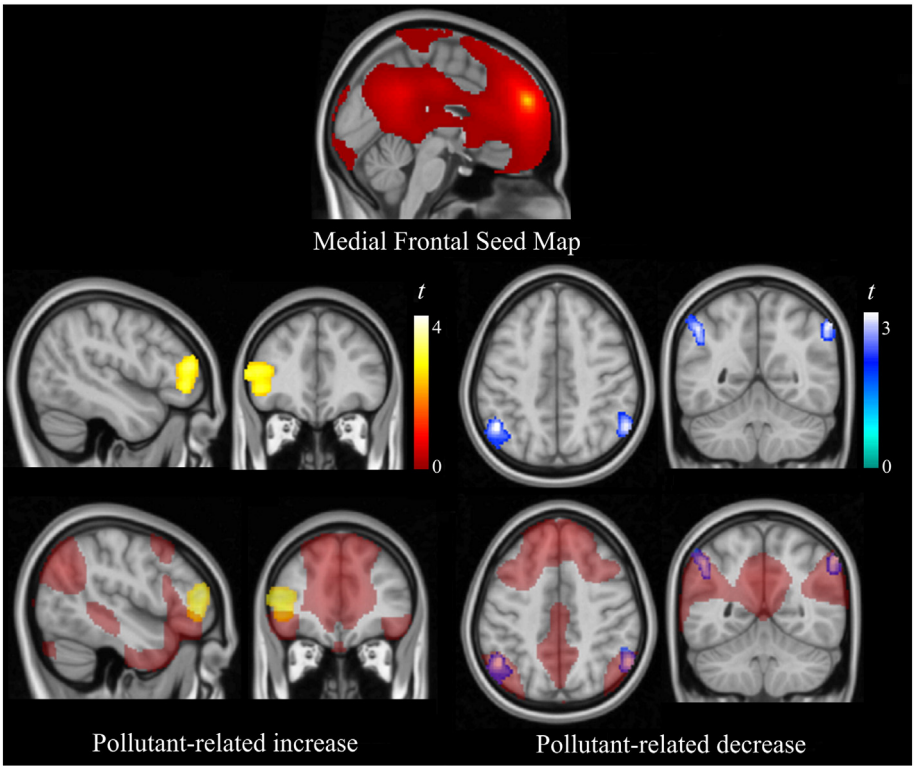

Fig. 1. Correlations of urban pollution with functional connectivity in the medial frontal seed map. Higher pollution levels were associated with higher functional connectivity between the medial frontal (seed) region and the lateral frontal cortex (left panels), and lower functional connectivity between the seed and both angular gyri (right panels). The right hemisphere corresponds to the right side of axial and coronal views.

used to test the association of air pollution with membrane precursors in white matter (Blüml et al., 2013). N-acetylaspartate (NAA) spectra width and the ratio creatine-to-noise (root-mean-square 'RMS' noise) were used to assess spectra quality. The quality criteria to be retained for statistical analyses were NAA linewidth (full width at half maximum of peak) of 0.09 ppm or less and creatine RMS noise of 8 or greater. A total of 34 participants were excluded as a result of poor spectrum quality. The final sample for the spectroscopy analysis included 229 children.

Functional MRI

Resting-state and task functional MRI preprocessing was carried out using SPM8 and involved motion correction, spatial normalization and smoothing using a Gaussian filter (full-width half-maximum, 8 mm). Data were normalized to the standard SPM-EPI template and re-sliced to 2 mm isotropic resolution in MNI space.

The following procedures were adopted to control for potential head motion effects: (i) Conventional SPM time-series alignment to the first image volume in each subject. (ii) Exclusion of 24 children in the resting-state analysis and 39 children in the task-activation analysis with large head motion. That is, outliers (and extremes) with regard to mean inter-frame motion were excluded using conventional boxplot criteria (cases beyond the quartile Q3 by one-and-a-half Q3-Q1 interquartile range [SPSS 15.0; SPSS Inc., Chicago IL]). The finally analyzed sample therefore included 239 children with valid resting-state and 224 children with valid task assessment. (iii) Both motion-related regressors (a total of 6 realignment parameters, including 3 translation and 3 rotation first-order derivatives) and estimates of global brain signal fluctuations were included as confounding variables in first-level (single-subject) analyses. (iv) Within-subject, censoring-based MRI signal artifact removal (scrubbing) (Power et al., 2014) was used to discard motion-affected volumes. For each subject, inter-frame motion measurements (Pujol et al., 2014b) served as an index of data quality to flag volumes of suspect quality across the run. At points with inter-frame motion >0.2 mm, that corresponding volume, the immediately preceding and the succeeding two volumes were discarded. Using this procedure, a mean ± SD of 11.2 (6.2%) ± 13.8 volumes out of 180 fMRI resting-state sequence volumes and 14.9 (12.4%) ± 15.8 volumes out of the 120 fMRI task volumes were removed. (v) Potential motion effects were further removed using a summary measurement for each participant (mean inter-frame motion across the fMRI run) as a regressor in the second-level (group) analyses in SPM (Pujol et al., 2014b).

Resting-state fMRI. Four functional connectivity MRI maps were generated using coordinates taken from a classical study (Fox et al., 2005), converted to MNI in mm and located at the medial frontal cortex [x = 1, y = 54, z = 26], posterior cingulate cortex [x = −2, y = −38, z = 38], dorsal frontal cortex [x = 28, y = −10, z = 58] and supplementary motor area [x = −2, y = −2, z = 55].

The maps obtained using the medial frontal cortex and the posterior cingulate cortex regions typically include all the elements of the Default Mode Network (DMN), which is highly active in inner mental processes and is negatively correlated (anticorrelated) with networks participating in attention-demanding tasks (Kelly et al., 2008). On the other hand, maps from the frontal cortex and supplementary motor area regions both capture networks commonly participating in attention-demanding tasks. As classically described, the dynamic relationship

Table 2
Functional MRI results.

Correlation with air pollution-	Non-adjusted			Adj. by age and sex	
	ml	*x y z*	*t*	*x y z*	*t*
Medial frontal seed map					
L Lateral frontal cortex—positive correlation	5.1	−48 46 16	3.6	−52 46 18	4.1
L Parietal cortex—negative correlation	2.6	−50 −58 44	3.5	−48 −56 44	3.2
R Parietal cortex—negative correlation	1.7	58 −56 46	3.5	58 −56 46	3.2
Dorsal frontal seed map					
L Parietal cortex—positive correlation	3.2	−32 −64 32	3.6	−32 −64 32	3.5
R Lateral frontal cortex—negative correlation	3.4	50 24 2	3.7	50 24 2	3.5
R Insula—negative correlation	1.4	38 2 −2	4.3	38 2 −2	4.3
Posterior cingulate cortex seed map					
R Lateral frontal cortex—positive correlation	1.5	56 36 −2	3.3	56 36 −2	3.2
Supplementary motor area seed map					
L Prefrontal cortex—positive correlation	6.1	−28 38 28	4.4	−28 38 28	4.6
R Prefrontal cortex—positive correlation	2.2	22 48 34	3.5	22 48 34	3.6
L Parietal cortex—positive correlation	3.5	−58 −46 36	3.3	−56 −46 36	3.4
R Parietal cortex—positive correlation	5.2	58 −46 40	4.1	58 −46 40	3.9
Anterior cingulate cortex—negative correlation	6.2	−14 34 −12	3.6	−14 36 −12	3.7
Sensory task					
R Somatosensory cortex—positive correlation	6.3	34 −44 64	3.7	34 −44 64	3.8
L Premotor cortex—positive correlation	1.4	−10 0 60	3.7	−10 0 60	3.6

Correlation with age			
Medial frontal seed map	*ml*	*x y z*	*t*
L Parietal cortex—positive correlation	10.7	−46 −70 52	4.9
Medial frontal cortex—positive correlation	1.5	−6 52 48	3.3
Cerebellum—positive correlation	5.8	−22 −48 −32	4.6
L Lateral frontal/insula—negative correlation	9.7	−36 22 0	4.8
R Lateral frontal/insula—negative correlation	10.4	40 16 2	3.5

Correlation with performance (motor speed)			
Medial frontal seed map			
Medial frontal cortex—positive correlation	7.6	−10 46 26	3.6
L Frontal lateral cortex—negative correlation	1.6	−32 44 −4	3.9

x y z, coordinates given in Montreal Neurological Institute (MNI) space. Statistics at corrected threshold $P_{FWE} < 0.05$ estimated using Monte Carlo simulations. Cluster size in ml.

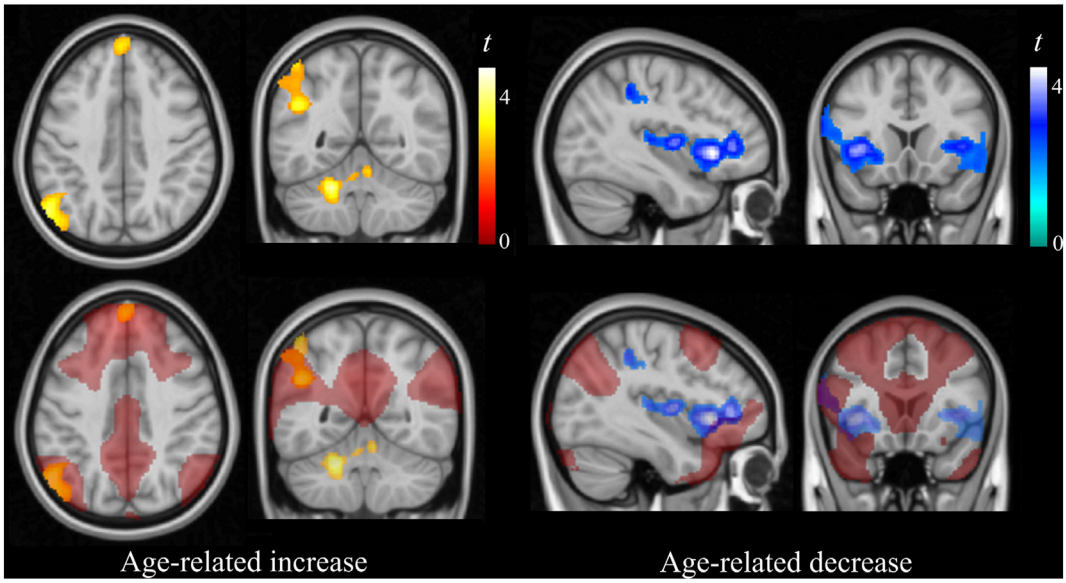

Fig. 2. Correlations of age with functional connectivity in the medial frontal seed map. Age was associated with higher functional connectivity between the medial frontal (seed) region and the left angular gyrus, medial frontal cortex and cerebellum (left panels), and with lower functional connectivity between the seed and the lateral frontal cortex/insula region bilaterally (right panels). The right hemisphere corresponds to the right side of axial and coronal views.

between the DMN and the anticorrelated task-related networks may reflect the largest-scale functional organization in the brain (Fox et al., 2005; Kelly et al., 2008). Interestingly, this network interaction maturates significantly in the age period targeted in the present study (Sherman et al., 2014).

Functional connectivity maps were generated using procedures detailed in previous reports (Harrison et al., 2013; Pujol et al., 2014a). For each location, the seed region was defined as a 3.5 mm radial sphere (sampling ~25 voxels in 2 mm isotropic space). This was performed using MarsBaR region of interest (ROI) toolbox in MNI stereotaxic space (Brett et al., 2003). Signals of interest were then extracted for each seed region respectively by calculating the mean ROI value at each time point across the time-series. To generate the seed maps, the signal time course of a selected seed region was used as a regressor to be correlated with the signal time course of every voxel in the brain in order to generate first-level (single-subject) voxel-wise statistical

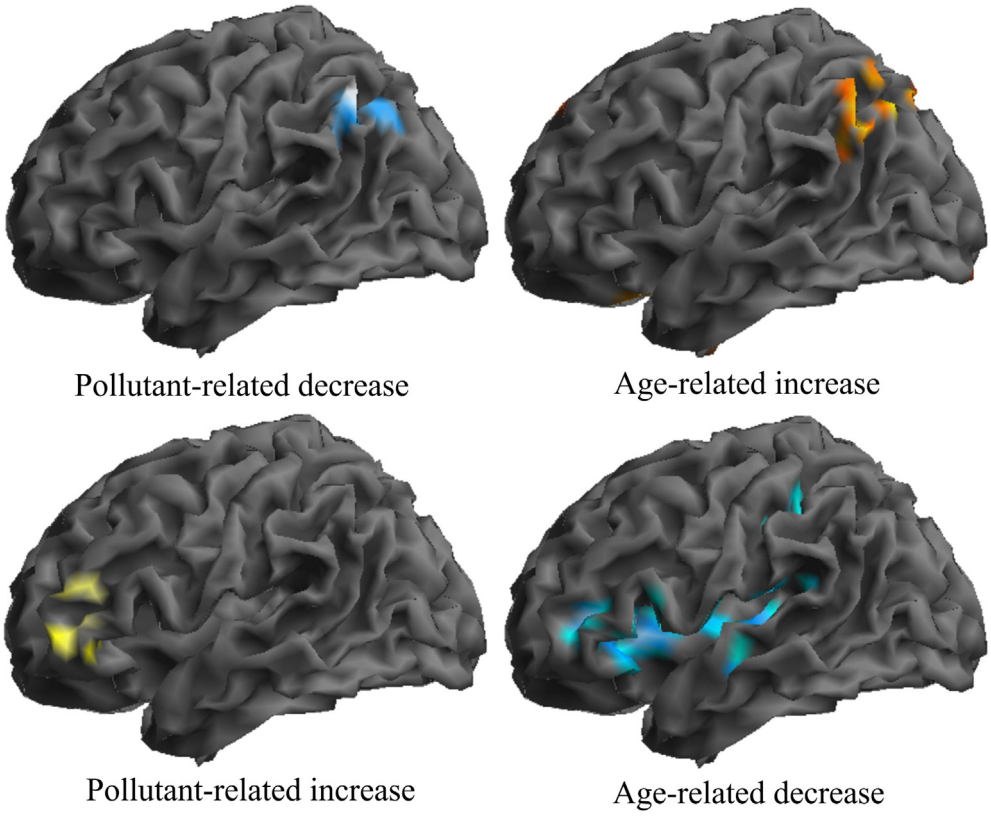

Fig. 3. 3D rendering display of urban pollution and age effects in the medial frontal seed map. Age and air pollution were associated with opposite effects on functional connectivity in notably similar areas, thus indicating that higher exposure may interfere with the normal development of functional connections.

parametric maps (contrast images). The maps were estimated for each seed separately. A high-pass filter set at 128 s was used to remove low frequency drifts below ~.008 Hz. In addition, we derived estimates of white matter, CSF and global brain signal fluctuations (using standard masks in MNI space from SPM) to include in the regression analyses as nuisance variables.

Task-activation fMRI. Functional interaction between brain systems may also be inferred using fMRI task paradigms by assessing the segregation between activated and deactivated areas during stimulation (Harrison et al., 2008; Pujol et al., 2012). Deactivated areas during our sensory task include part of the DMN, which are generally anticorrelated with networks participating in attention-demanding tasks (Chai et al., 2014; Kelly et al., 2008), although the deactivation pattern is not limited to the DMN. In the task analysis, single-subject (first-level) SPM contrast images were estimated for activations (stimulation condition > rest) and deactivations (rest > stimulation condition). For these analyses, the fMRI signal response at each voxel was modeled using the SPM canonical hemodynamic response function.

Before the statistical analysis, all the processed images (anatomical 3D, DTI, and functional MRI) were visually inspected to detect processing-induced artifacts and verify the accuracy of anatomical segmentation and FreeSurfer surface reconstructions.

Statistical analysis

Data was treated as quantitative variables and the analyses involved cross-correlations using SPM. After individual preprocessing of each imaging exam, separate second-level analyses were carried out to map voxel-wise the correlation across-subjects between individual brain images and individual age and pollutant measurements (obtained in the school of each participant). The correlations with pollutant measurements were performed both with and without adjusting by age and sex. The set of individual brain images included whole-brain estimates of regional white matter and gray matter volume and concentration, cortical thickness, DTI fractional anisotropy, resting-state functional connectivity and task-activation/deactivation. The association with choline-to-creatine metabolite ratio was obtained using simple bivariate Pearson correlation. Total creatine was examined first for an association with

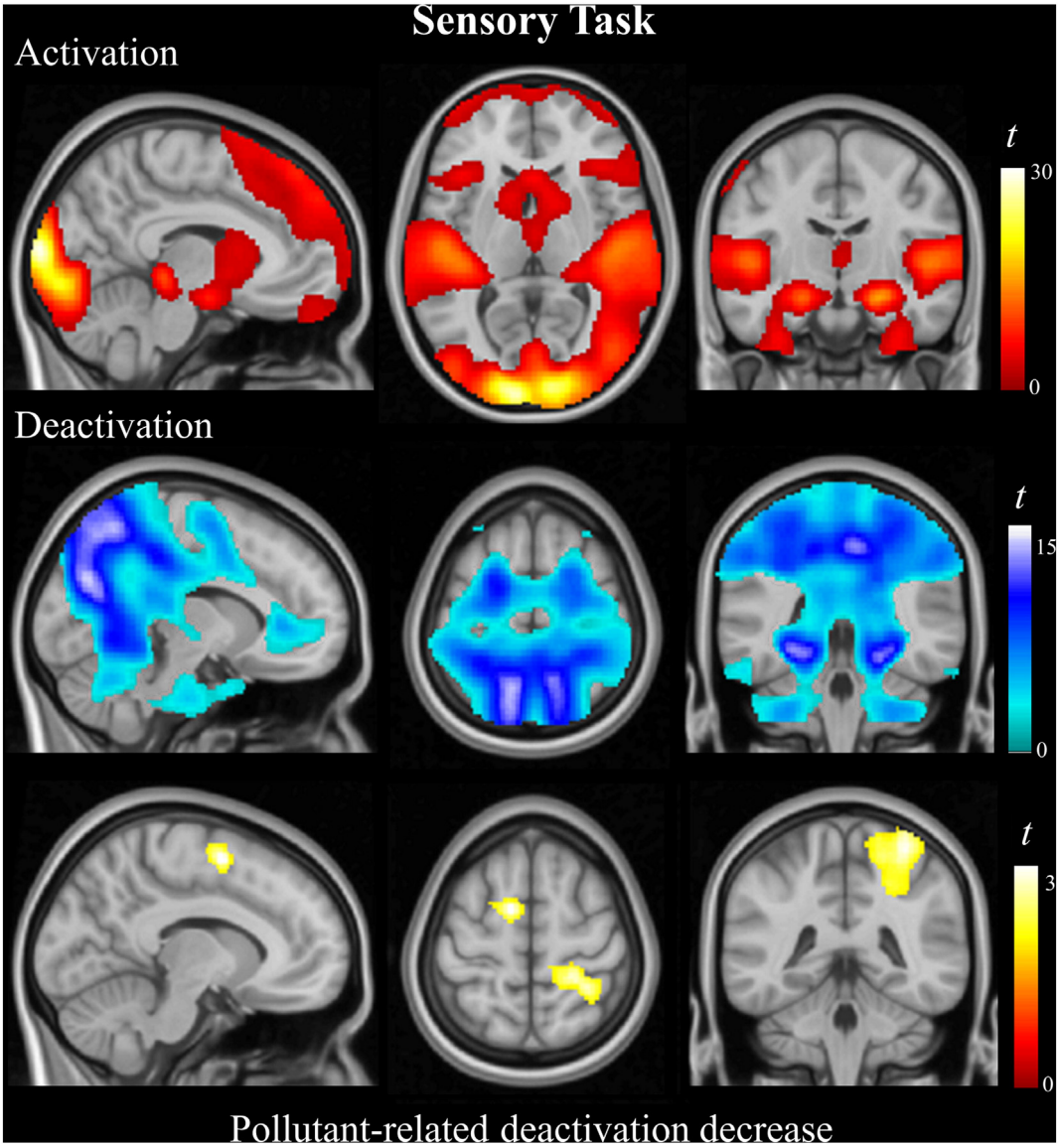

Fig. 4. Sensory task results. One-sample group activation (top panel) and deactivation (middle panel) maps showing brain response to passive viewing and listening. Air pollution was associated with lower deactivation in the supplementary motor area and somatosensory cortex included in the deactivation map (bottom panel). The right hemisphere corresponds to the right side of axial and coronal views.

traffic pollution. We found no association. As mentioned, the number of participants finally included in each analysis after exclusions on the basis of image quality criteria was: anatomic T1-weighted images, 253; DTI, 177; MR spectroscopy, 229; resting-state fMRI, 239; and sensory task fMRI 224. Finally, three additional children with outlier pollutant measurements were excluded from the correlation between brain measurements and air pollution.

Results were considered significant with clusters of 1.032 ml (e.g., 129 voxels with a resolution of $2 \times 2 \times 2$ mm) at a height threshold of $p < 0.005$, which satisfied the family-wise error (FWE) rate correction of $P_{FWE} < 0.05$ according to Monte Carlo simulations (Pujol et al., 2014c). Resting-state fMRI data were additionally adjusted for multiple testing (four functional connectivity maps) using Bonferroni (significant cluster size ≥1.4 ml). Maps in figures are displayed at $t > 2.3$.

Results

Traffic-related pollution at the children's schools was assessed using the weighted average of two reliable vehicle exhaust indicators, namely particulate elemental carbon and NO_2 (Methods). Table 1 reports ambient air concentrations of the measured pollutants. According to these data, air pollution levels at school in the city of Barcelona may be considered moderate-to-high when compared with other areas (Cyrys et al., 2012; Eeftens et al., 2012).

This summary pollution index was then whole-brain correlated with several MRI maps characterizing brain maturation. No significant association was identified between air pollution and any anatomical, structural or metabolic brain measurement. By contrast, the functional imaging analysis showed consistent results.

Our functional approach involved the generation of connectivity maps representative of key neural networks using coordinates taken from previous works (see Methods). The map obtained using the medial frontal cortex (seed) region of interest produced the most illustrative results. We found that traffic-related air pollution was significantly associated with weaker functional connectivity between regions belonging to the DMN (i.e., between the medial frontal cortex and the angular gyrus bilaterally), indicating lower intra-network integration (Fair et al., 2009). In addition, pollution also was associated with stronger functional connectivity between the (medial frontal cortex) seed region and the frontal operculum at the lateral boundary of the DMN, indicating lower network segregation (Fair et al., 2009) (Fig. 1 and Table 2).

The analysis of the correlation between children's age and functional connectivity in the DMN was useful in establishing the detrimental nature of the results (Fig. 2). Indeed, the age effect on functional connectivity in this network was the opposite of the pollutant effect. Age was significantly associated with stronger functional connectivity within the elements of the DMN (integration) and significantly associated with weaker functional connectivity with the bordering network (segregation), as shown in a previous longitudinal study (Sherman et al., 2014). Fig. 3 illustrates the opposite effects of age and pollutants using a 3D rendering display.

The analyses based on additional functional connectivity maps mirrored such findings with results in the same direction. The maps included the DMN identified from a seed region located in the posterior cingulate cortex (Table 2) and anticorrelated networks generated from dorsal frontal cortex (Supplementary Fig. 1) and supplementary motor area seeds (Supplementary Fig. 2).

The potential effects of air pollution on brain function were further tested by mapping the correlation between pollutant measurements and fMRI task activations and deactivations. Air pollutants were significantly associated with lower deactivations (rest > task map) during passive viewing and listening in the supplementary motor area and somatosensory cortex (Fig. 4). No significant findings were observed in the task > rest map.

To test whether measured pollution was associated with cognitive performance, we used children's performance in working memory, motor response speed and attention (Methods). The only significant result involved motor speed. Higher pollution predicted slower reaction time in 248 participants with complete MRI and behavioral testing (standardized $\beta = 0.154$; $p = 0.015$). A further imaging analysis was performed to correlate children's reaction time with functional connectivity in the DMN map (Fig. 5). Interestingly, a faster reaction time was associated with stronger connectivity within the DMN (network integration) and weaker connectivity in the frontal operculum (network segregation).

The effect of potential confounders was tested for each significant finding including age, sex, academic achievement, difficulties scores, obesity, parental education, home and school vulnerability index, distance from home to school and public/non-public school category as covariates. Each potential confounder was both individually entered into the model and combined with other confounders. No single confounder or combination showed a relevant effect. That is, decreases in β estimates after the inclusion of confounders in a regression model were

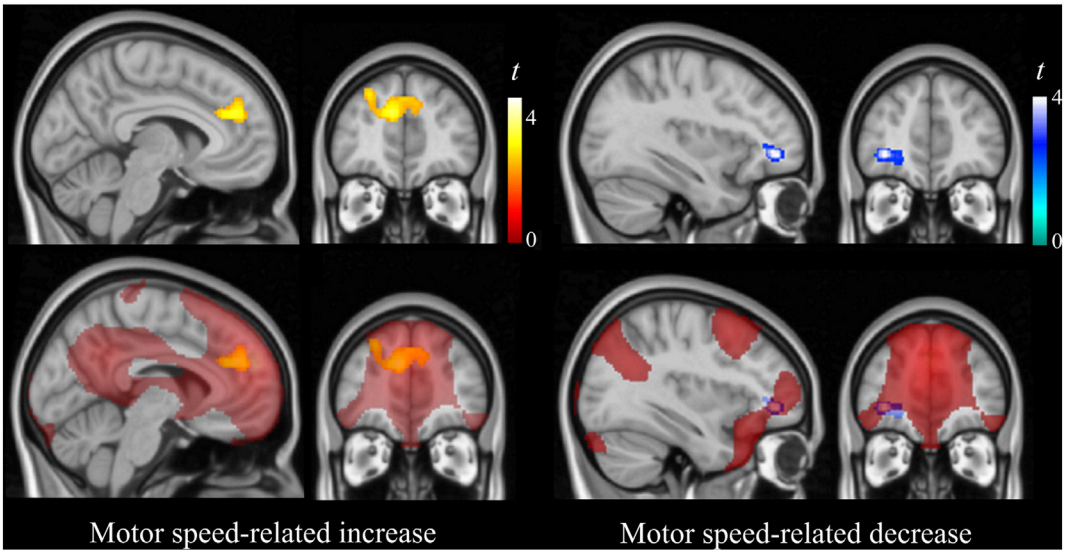

Fig. 5. Correlations of performance (motor speed) with functional connectivity in the medial frontal seed map. Faster responses were associated with higher functional connectivity within a core region of the network (medial frontal cortex), and with lower functional connectivity in the lateral boundary of the network. The right hemisphere corresponds to the right side of coronal views.

very small (mean ± SD, 1.2% ± 1.0%) with no variables affecting the primary results with β reductions greater than 7%.

Discussion

Vehicle exhaust-related air pollution exposure was associated with brain changes of a functional nature, with no evident effect on brain anatomy, structure or membrane metabolism. Children from schools with higher traffic-related pollution showed lower functional integration and segregation in key brain networks. Age and performance (i.e., motor response speed) both showed the opposite effect to that of pollution on brain function, thus indicating that higher exposure is associated with slower brain maturation.

The functional findings were highly consistent, as similar effects were observed in different functional networks and the age-sensitive areas notably coincided with the areas showing significant correlation with air pollution. Similarly, the regions identified with the mapping of correlations with motor speed also showed a notable correspondence with the anatomy of findings from both pollutant and age analyses. Nonetheless, despite the evident effect on functional connectivity, the overall brain repercussion may, to some extent, be considered subtle, as changes did not involve any measurement of brain structure. In such a context, one may speculate on the reversibility of the brain damage and the potential effectiveness of actions addressed to reduce pollution. Epidemiological data also support the notion of a subtle repercussion, as large samples are required to demonstrate robust associations (Sunyer et al., 2015).

The effect of air pollution may, however, be more dramatic when the exposure involves early developmental periods. Indeed, Peterson et al. (2015) have provided evidence of brain structural alterations in later childhood associated with prenatal pollutant exposure affecting large areas of the left-hemisphere white matter, and a less severe effect associated with postnatal exposures at age 5 years. Also, recent studies have revealed that long-term ambient air pollution exposure may ultimately affect brain tissue volume in older people (Chen et al., 2015; Wilker et al., 2015).

We have used a general marker of vehicle exhaust traffic-related air pollution based on elemental carbon and NO_2. Although this indicator reflects the amount of pollution from the traffic source, carbon and NO_2 are not necessarily the agents causing the toxic effect on the brain. Traffic pollution contains a variety of elements with greater potential neurotoxicity, such as manganese, aluminum, lead and copper (Amato et al., 2014). We have recently identified the effects of airborne copper pollution, which is road traffic-related, although a significant proportion also comes from industry, and a third source is the result of railway traffic (submitted). Brain alterations associated with copper were neural system specific and affected the basal ganglia with damage to both structure and function. In contrast, our current study based on a general indicator does not inform on which specific neurotoxicant or a combination thereof may be responsible for the identified effect restricted to functional measurements.

A concern in traffic pollution studies is potential residual confounding by socio-demographic characteristics (e.g., when a relationship exists between proximity to traffic and economically disadvantaged areas). In the city of Barcelona, however, there was a small and inverse relation between air pollution and socioeconomic vulnerability, with higher pollution levels in schools with lower vulnerability (Sunyer et al., 2015). Also, we found no significant associations between school pollution levels and parental education, employment or educational quality. Besides, the associations between air pollution and fMRI remained after adjusting for all the potential confounders (see Results), which is opposed to a potential role of these variables.

A general limitation when assessing children with MRI is the potential effect of head movements on image quality, particularly on functional MRI and DTI acquisitions. We considered this issue carefully and adopted several means to rigorously control the effects of motion (Methods). However, it is relevant to emphasize that a rigorous control of potential head motion may introduce spurious changes (e.g., regressing out global brain signal may introduce negative correlations) or even remove changes related to genuine neural activity (Pujol et al., 2014b). Also, a higher MRI signal may be obtained using a higher magnetic field (i.e., 3-Tesla magnets). Although we did have the 3-Tesla option, the present study was developed using a 1.5-Tesla magnet following the recommendations of the FP7-ERC Ethics Review Committee to limit magnetic field strength in children.

Conclusion

Although children's brains may be vulnerable at each developmental stage, preadolescence is notably transcendent in establishing solid bases for large-scale functional network organization. Urban traffic pollution appears to be capable of affecting the normal development of the proto-adult brain and significantly interfering with functional network maturation.

Conflicts of interest

The authors declare no conflict of interest.

Acknowledgments

This work was supported by the European Research Council under the ERC [grant number 268479]—the BREATHE project. The Agency of University and Research Funding Management of the Catalonia Government participated in the context of Research Group SGR2014-1673. We acknowledge Cecilia Persavento, Judit González, Laura Bouso, Mónica López and Pere Figueras for their contribution to the field work. We also acknowledge all the families and schools participating in the study.

Appendix A. Supplementary data

Supplementary data to this article can be found online at http://dx.doi.org/10.1016/j.neuroimage.2016.01.036.

References

Amato, F., Rivas, I., Viana, M., et al., 2014. Sources of indoor and outdoor PM2.5 concentrations in primary schools. Sci. Total Environ. 490, 757–765.
Anderson, P., 2002. Assessment and development of executive function (EF) during childhood. Child Neuropsychol. 8, 71–82.
Block, M.L., Calderón-Garcidueñas, L., 2009. Air pollution: mechanisms of neuroinflammation and CNS disease. Trends Neurosci. 32, 506–516.
Blüml, S., Wisnowski, J.L., Nelson Jr., M.D., et al., 2013. Metabolic maturation of the human brain from birth through adolescence: insights from in vivo magnetic resonance spectroscopy. Cereb. Cortex 23, 2944–2955.
Brett, M., Valabregue, R., Poline, J., 2003. Region of Interest analysis using an SPM toolbox. NeuroImage (16(Suppl.)).
Brines, M., Dall'osto, M., Beddows, D.C.S., et al., 2015. Traffic and nucleation events as main sources of ultrafine particles in high insolation developed world cities. Atmos. Chem. Phys. 15, 5929–5945.
Calderón-Garcidueñas, L., 2012. White matter hyperintensities, systemic inflammation, brain growth, and cognitive functions in children exposed to air pollution. J. Alzheimers Dis. 31, 183–191.
Chai, X.J., Ofen, N., Gabrieli, J.D., Whitfield-Gabrieli, S., 2014. Selective development of anticorrelated networks in the intrinsic functional organization of the human brain. J. Cogn. Neurosci. 26, 501–513.
Chen, J.C., Wang, X., Wellenius, G.A., et al., 2015. Ambient air pollution and neurotoxicity on brain structure: Evidence from Women's Health Initiative Memory Study. Ann. Neurol. 78, 466–476.
Cyrys, J., Eeftens, M.R., Heinrich, J., et al., 2012. Variation of NO_2 and NO_x concentrations between and within 36 European study areas: results from the ESCAPE study. Atmos. Environ. 62, 374–390.
de Onis, M., Garza, C., Onyango, A.W., Rolland-Cachera, M.F., 2009. WHO development standards for infants and young children. Arch. Pediatr. 16, 47–53.
Di Martino, A., Fair, D.A., Kelly, C., et al., 2014. Unraveling the miswired connectome: a developmental perspective. Neuron 83, 1335–1353.
Dwyer, D.B., Harrison, B.J., Yücel, M., et al., 2014. Large-scale brain network dynamics supporting adolescent cognitive control. J. Neurosci. 34, 14096–14107.
Eeftens, M., Tsai, M.Y., Ampe, C., et al., 2012. Spatial variation of PM2.5, PM10, PM2.5 absorbance and PM coarse concentrations between and within 20 European study areas

and the relationship with NO_2—results of the ESCAPE project. Atmos. Environ. 62, 303–317.
Fair, D.A., Cohen, A.L., Power, J.D., et al., 2009. Functional brain networks develop from a "local to distributed" organization. PLoS Comput. Biol. 5, e1000381.
Fischl, B., Sereno, M.I., Dale, A.M., 1999. Cortical surface-based analysis. II: inflation, flattening, and a surface-based coordinate system. NeuroImage 9, 195–207.
Forns, J., Esnaola, M., López-Vicente, M., et al., 2014. The n-back test and the attentional network task as measures of child neuropsychological development in epidemiological studies. Neuropsychology 28, 519–529.
Fox, M.D., Snyder, A.Z., Vincent, J.L., et al., 2005. The human brain is intrinsically organized into dynamic, anticorrelated functional networks. Proc. Natl. Acad. Sci. U. S. A. 102, 9673–9678.
Goodman, R., 2001. Psychometric properties of the strengths and difficulties questionnaire. J. Am. Acad. Child Adolesc. Psychiatry 40, 1337–1345.
Grice, S., Stedman, J., Kent, A., et al., 2009. Recent trends and projections of primary NO2 emissions in Europe. Atmos. Environ. 43, 2154–2167.
Harrison, B.J., Pujol, J., Cardoner, N., et al., 2013. Brain corticostriatal systems and the major clinical symptom dimensions of obsessive–compulsive disorder. Biol. Psychiatry 73, 321–328.
Harrison, B.J., Pujol, J., López-Solà, M., et al., 2008. Consistency and functional specialization in the default mode brain network. Proc. Natl. Acad. Sci. U. S. A. 105, 9781–9786.
Kelly, A.M., Uddin, L.Q., Biswal, B.B., et al., 2008. Competition between functional brain networks mediates behavioral variability. NeuroImage 39, 527–537.
Langner, R., Eickhoff, S.B., 2013. Sustaining attention to simple tasks: a meta-analytic review of the neural mechanisms of vigilant attention. Psychol. Bull. 139, 870–900.
Menon, V., 2013. Developmental pathways to functional brain networks: emerging principles. Trends Cogn. Sci. 17, 627–640.
Paus, T., 2010. Population neuroscience: why and how. Hum. Brain Mapp. 31, 891–903.
Perera, F.P., Li, Z., Whyatt, R., et al., 2009. Prenatal airborne polycyclic aromatic hydrocarbon exposure and child IQ at age 5 years. Pediatrics 124, e195–e202.
Peterson, B.S., Rauh, V.A., Bansal, R., et al., 2015. Effects of prenatal exposure to air pollutants (polycyclic aromatic hydrocarbons) on the development of brain white matter, cognition, and behavior in later childhood. JAMA Psychiatry 72, 531–540.
Power, J.D., Mitra, A., Laumann, T.O., et al., 2014. Methods to detect, characterize, and remove motion artifact in resting state fMRI. NeuroImage 84, 320–341.
Pujol, J., del Hoyo, L., Blanco-Hinojo, L., et al., 2014a. Anomalous brain functional connectivity contributing to poor adaptive behavior in Down syndrome. Cortex 64C, 148–156.
Pujol, J., Macià, D., Blanco-Hinojo, L., et al., 2014b. Does motion-related brain functional connectivity reflect both artifacts and genuine neural activity? NeuroImage 101, 87–95.
Pujol, J., Macià, D., Garcia-Fontanals, A., et al., 2014c. The contribution of sensory system functional connectivity reduction to clinical pain in fibromyalgia. Pain 155, 1492–1503.
Pujol, J., Batalla, I., Contreras-Rodríguez, O., et al., 2012. Breakdown in the brain network subserving moral judgment in criminal psychopathy. Soc. Cogn. Affect. Neurosci. 7, 917–923.
Pujol, J., Soriano-Mas, C., Ortiz, H., et al., 2006. Myelination of language-related areas in the developing brain. Neurology 66, 339–343.
Reche, C., Querol, X., Alastuey, A., et al., 2011. New considerations for PM, black carbon and particle number concentration for air quality monitoring across different European cities. Atmos. Chem. Phys. 11, 6207–6227.
Rivas, I., Viana, M., Moreno, T., et al., 2014. Child exposure to indoor and outdoor air pollutants in schools in Barcelona, Spain. Environ. Int. 69, 200–212.
Rueda, M.R., Fan, J., McCandliss, B.D., et al., 2004. Development of attentional networks in childhood. Neuropsychologia 42, 1029–1040.
Sherman, L.E., Rudie, J.D., Pfeifer, J.H., et al., 2014. Development of the default mode and central executive networks across early adolescence: a longitudinal study. Dev. Cogn. Neurosci. 10, 148–159.
Smith, S.M., Jenkinson, M., Johansen-Berg, H., et al., 2006. Tract-based spatial statistics: voxelwise analysis of multi-subject diffusion data. NeuroImage 31, 1487–1505.
Smith, S.M., Jenkinson, M., Woolrich, M.W., et al., 2004. Advances in functional and structural MR image analysis and implementation as FSL. NeuroImage 23 (Suppl. 1), S208–S219.
Suglia, S.F., Gryparis, A., Wright, R.O., et al., 2008. Association of black carbon with cognition among children in a prospective birth cohort study. Am. J. Epidemiol. 167, 280–286.
Sunyer, J., Esnaola, M., Alvarez-Pedrerol, M., et al., 2015. Traffic-related air pollution in schools impairs cognitive development in primary school children. PLoS Med. 2, e1001792.
Toga, A.W., Thompson, P.M., Sowell, E.R., 2006. Mapping brain maturation. Trends Neurosci. 29, 148–159.
Uddin, L.Q., Supekar, K., Menon, V., 2010. Typical and atypical development of functional human brain networks: insights from resting-state FMRI. Front. Syst. Neurosci. 4, 21.
Vogel, A.C., Power, J.D., Petersen, S.E., Schlaggar, B.L., 2010. Development of the brain's functional network architecture. Neuropsychol. Rev. 20, 362–375.
Wang, S., Zhang, J., Zeng, X., et al., 2009. Association of traffic-related air pollution with children's neurobehavioral functions in Quanzhou, China. Environ. Health Perspect. 117, 1612–1618.
Wilker, E.H., Preis, S.R., Beiser, A.S., et al., 2015. Long-term exposure to fine particulate matter, residential proximity to major roads and measures of brain structure. Stroke 46, 1161–1166.
Yoshida, S., Oishi, K., Faria, A.V., Mori, S., 2013. Diffusion tensor imaging of normal brain development. Pediatr. Radiol. 43, 15–27.

Video Gaming in School Children: How Much Is Enough?

Jesus Pujol, MD,[1,2] Raquel Fenoll, MSc,[1] Joan Forns, PhD,[3,4,5] Ben J. Harrison, PhD,[6] Gerard Martínez-Vilavella, MSc,[1] Dídac Macià, MSc,[1] Mar Alvarez-Pedrerol, PhD,[3,4,5] Laura Blanco-Hinojo, PhD,[1] Sofía González-Ortiz, MD,[7] Joan Deus, PhD,[1,8,9] and Jordi Sunyer, MD[3,4,5,10]

Objective: Despite extensive debate, the proposed benefits and risks of video gaming in young people remain to be empirically clarified, particularly as regards an optimal level of use.
Methods: In 2,442 children aged 7 to 11 years, we investigated relationships between weekly video game use, selected cognitive abilities, and conduct-related problems. A large subgroup of these children (n = 260) was further examined with magnetic resonance imaging approximately 1 year later to assess the impact of video gaming on brain structure and function.
Results: Playing video games for 1 hour per week was associated with faster and more consistent psychomotor responses to visual stimulation. Remarkably, no further change in motor speed was identified in children playing >2 hours per week. By comparison, the weekly time spent gaming was steadily associated with conduct problems, peer conflicts, and reduced prosocial abilities. These negative implications were clearly visible only in children at the extreme of our game-playing distribution, with 9 hours or more of video gaming per week. At a neural level, changes associated with gaming were most evident in basal ganglia white matter and functional connectivity.
Interpretation: Significantly better visuomotor skills can be seen in school children playing video games, even with relatively small amounts of use. Frequent weekly use, by contrast, was associated with conduct problems. Further studies are needed to determine whether moderate video gaming causes improved visuomotor skills and whether excessive video gaming causes conduct problems, or whether children who already have these characteristics simply play more video games.

ANN NEUROL 2016;00:000–000

The pros and cons of video gaming in children remain openly debated.[1,2] Although there is some evidence to suggest that video gaming can improve particular cognitive abilities in youth,[3,4] other evidence links it with conduct-related problems and increased risk toward disorders of addiction.[5,6] One possibility is that video gaming per se is neither good nor bad, but its level of use makes it so, which begs the question, how much is enough?

We performed the current study in 2,442 school-age children to investigate relationships between average weekly video game use and both cognitive performance and conduct-related problems. Considering video gaming as a training exercise based on repetitive use and on the basis of previous research,[3] we predicted that video gaming in school children would have a principal beneficial effect on speed of mental processing (eg, reaction time and chronometric measurements of attention) and a marginal influence on more innate cognitive capabilities (eg, working memory[7,8]).

A subgroup of this population (n = 260) was further examined with magnetic resonance imaging (MRI)

View this article online at wileyonlinelibrary.com. DOI: 10.1002/ana.24745

Received Apr 1, 2016, and in revised form Jul 12, 2016. Accepted for publication Jul 24, 2016.

Address correspondence to Dr Pujol, MRI Department, Hospital del Mar, Passeig Marítim 25-29. 08003, Barcelona, Spain. E-mail: 21404jpn@comb.cat

From the [1]Magnetic Resonance Imaging Research Unit, Department of Radiology, Hospital del Mar, Barcelona, Spain; [2]Biomedical Research Center Network for Mental Health (CibersamG21), Barcelona, Spain; [3]Center for Research in Environmental Epidemiology, Barcelona, Spain; [4]Pompeu Fabra University, Barcelona, Spain; [5]Biomedical Research Center Network for Epidemiology and Public Health (Ciberesp), Madrid, Spain; [6]Melbourne Neuropsychiatry Centre, Department of Psychiatry, University of Melbourne, Melbourne, Australia; [7]Department of Radiology, Hospital del Mar, Barcelona, Spain; [8]Guttmann Neurorehabilitation Institute, Autonomous University of Barcelona, Barcelona, Spain; [9]Department of Clinical and Health Psychology, Autonomous University of Barcelona, Barcelona, Spain; and [10]Hospital del Mar Medical Research Institute, Barcelona, Spain

Additional supporting information can be found in the online version of this article.

TABLE 1. Frequency of Video Games Used as a Percentage

Game	Use, %
Visuomotor skill-based games[a]	78
Platforms	
Mario Bros/Super Mario Bros/ Luigi/Super Mario Galaxy	46
Donkey Kong	12
Sports simulation	
FIFA	33
Pro Evolution Soccer	8
Inazuma Eleven	8
NBA	4
Driving simulation	
Mario Karts	7
Formula 1	3
Gran Turismo	2
Shooting	
Call of Duty	2
Fighting	
Dragon Ball	2
Adventure with action	
Lego City	5
Grand Theft Auto	3
Full-body active games/exergames[a]	58
Wii Sports	48
Just Dance	20
Mario Party	17
Wii Party	4
Adventure/strategy games[a]	49
Animal Crossing	12
Pokemon	11
Minecraft	6
Dogz/Horsez	4
Others	12
Visuomotor skill-based games and/or full-body active games	96
Adventure/strategy games alone	4

Based on reports from 100 families indicating up to 3 games played the most in the year before magnetic resonance imaging.
[a]Alone or combined.

approximately 1 year later to assess the impact of video gaming on brain structure and function. In the brain, video gaming could more notably reinforce neural connections, with a major effect presumably on frontal–basal ganglia circuits, which are central for the acquisition of new skills through practice.[9–11]

Subjects and Methods

Participants

This study was developed in the context of a large-scale project designed to assess the effects of environmental factors on brain development in children (BREATHE, European Commission FP7-ERC-2010-AdG, ID 268479). Study design and participant selection have been described in full detail elsewhere.[12,13] In short, the BREATHE project recruited 2,897 children from 39 schools to form a representative sample of children in Barcelona aged between 7 and 11 years.[12] A representative subsample of 278 children was recruited from the larger cohort to participate in neuroimaging. For the present video game study, we included children with complete cognitive and behavioral evaluation, and excluded statistically defined extreme video gamers (n = 23 children playing $\geq$18 hours per week). The final sample comprised 2,442 children (mean $\pm$ standard deviation [SD] age at the baseline = 8.6 $\pm$ 0.9 years, range = 7.0–11.1 years, including 1,223 boys and 1,219 girls). The neuroimaging subsample comprised 260 children (mean $\pm$ SD age at baseline = 8.4 $\pm$ 0.8 years, range = 7.1–10.3 years, including 134 boys and 126 girls) with complete imaging assessment, after the exclusion of statistically defined extreme video gamers (n = 3).

All parents or tutors signed the informed consent form approved by the Research Ethical Committee (No. 2010/41221/I) of the Hospital del Mar Medical Research Institute, Barcelona, Spain and the FP7-ERC-2010-AdG Ethics Review Committee (268479-22022011).

Behavioral Measurements

VIDEO GAME USE. At baseline, parents were asked to estimate how much time (in hours) their child was currently playing video games on an average weekday and weekend. A single score was computed from these estimates to indicate average hours of play per week. To document the video games most frequently used, 100 families from the MRI group completed a follow-up questionnaire indicating which games were most frequently played in the previous year. As shown in Table 1, 96% of children played visuomotor skill-based games (eg, Super Mario Bros), full-body active games (exergames; eg, Wii Sports), or both.

COGNITIVE TESTING. The selected cognitive assessment included motor response speed, attention, and working memory. Speed of motor responses and attention were assessed using the computerized child version of the Attentional Network Test (ANT).[14] Overall reaction time was used to index speed of motor responses to visual stimulation and its SD was used to index motor response consistency as a measurement of sustained attention.[15] Specific visual attention features additionally measured by

the ANT task are "alerting," "orienting," and "interference." Commission and omission errors were also registered. Cases with >30% commission or omission errors were excluded from further analyses (total 9 cases in the whole sample and 2 cases in the MRI sample). In the final whole sample, commission errors were 3.1% and omission errors were 1.1%.

A computerized version of the N-Back task[16] was used to assess working memory. "Detectability" (normalized hit rate minus normalized false alarm rate) on 2-back and 3-back loads was used to overall index test performance accuracy. See Forns et al[17] for more detail.

BEHAVIORAL ASSESSMENT. Parents completed the Strengths and Difficulties Questionnaire (SDQ) of child behavioral problems.[18] The questionnaire includes 25 questions on psychological attributes, some positive and some negative, which are rated from 0 to 2 points each. Responses are divided in 5 separate scales: "emotional symptoms," "conduct problems," "inattention/hyperactivity," "peer relationship problems," and "prosocial behavior." A "difficulties" score ranging from 0 to 40 was generated by summing the scores for the scales 1 to 4. Parents were also asked to report the average daily sleeping time (in hours) of their children. Overall school achievement was rated by teachers using a 5-point scale (from the worse = 1 to the best = 5).

ADDITIONAL CONTEXTUAL ASSESSMENTS. A neighborhood socioeconomic status vulnerability index (Urban Vulnerability Atlas of Spain, 2012; http://www.fomento.gob.es/MFOM/LANG_CASTELLANO/DIRECCIONES_GENERALES/ARQ_VIVIENDA/SUELO_Y_POLITICAS/OBSERVATORIO/Atlas_Vulnerabilidad_Urbana/), at both school and home addresses, was used as a composite measure of sociodemographic factors including level of education, unemployment, and occupation at the census tract. Parental education was registered using a 5-point scale (1 = illiterate; 2 = less than primary; 3 = primary; 4 = secondary; 5 = university).

MRI Acquisition

MRI was administered a mean ± SD of 1.2 ± 0.4 years after study baseline. A 1.5T Signa Excite system (General Electric, Milwaukee, WI) equipped with an 8-channel phased-array head coil and single-shot echo planar imaging (EPI) software were used. The imaging protocol included high-resolution T1-weighted 3-dimensional (3D) anatomical images, diffusion tensor imaging (DTI), and a 6-minute functional MRI sequence acquired in the resting state with eyes closed. Acquisition parameters for the 3 sequences are fully described in a previous report.[13]

Image Preprocessing

ANATOMICAL 3D. After visual inspection by a trained operator, images from 9 children were discarded as a result of poor image quality, and thus the final sample for the anatomical analysis included 251 children. Statistical parametric mapping (SPM) voxel-based morphometry algorithms with DARTEL registration were used to measure gray and white matter tissue concentration and volume at a voxel level. The preprocessing steps are detailed elsewhere.[13] Such a preprocessing approach implied the generation of a study-specific template. Normalized images were transformed to the standard SPM template, resliced to 1.5mm resolution in Montreal Neurological Institute (MNI) space.

DTI. The Functional MRI of the Brain (FMRIB) Software Library 5.0 (FSL), developed by the Analysis Group at the Oxford Centre for FMRIB,[19] was used to process DTI images. Image quality control was rigorous in this study. A total of 86 children were removed from the DTI analysis on the basis of suboptimal image quality (see Pujol et al[13]). The final DTI sample involved 174 children with a mean ± SD of 23.5 (94%) ± 1.9 optimal-quality volumes. Fractional anisotropy (FA) maps were estimated using FMRIB's Diffusion Toolbox in FSL after local fitting of the diffusion tensor model at each voxel ("dtifit"). Tract-Based Spatial Statistics[20] was used to process diffusion data. FA data sets were resliced to a 1mm × 1mm × 1 mm anatomical resolution and normalized to standard MNI space via the FMRIB58_FA template and the Nonlinear Registration Tool.

FUNCTIONAL MRI. Preprocessing was carried out using SPM8 and involved motion correction, spatial normalization, and smoothing using a Gaussian filter (full-width half-maximum = 8mm). Data were normalized to the standard SPM-EPI template and resliced to 2mm isotropic resolution in MNI space.

The comprehensive procedures adopted to control for potential head motion effects are fully described in our previous report.[13] In short, the procedures included: (1) conventional SPM time-series alignment; (2) exclusion of 24 children with outlier head motion (mean interframe motion > 0.12mm; the finally analyzed sample therefore included 236 children); (3) use of both motion-related regressors and estimates of global brain signal fluctuations as confounding variables in first-level analyses; (4) within-subject, censoring-based MRI signal artifact removal (scrubbing)[21,22]; and (5) use of the mean interframe motion across the functional MRI run for each participant as a regressor in the second-level analyses.[22]

Based on the results obtained from the anatomical and DTI assessments, our functional connectivity analysis was focused on the left basal ganglia. To systematically explore basal ganglia, we targeted 4 key subregions: the dorsal and ventral aspects of both caudate nucleus and putamen. Based on a widely applied method for mapping basal ganglia functional connectivity, the regions of interest (or "seeds") were centered at MNI coordinates (in millimeters): (1) dorsal caudate nucleus (x = −13, y = 15, z = 9); (2) dorsal putamen (x = −28, y = 1, z = 3); (3) ventral caudate nucleus, corresponding approximately to the nucleus accumbens (x = −9, y = 9, z = −8); and (4) ventral putamen (x = −20, y = 12, z = −3).[22–25]

The procedures adopted to generate functional connectivity maps from the selected regions are detailed in our previous report.[13]

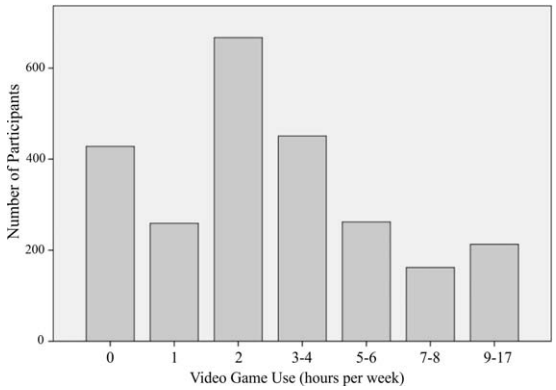

FIGURE 1: Participant distribution according to playing time.

Statistical Analysis

BEHAVIORAL DATA. Student *t* test was used to compare sex and age group means as to hours of play per week. Analysis of variance (ANOVA) adjusted by age and sex (ANCOVA) was used to compare gamers and nongamers as to the behavioral variables. Assumptions under the ANCOVA were met in these analyses including homogeneity of variance, homogeneity of regression slopes of covariates, and noncollinearity. Linear regression adjusted by age and sex was used to assess the relationship between video game playing time and behavioral variables within the user group. Bonferroni correction was applied to account for multiple testing within each analysis. Only probability values < 0.006 (0.05/8) were considered significant. Finally, to easily illustrate the identified associations of gaming with behavior variables, the data were plotted as discrete groups on the basis of playing time in hours (Figs 1 and 2).

IMAGING ANALYSES. ANOVA with age and sex as covariates (ANCOVA) and cross-correlations were estimated using SPM. Separate second-level (group) analyses were carried out for whole-brain estimates of regional white matter and gray matter volume, DTI fractional anisotropy, and resting-state functional connectivity. The behavioral results obtained in the large sample helped to guide the subsequent imaging analysis. Specifically, 3 groups of children were defined on the basis of video game use: 45 nongamers, 113 low-use gamers (playing 1–2 hours per week), and 102 high-use gamers (playing 3 or more hours per week). The cutoff between low and high use corresponds to the median of time of play per week in all gamers. In each case, ANCOVA allowed us to first identify brain areas showing overall differences among these groups. From each analysis, a plot was then generated using brain measurements extracted at representative peak differences to characterize the direction of findings with no bias. That is, the 3-group model allowed us to fairly capture any change combination among the 3 groups (nonplaying, low use, and high use) in a single model sensitive to both the effect of playing versus nonplaying and the effect of low versus high use. Finally, post hoc whole-brain *t* tests were used to compare nongamers with high-use gamers. In addition, we mapped voxelwise the correlation across subjects between individual brain images and the child's age at the time of MRI acquisition.

Results were considered significant with clusters of 1.032ml (eg, 129 voxels with a resolution of $2 \times 2 \times 2$mm) at a height threshold of $p < 0.005$, which satisfied the family-wise error (FWE) rate correction of $p_{FWE} < 0.05$ according to Monte Carlo simulations.[26]

Results

Behavioral Results

The overall study sample comprised 428 nongamers and 2,014 gamers (ie, playing 1 hour or more per week). As a group, gamers played a mean of 4.0 ± 2.9 hours per week (see Fig 1 for participant distribution according to playing time). Boys overall played video games 1.7 hours per week more than girls (95% confidence interval [CI] = 1.4–1.9 hours). There was also a significant effect of age, with older children (above sample median age) playing 0.4 hours per week more than younger children (95% CI = 0.2–0.7 hours). Although the correlation between age and gaming hours was significant in the whole group ($p = 0.0004$), collinearity between both variables was very low ($r = 0.07$, tolerance = 0.995).

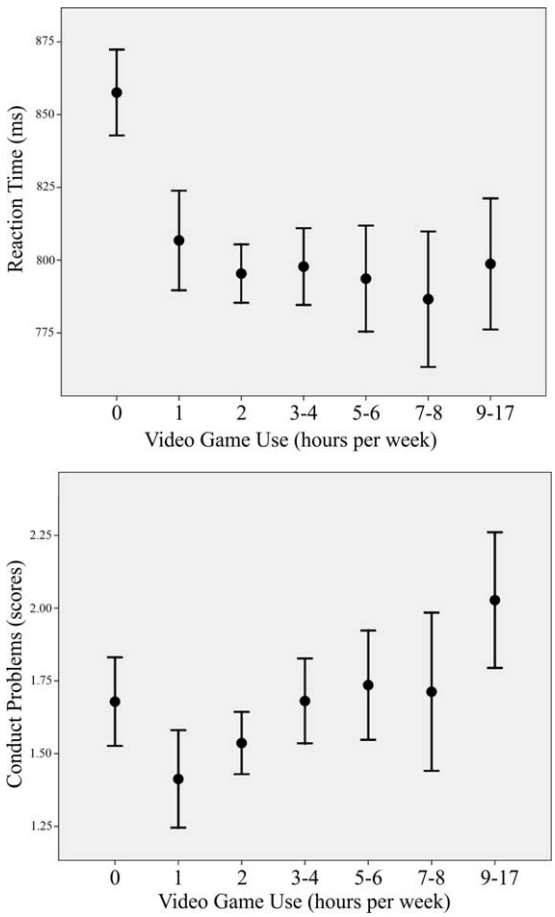

FIGURE 2: Mean reaction time (top) and conduct scores (bottom) plotted for discrete playing time groups. Both plots are adjusted by age and sex and display 95% confidence interval estimates.

No significant differences were found between gamers and nongamers as to parents' education. For example, 59.1% of mothers of gamers had university-level education versus 61.0% in nongamers (chi-square = 0.5, p = 0.511). All further statistical analyses were adjusted for sex and age (ie, age and sex were included as covariates in both group comparisons and correlations).

Video gamers showed faster motor response to visual stimulation (ie, shorter reaction time) than nongamers, with a mean group difference of 65 milliseconds (Table 2). Such a difference was statistically robust (t = 8.1, p = $6e^{-16}$) and was also significant in the smaller subsample of children who underwent MRI (t = 4.5, p = 0.0001). Video game use was also associated with higher consistency of motor responses, measured as reaction time SD (see Table 2). However, there were no effects on specific attentional features or working memory. Remarkably, most of the advantage in motor responsiveness was observed in children playing 1 hour per week (mean difference of 52 milliseconds with respect to nongamers), with minimal further change observed after 2 hours per week (illustrated in Fig 2).

By contrast, in the gaming group, the weekly time spent gaming was steadily associated with higher scores in parental ratings of strengths and difficulties (SDQ), particularly in regard to conduct problems (see Fig 2), peer conflicts, and reduced prosocial abilities (see Table 2). In our post hoc analyses, children gaming in the range of 9 to 17 hours per week showed significantly more behavioral problems than nongamers (eg, conduct problems; t = 3.3, p = 0.001). In addition, the amount of time that was spent gaming was negatively associated with sleeping time. However, as a group, gamers and nongamers did not differ as to strengths and difficulties ratings. Interestingly, gamers showed significantly higher school achievement scores (see Table 2).

A further analysis stratified by sex and age showed that the identified associations were notably consistent across the subgroups. In both boys and girls, most of the attained group difference in motor responsiveness was observed playing 1 hour per week, as in the older children subgroup. It is relevant, however, that further improvement was observed up to 3 to 4 hours of play in the younger children. In each stratified group, differences between gamers and nongamers were highly significant (boys, p = $2e^{-10}$; girls, p = $5e^{-8}$; younger, p = $3e^{-10}$; older, p = $9e^{-9}$). However, such differences between gamers and nongamers were significantly stronger in girls compared to boys (interaction t = 2.6, p = 0.008). No significant interaction was identified for age. Similarly, gamers showed a significant linear correlation between playing hours and conduct problems in each subgroup analysis (boys, p = 0.001; girls, p = $1e^{-5}$; younger, p = $8e^{-6}$; older, p = 0.002). No significant interaction was found in the correlation analysis. Also, we found no significant differences between gamers and nongamers in any subgroup (boys, girls, younger, and older children) as to conduct problems. All associations remained highly significant when analyses were further adjusted for other potential confounding variables, including parental education and neighborhood vulnerability index as the most representative indicators of children's close environment.

Imaging Results

Age and sex were included as covariates in all imaging analyses.

T1-WEIGHTED 3D ANATOMICAL IMAGES. When examining differences among nongamers and low- and high-use gamers in white matter volume measurements (ANCOVA), significant results were observed in a region adjacent to the ventral and lateral aspect of the striatum and extending to the temporal lobe (Fig 3 and Supplementary Table). A plot of white matter volume measurements from the left ventral striatal region revealed a similar increase of white matter volume in both low- and high-user groups compared with nonusers. Figure 3 illustrates this effect in post hoc comparison between nonusers and high users. In addition, the primary ANCOVA identified significant effects in the brainstem (see Supplementary Table), which were not observed in the post hoc analysis. No significant results were obtained for gray matter volumes.

DTI FA. ANCOVA consistently showed significant differences among groups in a region adjacent to the lateral aspect of the striatum (see Fig 3, Supplementary Table). The plot of FA measurements from this left striatal region revealed a relevant FA increase, but only in the high-use group (see Fig 3). Direct comparison of nongamers with high-use gamers confirmed the increase of FA in this region and detected additional significant changes in the ventral striatal region bilaterally, as well as the right thalamus and left occipital white matter.

BASAL GANGLIA FUNCTIONAL CONNECTIVITY. Video gaming was associated with higher functional connectivity in the putamen and caudate nucleus maps (Fig 4 and Supplementary Table). Specifically in the putamen maps, a significant connectivity increase was identified with the left motor cortex and prefrontal cortex in both low- and high-use groups. In the ventral caudate map, the most relevant finding involved the dorsal anterior cingulate cortex (ACC), which demonstrated a strong effect in the high-use group and an intermediate effect in the low-use group compared with nongamers. The post

TABLE 2. Behavioral Results

Measure	Group Comparison					Correlation with Weekly Play Time, Users, n = 2,014		
	Nonusers, n = 428, Adj. Mean (95% CI)	Users, n = 2,014, Adj. Mean (95% CI)	Difference (95% CI)	*t*	*p*	*β*	*t*	*p*
Cognitive tests								
Reaction time, ms	861 (847 to 875)	796 (790 to 802)	65 (49 to 81)	8.1[a]	$6e^{-16}$[a]	−0.559	−0.5	0.619
Reaction time SD, ms	286 (278 to 294)	267 (264 to 271)	19 (10 to 28)	4.0[a]	0.00005[a]	−0.201	−0.3	0.761
Alerting, ms	43 (35 to 50)	49 (46 to 53)	−6 (−15 to 2)	−1.5	0.128	1.161	2.0	0.045
Orienting, ms	32 (25 to 40)	35 (31 to 38)	−3 (−11 to 6)	−0.6	0.575	−1.102	−2.0	0.057
Interference, ms	66 (60 to 72)	63 (60 to 66)	3 (−3 to 10)	1.0	0.340	1.082	2.3	0.021
2B working memory, d′	2.2 (2.1 to 2.3)	2.3 (2.2 to 2.3)	−0.08 (−0.2 to 0.05)	−1.2	0.229	−0.015	−1.6	0.118
3B working memory, d′	1.1 (1.0 to 1.2)[b]	1.2 (1.2 to 1.3)[c]	−0.07 (−0.2 to 0.04)	−1.3	0.210	−0.012	−1.5	0.124
Behavior								
School achievement	3.41 (3.31 to 3.51)	3.60 (3.55 to 3.64)	−0.19 (−0.26 to −0.03)	−3.2[a]	0.001[a]	−0.002	−0.3	0.780
Sleeping time, h	9.63 (9.56 to 9.7)	9.56 (9.53 to 9.59)	0.07 (−0.007 to 0.1)	1.8	0.076	−0.029	−5.3[a]	$1e^{-7}$[a]
Total SDQ score	8.6 (8.1 to 9.1)	8.3 (8.1 to 8.6)	0.27 (−0.30 to 0.84)	0.9	0.353	0.188	4.6[a]	$5e^{-6}$[a]
Conduct problems	1.7 (1.5 to 1.8)	1.6 (1.6 to 1.7)	0.04 (−0.13 to 0.21)	0.4	0.661	0.065	5.4[a]	$8e^{-8}$
Problems with peer	1.2 (1.0 to 1.3)	1.1 (1.1 to 1.2)	0.07 (−0.09 to 0.23)	0.8	0.420	0.061	5.2[a]	$2e^{-7}$[a]
Emotional symptoms	1.9 (1.7 to 2.1)	1.9 (1.9 to 2.0)	−0.03 (−0.22 to 0.17)	−0.3	0.787	0.030	2.1	0.033
Inattention/ hyperactivity	3.8 (3.6 to 4.1)	3.7 (3.6 to 3.8)	0.19 (−0.08 to 0.46)	1.4	0.169	0.033	1.7	0.094
Prosocial behavior	8.5 (8.3 to 8.7)	8.5 (8.4 to 8.6)	<−0.006 (−0.18 to 0.16)	−0.1	0.941	−0.039	−3.2[a]	0.002[a]

All the analyses were adjusted by sex and age. 2B and 3B indicate 2-back and 3-back, respectively.
[a]Significant after Bonferroni correction.
[b]n = 408.
[c]n = 1967.
Adj. = adjusted; CI = confidence interval; d′ = detectability; SD = standard deviation; SDQ = Strengths and Difficulties Questionnaire.

hoc analysis confirmed a robust connectivity increase with the ACC and additionally with the left and right anterior insula region (see Fig 4 and Supplementary Table).

CORRELATION ANALYSIS WITH AGE. White matter volume increased with age in the visual system and sensory–motor projection tracts at the level of basal ganglia and thalamus, with no areas showing negative correlations with age (Fig 5). FA increased significantly with age mostly in the internal capsule and basal ganglia. Therefore, the identified associations of video gaming with white matter measurements were generally consistent with the effects of age in

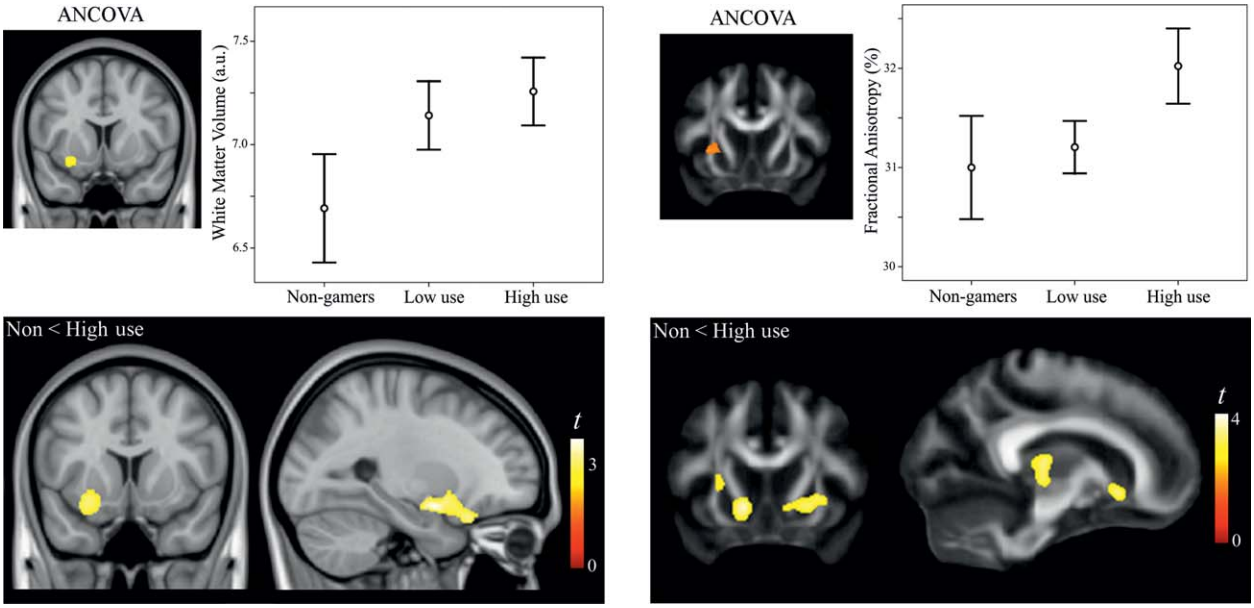

FIGURE 3: Gaming group differences in white matter volume measurements (top left) and diffusion tensor imaging fractional anisotropy (top right). Analysis of variance adjusted by age and sex (ANCOVA) indicated significant changes adjacent to the striatum in both analyses. Mean and 95% confidence intervals are plotted for each modality, reflecting regional peak differences among gaming groups. The bottom left and right images illustrate corresponding differences identified between nongamers versus high-use gamers. The left hemisphere corresponds to the left side of coronal views.

terms of their positive direction and (partial) anatomical overlap. Similarly, age was associated with higher functional connectivity between the putamen and motor cortex in the area associated with video game use, albeit significant only for right hemispheric effects. For the ventral caudate, age was instead negatively associated with its functional connectivity with a medial frontal area adjacent to the ACC region that was positively associated with gaming use (and additionally with the upper brainstem and amygdala).

Discussion

In the cognitive domain, video game use was associated with faster motor response to visual stimulation. Importantly, no further change in motor speed was identified in children playing >2 hours per week, suggesting an early ceiling effect for this measurement. Video gamers, overall, did not demonstrate more problematic behavior that nongamers, although, within the gaming group, we observed a positive association between time weekly spent gaming and conduct problems, peer conflicts, and reduced prosocial abilities, as well as a negative association with sleeping time. At a neural level, structural and functional brain changes associated with gaming use were most evident with respect to basal ganglia circuitry.

Our cognitive assessment selectively measured processing speed, attention, and working memory as primary cognitive domains of interest. In the literature, there is some consensus that gaming may improve speed of information processing and motor response[3,27,28]; however, the reported effects on executive function and working memory, as well as general intelligence, have been less consistent.[3] For example, working memory has been shown to improve in some studies, whereas others reported only partial associations or negative results.[29–31] In our study, larger differences in reaction time than in working memory support the contention that several abilities are more trainable than others with commercial video games.[3,7,8]

We observed an association between gaming use and changes in basal ganglia circuits in the form of structural (white matter) and functional connectivity increases. These findings are intuitive in many respects, as it is well known that basal ganglia circuits are critical for procedural learning based on the acquisition of new skills through practice.[7–9] Our results are also generally consistent with other imaging studies reporting significant effects of gaming use on the frontobasal ganglia system structure and function.[32–37] Specifically, Erickson et al[37] showed that the acquisition of skills on demanding video games may be predicted by variations in the volume of the striatum. Children traditionally acquire procedural skills through action, for instance in relation to sports and outdoor games. Neuroimaging research now suggests that training with desktop virtual environments is also capable of modulating brain systems that support procedural learning. However, the type of video game is likely to be particularly relevant with regard to the modulation of specific neural systems. For example, the use of logic

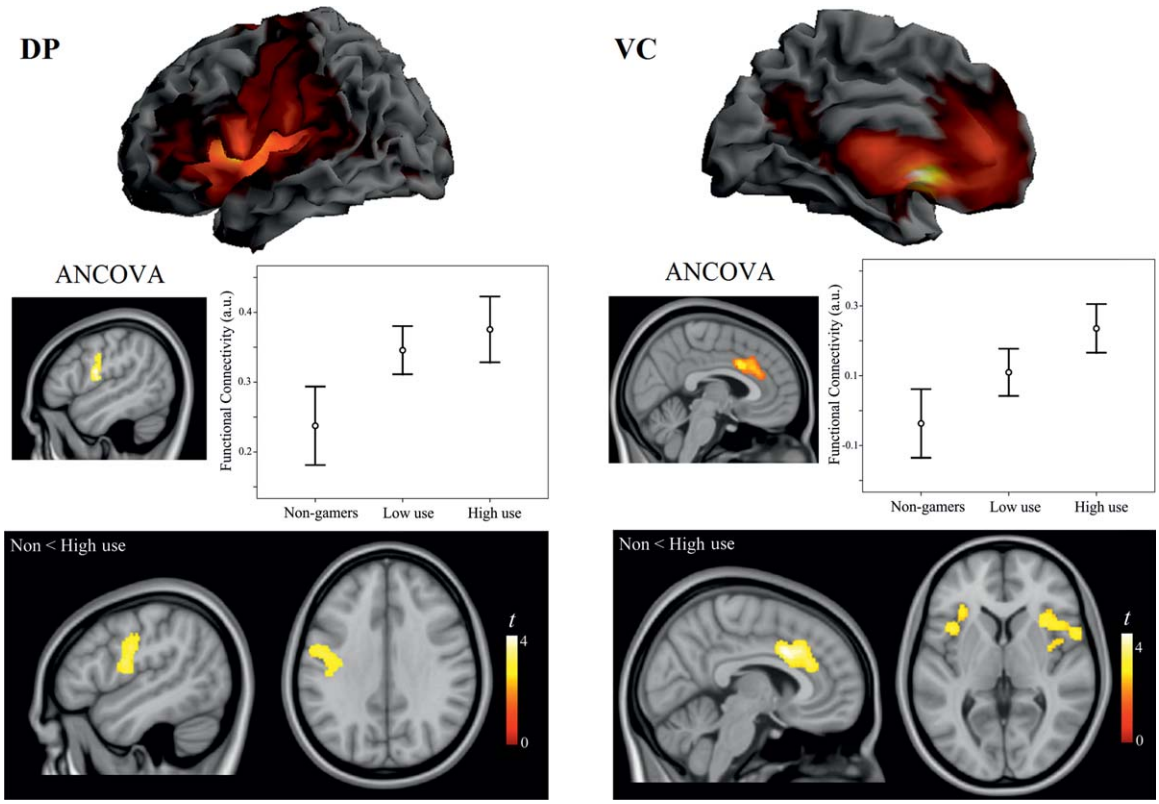

FIGURE 4: Gaming group differences in basal ganglia functional connectivity. Analysis of covariance (ANCOVA) indicated significant changes in functional connectivity between the dorsal putamen (DP) and motor cortex at the level of the frontal operculum. In the ventral caudate (VC) analysis, the most relevant finding involved the anterior cingulate cortex. Mean and 95% confidence intervals are plotted, reflecting regional peak differences among gaming groups. The bottom left and right images illustrate corresponding differences identified between nongamers versus high-use gamers. The left hemisphere corresponds to the left side of axial views.

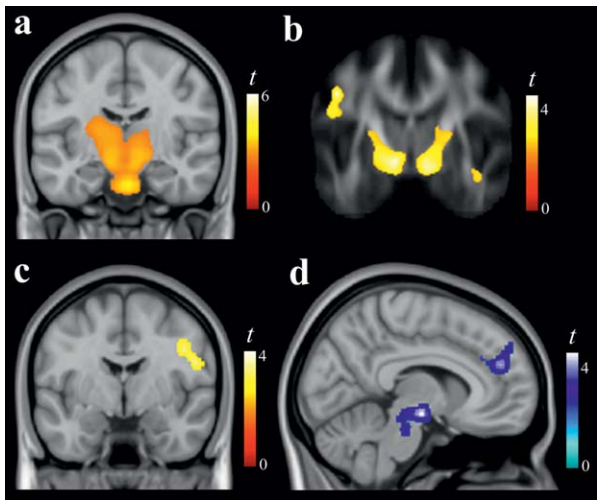

FIGURE 5: Correlations between age and brain measurements. White matter volume (A) increased significantly with age in projection tracts (and the visual system). Fractional anisotropy (B) increased with age mostly in the internal capsule and basal ganglia. Age was also associated with stronger functional connectivity between the putamen and motor cortex (C) and weaker functional connectivity between the caudate nucleus and the medial frontal cortex (D) and additionally with the upper brainstem (and amygdala).

and "platform jumping" games has been associated with anatomical changes implicating the hippocampal system in adults.[38,39]

Reviews of the literature generally conclude that excessive video game use has negative effects on some aspects of behavior in children.[1,3,5,40] Most of the identified problems relate to the extent to which gaming can become a behavioral addiction, or to the violent content of some of the games themselves. We did not include children with probable gaming addiction, and the amount of time spent on playing in our population (mean = 4 hours per week, = range 0–17 hours) was far less than the gaming level that has been associated with severe psychosocial health disturbances. Despite this, gaming use in our study was positively related to the presence of conduct problems, peer conflicts, and reduced prosocial abilities. This finding is in agreement with the results of a national survey of 10- to 15-year-old children in the United Kingdom, in which gaming use of >3 hours per day was associated with similar behavioral problems.[41] Thus, frequent video game use does appear to be associated with behavioral problems in

children even in the absence of a recognized gaming disorder, although the direction of the relationship is less clear.[6] That is, children with peer conflicts and reduced prosocial abilities may show a tendency to isolate and spend more time playing video games. Conversely, highly frequent use likely consumes a proportion of the child's leisure time and invades other activities that may ultimately affect the normal development of prosocial abilities.

Our study was limited in that we applied a selective cognitive and behavioral assessment that did not comprehensively cover all domains. Also, we estimated the time spent gaming from parental reports but with no formal assessment of the fidelity of these reports in terms of their reliability and accuracy. It is also relevant to mention that the estimation of video game use was based on a single cross-sectional measurement. Finally, the type of video games played varied, and we were unable to perform specific analyses stratified by game content or type.

In conclusion, we have investigated relationships between weekly video game use, selected cognitive abilities, conduct-related problems, and brain correlates in a large group of children. Relatively small amounts of video gaming were associated with better performance in certain visuomotor skills and, by contrast, a frequent use was associated with the presence of conduct problems. Whereas motor response differences between gamers and nongamers were already established with 2 hours per week of video gaming, conduct problems appear to be more common in school children playing 9 hours weekly or more. It is important to emphasize that this is a correlational study and, as such, does not permit direct inferences regarding causal relationships. Further studies will be needed to explore the extent to which better visuomotor skills and conduct problems are a cause or consequence of gaming.

Acknowledgment

This work was supported by the European Research Council (grant number 268479; the BREATHE project). The Agency of University and Research Funding Management of the Catalonia Government participated in the context of Research Group SGR2014-1673.

We thank C. Persavento, J. González, L. Bouso, M. López, and P. Figueras for their contribution to the field work; and the families and schools participating in the study.

Author Contributions

J.P., J.S., L.B.-H., and J.D. contributed to the study concept and design; J.P., M.A.-P., J.F., S.G.-O., R.F., D.M., and G.M.-V. contributed to data acquisition and analysis; J.P. and B.J.H. contributed to drafting the manuscript and figures.

Potential Conflicts of Interest

Nothing to report.

References

1. Bavelier D, Green CS, Han DH, et al. Brains on video games. Nat Rev Neurosci 2011;12:763–768.
2. Ferguson CJ. Do angry birds make for angry children? a meta-analysis of video game influences on children's and adolescents' aggression, mental health, prosocial behavior, and academic performance. Perspect Psychol Sci 2015;10:646–666.
3. Powers KL, Brooks PJ, Aldrich NJ, et al. Effects of video-game play on information processing: a meta-analytic investigation. Psychon Bull Rev 2013;20:1055–1079.
4. Bavelier D, Green CS, Pouget A, Schrater P. Brain plasticity through the life span: learning to learn and action video games. Annu Rev Neurosci 2012;35:391–416.
5. Anderson CA, Shibuya A, Ihori N, et al. Violent video game effects on aggression, empathy, and prosocial behavior in Eastern and Western countries: a meta-analytic review. Psychol Bull 2010; 136:151–173.
6. Gentile DA, Choo H, Liau A, et al. Pathological video game use among youths: a two-year longitudinal study. Pediatrics 2011;127: e319–e329.
7. Melby-Lervåg M, Hulme C. Is working memory training effective? A meta-analytic review. Dev Psychol 2013;49:270–291.
8. Shipstead Z1, Redick TS, Engle RW. Is working memory training effective? Psychol Bull 2012;138:628–654.
9. Doyon J, Penhune V, Ungerleider LG. Distinct contribution of the cortico-striatal and cortico-cerebellar systems to motor skill learning. Neuropsychologia 2003;41:252–262.
10. Graybiel AM. Habits, rituals, and the evaluative brain. Annu Rev Neurosci 2008;31:359–387.
11. Yin HH, Knowlton BJ. The role of the basal ganglia in habit formation. Nat Rev Neurosci 2006;7:464–476.
12. Sunyer J, Esnaola M, Alvarez-Pedrerol M, et al. Traffic-related air pollution in schools impairs cognitive development in primary school children. PLoS Med 2015;2:e1001792.
13. Pujol J, Martínez-Vilavella G, Macià D, et al. Traffic pollution exposure is associated with altered brain connectivity in school children. Neuroimage 2016;129:175–184.
14. Rueda MR, Fan J, McCandliss BD, et al. Development of attentional networks in childhood. Neuropsychologia 2004;42:1029–1040.
15. Langner R, Eickhoff SB. Sustaining attention to simple tasks: a meta-analytic review of the neural mechanisms of vigilant attention. Psychol Bull 2013;139:870–900.
16. Anderson P. Assessment and development of executive function (EF) during childhood. Child Neuropsychol 2002;8:71–82.
17. Forns J, Esnaola M, López-Vicente M, et al. The n-back test and the attentional network task as measures of child neuropsychological development in epidemiological studies. Neuropsychology 2014;28:519–529.
18. Goodman R. Psychometric properties of the strengths and difficulties questionnaire. J Am Acad Child Adolesc Psychiatry 2001;40: 1337–1345.

19. Smith SM, Jenkinson M, Woolrich MW, et al. Advances in functional and structural MR image analysis and implementation as FSL. Neuroimage 2004;23(suppl 1):S208–S219.
20. Smith SM, Jenkinson M, Johansen-Berg H, et al. Tract-based spatial statistics: voxelwise analysis of multi-subject diffusion data. Neuroimage 2006;31:1487–1505.
21. Power JD, Mitra A, Laumann TO, et al. Methods to detect, characterize, and remove motion artifact in resting state fMRI. Neuroimage 2014;84:320–341.
22. Pujol J, Macià D, Blanco-Hinojo L, et al. Does motion-related brain functional connectivity reflect both artifacts and genuine neural activity? Neuroimage 2014;101:87–95.
23. Di Martino A, Fair DA, Kelly C, et al. Unraveling the miswired connectome: a developmental perspective. Neuron 2014;83:1335–1353.
24. Harrison BJ, Soriano-Mas C, Pujol J, et al. Altered corticostriatal functional connectivity in obsessive-compulsive disorder. Arch Gen Psychiatry 2009;66:1189–1200.
25. Harrison BJ, Pujol J, Cardoner N, et al. Brain corticostriatal systems and the major clinical symptom dimensions of obsessive-compulsive disorder. Biol Psychiatry 2013;73:321–328.
26. Pujol J, Macià D, Garcia-Fontanals A, et al. The contribution of sensory system functional connectivity reduction to clinical pain in fibromyalgia. Pain 2014;155:1492–1503.
27. Latham AJ, Patston LL, Tippett LJ. The virtual brain: 30 years of video-game play and cognitive abilities. Front Psychol 2013;4:629.
28. Dye MW, Green CS, Bavelier D. Increasing speed of processing with action video games. Curr Dir Psychol Sci 2009;18:321–326.
29. Oei AC, Patterson MD. Enhancing cognition with video games: a multiple game training study. PLoS One 2013;8:e58546.
30. Blacker KJ, Curby KM, Klobusicky E, Chein JM. Effects of action video game training on visual working memory. J Exp Psychol Hum Percept Perform 2014;40:1992–2004.
31. Boot WR, Kramer AF, Simons DJ, et al. The effects of video game playing on attention, memory, and executive control. Acta Psychol (Amst) 2008;129:387–398.
32. Kim YH, Kang DW, Kim D, et al. Real-time strategy video game experience and visual perceptual learning. J Neurosci 2015;35:10485–10492.
33. Lorenz RC, Gleich T, Gallinat J, Kühn S. Video game training and the reward system. Front Hum Neurosci 2015;9:40.
34. Kühn S, Romanowski A, Schilling C, et al. The neural basis of video gaming. Transl Psychiatry 2011;1:e53.
35. Kühn S, Lorenz R, Banaschewski T, et al. Positive association of video game playing with left frontal cortical thickness in adolescents. PLoS One 2014;9:e91506.
36. Hyun GJ, Shin YW, Kim BN, et al. Increased cortical thickness in professional on-line gamers. Psychiatry Investig 2013;10:388–392.
37. Erickson KI, Boot WR, Basak C, et al. Striatal volume predicts level of video game skill acquisition. Cereb Cortex 2010;20:2522–2530.
38. Kühn S, Gleich T, Lorenz RC, et al. Playing Super Mario induces structural brain plasticity: gray matter changes resulting from training with a commercial video game. Mol Psychiatry 2014;19:265–271.
39. Kühn S, Gallinat J. Amount of lifetime video gaming is positively associated with entorhinal, hippocampal and occipital volume. Mol Psychiatry 2014;19:842–847.
40. Straker L, Abbott R, Collins R, Campbell A. Evidence-based guidelines for wise use of electronic games by children. Ergonomics 2014;57:471–489.
41. Przybylski AK. Electronic gaming and psychosocial adjustment. Pediatrics 2014;134:e716–e722.

Journal of Alzheimer's Disease 57 (2017) 61–70
DOI 10.3233/JAD-161112
IOS Press

Anomalous White Matter Structure and the Effect of Age in Down Syndrome Patients

Raquel Fenoll[a], Jesus Pujol[a,b,*], Susanna Esteba-Castillo[c], Susana de Sola[d,e], Núria Ribas-Vidal[c], Javier García-Alba[f], Gonzalo Sánchez-Benavides[d], Gerard Martínez-Vilavella[a], Joan Deus[a,g], Mara Dierssen[e,h,1], Ramón Novell-Alsina[c,1] and Rafael de la Torre[d,i,j,1]

[a]*MRI Research Unit, Department of Radiology, Hospital del Mar, Barcelona, Spain*
[b]*Centro Investigación Biomédica en Red de Salud Mental, CIBERSAM G21, Barcelona, Spain*
[c]*Specialized Department in Mental Health and Intellectual Disability, Institut d'Assistència Sanitària (IAS), Girona, Catalonia, Spain*
[d]*Integrative Pharmacology and Neuroscience Systems Research Group, Hospital del Mar Medical Research Institute, Barcelona, Spain*
[e]*Cellular & Systems Neurobiology, Centre for Genomic Regulation (CRG), Barcelona, Spain*
[f]*Department of Adults with Down Syndrome, Hospital Universitario de La Princesa, Madrid, Spain*
[g]*Department of Clinical and Health Psychology, Autonomous University of Barcelona, Spain*
[h]*Centro de Investigación Biomédica en Red de Enfermedades Raras (CIBERER), Madrid, Spain*
[i]*Centro de Investigación Biomédica en Red de Fisiopatología de la Obesidad y Nutrición (CIBEROBN), Madrid, Spain*
[j]*Department de Ciències Experimentals i de la Salut Universitat Pompeu Fabra (CEXS-UPF), Barcelona, Spain*

Handling Associate Editor: Juan Fortea

Accepted 27 December 2016

Abstract.
Background: Neural tissue alterations in Down syndrome are fully expressed at relatively late developmental stages. In addition, there is an early presence of neurodegenerative changes in the late life stages.
Objective: The aims of this study were both to characterize white matter abnormalities in the brain of adult Down syndrome patients using diffusion tensor imaging (DTI) and to investigate whether degenerative alterations in white matter structure are detectable before dementia is clinically evident.
Methods: Forty-five adult non-demented Down syndrome patients showing a wide age range (18–52 years) and a matched 45-subject control group were assessed. DTI fractional anisotropy (FA) brain maps were generated and selected cognitive tests were administered.
Results: Compared with healthy controls, non-demented Down syndrome patients showed lower DTI FA in white matter involving the major pathways, but with more severe alterations in the frontal-subcortical circuits. White matter FA decreased with age at a similar rate in both DS and control groups.
Conclusions: Our results contribute to characterizing the expression of white matter structural alterations in adult Down syndrome. However, an accelerated aging effect was not demonstrated, which may suggest that the FA measurements used are not sufficiently sensitive or, alternatively, age-related white matter neurodegeneration is not obvious prior to overt clinical dementia.

Keywords: Accelerated aging, diffusion tensor imaging, magnetic resonance imaging, neurodegeneration

[1]These authors contributed equally to this work.

*Correspondence to: Dr. Jesus Pujol, MD, MRI Research Unit, Department of Radiology, Hospital del Mar, Barcelona, Spain. Tel.: +34 932212180; Fax: +34 932212181; E-mail: 21404jpn@comb.cat.

INTRODUCTION

Although research in Down syndrome has substantially progressed in the understanding of basic mechanisms via which gene overexpression interferes with brain development, there is less information as to the general organization of the adult brain and the effect of age [1, 2]. The brain contains billion of neurons that communicate with each other via axons to create complex neural networks. The structural mapping of these networks is essential for understanding brain function [3]. However, although new imaging techniques have emerged in recent years, our knowledge of structural connectivity in Down syndrome is still limited.

Diffusion tensor imaging (DTI) is a noninvasive method that provides information about the microstructural properties of brain tissue by measuring the magnitude and direction of water molecule diffusion [4]. In white matter, the diffusion of water molecules is less restricted along the long axis of a group of aligned tissue fibers than perpendicular to it. This condition of directionally-dependent diffusion is referred to as "anisotropic". The most commonly used measure for diffusion anisotropy is fractional anisotropy (FA), which serves to characterize white matter tracts by mapping directional diffusion restrictions related mainly to fiber density, axonal diameter and myelination degree [3, 4].

DTI has been used to characterize both age-related changes and disease [5–8]. Results from leading studies have shown that age-related changes are associated with FA decreases [5]. DTI findings have been validated by postmortem histological studies showing that advanced age is linked to alterations of almost all white matter components. Segments of axons degenerate and swell, myelin becomes less compact and glial cells accumulate cellular debris, form glial scars and increase in number [9–11].

In Down syndrome, a number of magnetic resonance imaging (MRI) studies have identified a variety of anatomical [12–17] and functional [18, 19] alterations. The frontal lobes [16, 20] and related circuits [18, 19], as representative of late maturing structures, generally show the most relevant alteration. By contrast, some studies have reported a relative preservation of tissue volume in temporal and parietal regions [16, 20, 21]. Nevertheless, white matter alterations and their functional significance have not been fully characterized using FA measurements. There is one previous study indicating that white matter in adult Down syndrome is abnormal in terms of FA, particularly when dementia is clinically evident [22]. Nevertheless, the number of Down syndrome patients without dementia was small in this study ($n = 10$) and the study design did not allow a distinction between the effect of aging and pre-existing changes. It is not currently evident whether the neurodegenerative effect on white matter structure is detectable before dementia is expressed. If this were indeed the case, age-related FA changes could serve as early markers of neurodegeneration, which could be of high practical interest given the difficulty in identifying the cognitive deficits related to dementia in a population with significant baseline alteration in cognition [1, 2].

The aims of this study were both to characterize white matter abnormalities in the brain of adult non-demented Down syndrome patients using DTI and to investigate whether degenerative changes in white matter structure are detectable before dementia becomes clinically evident. We predicted that Down syndrome patients would exhibit both widespread FA reduction in white matter and an accelerated aging effect, and that the alteration would be associated with poorer cognitive performance.

METHODS

Participants

Sixty-eight Down syndrome patients were initially recruited in the study. Candidates were recruited from the community via parent organizations and underwent comprehensive medical, psychiatric, neuropsychological, and laboratory evaluation. Individuals with seizure or neurological disease (other than Down syndrome) and non-stable medical conditions were not considered eligible. Participants were selected on the basis of age (18 years old and upwards), Down syndrome confirmed by karyotype, capability to understand MRI instructions, follow commands and keep still, and also optimal attitude and willingness (patients and parents) to participate. Five patients did not complete the image acquisition protocol and a further 18 subjects were ultimately excluded due to head motion during MRI (see below). The final sample, therefore, included 45 relatively high-functioning Down syndrome patients (29 females, 16 males) with genotype-confirmed trisomy 21 and a mean $\pm$ SD age of 35.3 ± 10.8 years, range 18–52 (Table 1). The included and excluded patient subgroups did not significantly differ as to age, performance IQ, semantic fluency, and working

Table 1
Characteristics of study participants

	Down Syndrome	Healthy Controls
Age (mean, SD years)[a]	35.3 (10.8)	34.6 (10.0)
Gender (men/women)	16/29	19/26
Medical Background (%)		
Cardiovascular	28.9%	
Respiratory	24.4%	
Metabolic / Endocrine	46.7%	
Ophthalmological	66.7%	
Otorhinolaryngological	6.7%	
Disability Levels (%)$^{DSM-IV-TR}$		
Mild	57.8%	
Moderate	42.2%	
Severe	0%	
Profound	0%	
Knowledge (%)		
Illiterate	51.1%	
Read/Write	48.9%	
Years of Schooling (mean, SD years)	9.3 (3.9)	
Neuropsychological Assessment:		
Performance IQ, K-BIT (mean, SD)[b]	60.5 (8.0)	
Semantic Fluency (mean, SD)[c]	9.8 (3.4)	
Digit Span Test (mean, SD)[d]		
Forward Span	2.7 (1.2)	
Backward Span	1.2 (1.1)	
Forward Score	3.3 (1.5)	
Backward Score	1.2 (1.2)	
Total Score	4.5 (2.3)	

SD, standard deviation. [a]Between-group differences for age were not significant ($p = 0.76$). [b]K-BIT, Kaufman Brief Intelligent Test (2nd edition); matrices test. [c]Semantic fluency, animals in 1 minute. [d]Digit span, verbal short-term memory test.

memory. Excluded patients, however, were predominantly males (6 females, 17 males).

A control group of 45 healthy volunteers were selected matched for age with the patient sample (34.6 ± 10.0 years, range 19–51) and showing similar sex distribution (Table 1). Participants were either friends or family of subjects participating in the current and other studies, or were recruited from local advertisements. A complete medical interview was carried out to exclude individuals with relevant medical or neurological disorders, cerebrovascular risk factors, substance abuse, psychiatric disease, or undergoing medical treatment. In all included control subjects, the brain showed a normal appearance on high resolution anatomical MRI scans.

This study was conducted according to the principles expressed in the Declaration of Helsinki. Anxiolytics were not administered in this study. The study protocol was approved by the Clinical Research Ethical Committee of the Parc de Salut Mar of Barcelona. Written informed consent was obtained from parents and control subjects. Verbal or written assent was additionally obtained from Down syndrome patients.

Cognitive testing

Selected cognitive assessment in all Down syndrome patients included Performance IQ estimated with the Kaufman Brief Intelligent Test, Second Edition (K-BIT) [23] matrices subtest as a general cognitive assessment, the Wechsler Adult Intelligence Scale (WAIS) backward digit span task as one of conventional measurements of working memory [24], and semantic fluency as a sensitive measurement of verbal output [25].

Additionally, each patient underwent comprehensive neurological and psychiatric history and subsequent tailored neuropsychological testing to clinically rule out the presence of dementia (and mild cognitive impairment, MCI) in terms of cognitive deterioration overlapping with developmental cognitive deficits associated with Down syndrome. Clinical diagnosis (or exclusion) of dementia in Down syndrome by experienced clinicians is recommended as being more accurate and reliable than operative diagnostic tools at a relatively early stage of the disease [26]. Nevertheless, apart from expert clinical diagnosis (by SE and SdS), no patient met International

Classification of Diseases (ICD)-10 [27] or Diagnostic and Statistical Manual of Mental Disorder-IV-Text Revision (DSM-IV-TR) [28] criteria for dementia. A total of 3 patients, however, did meet criteria for mild MCI [29], adapted to adults with intellectual disability [30]. The clinical diagnosis of MCI in these 3 cases was established by an experienced neuropsychologist (SEC) on the basis of (i) a report of cognitive impairment by the patient (confirmed by a reliable informant) or by a reliable informant that implies a change from previous capacities, (ii) abnormal performance in the corresponding neuropsychological testing, and (iii) no clinically relevant decline in overall adaptive skills and insufficient ICD-10 and DSM-IV-TR criteria for dementia.

MRI acquisition

A 1.5 Tesla Signa Excite System (General Electric, Milwaukee, WI, USA) equipped with an eight-channel phased-array head coil and single-shot echoplanar imaging (EPI) software was used. Diffusion-weighted scans were obtained using spin-echo single-shot echo-planar sequences of 25 directions with a B-factor of 1000 s/mm^2. Acquisition parameters were repetition time 8300 ms; echo time 94 ms; thickness 5 mm, no gap; pulse angle 90°; field of view 26 cm; 128 × 128 acquisition matrix reconstructed into a 256 × 256 matrix, and scan duration was 3 m 52 s. Twenty-six slices were prescribed parallel to the anterior-posterior commissure line covering the whole brain. Participants were instructed to relax, stay awake and lie still.

Image preprocessing

DTI was processed using Functional MRI of the Brain (FMRIB) Software Library 5.0 (FSL), developed by the Analysis Group at the Oxford Centre for FMRIB [31]. Diffusion-weighted images were aligned to the B0 image using affine registration and corrected for motion and eddy current distortions ("Eddy Current Correction" option in the FMRIB Diffusion Toolbox [FDT] version 2.0 in FSL). A whole-brain mask, generated with the FSL Brain Extracting Tool, was applied to the DTI images. Subsequently, we estimated FA maps using FDT in FSL by local fitting of the diffusion tensor model at each voxel ("dtifit"). FA maps were then aligned to a common target (FMRIB58_FA template) using Tract-Based Spatial Statistics [32], re-sliced to a 1 mm × 1 mm × 1 mm anatomical resolution and normalized to standard MNI space via the FMRIB58_FA template using the FMRIB's Nonlinear Registration Tool. All the images were visually inspected by a trained researcher before and after the preprocessing steps to avoid the inclusion of poor-quality images. An additional rigorous image quality control was carried out to identify potential effects of head motion on raw images, which involved the visual inspection of each DTI slice for all 25 DTI volumes in all participants. The effect of motion can generally be observed as signal loss in the whole or a part of one slice compared with the other slices. Volumes with slices showing signal loss (greater than ∼10% compared with slices normal in signal and measured using the conventional MRIcron display tool) or residual artifacts were identified by an expert researcher. DTI full examinations showing more than 5 degraded volumes were discarded. A total of 18 participants were removed from the DTI analysis on the basis of this criterion (in addition to 5 cases showing gross image degradation). The final DTI sample involved 45 patients with a mean ± SD of 23.0 (92%) ± 1.6 optimal-quality volumes.

After the full pre-processing, FA maps were transferred to the SPM8 platform and smoothed with an 8 mm Gaussian Kernel to carry out group statistical analyses.

Statistical analysis

Individual FA maps were included in second-level (group) SPM analyses using 2-sample *t*-test between the 45 Down syndrome patients and 45 healthy controls. Voxel-wise analyses in SPM were also performed to map the correlation between age and whole-brain FA measurements in both groups. Finally, voxel-wise analyses were performed to map the correlation between individual ratings in the selected cognitive tests and FA measurements in the Down syndrome group.

Results were considered significant with clusters of 1.032 ml (1,032 voxels) at a height threshold of $p < 0.005$, which satisfied the family-wise error (FWE) rate correction of $P_{FWE} < 0.05$ according to Monte Carlo simulations [33].

RESULTS

Fractional anisotropy differences between Down syndrome and control subjects

Down syndrome patients showed a widespread white matter FA reduction compared with healthy

Table 2
Diffusion tensor imaging fractional anisotropy results

	Cluster size, ml	x y z	t (r)	t** (r)**
Down < Controls				
R semioval center	354.0*	18 –7 53	6.3	5.9
L semioval center	*	–13 2 51	6.1	5.7
R frontal lobe	*	20 45 15	7.9	7.5
L frontal lobe	*	–19 47 13	8.2	7.8
Corpus callosum	*	4 30 –3	4.3	4.0
R putamen	*	24 13 16	7.4	7.0
L putamen	*	–21 11 17	8.0	7.7
R thalamus	*	10 –9 17	7.2	7.0
L thalamus	*	–11 –11 18	8.4	8.3
R pyramidal tract	*	19 –18 –7	7.9	7.4
L pyramidal tract	*	–19 22 –6	9.2	8.7
Brainstem	*	1 –32 –23	8.3	7.8
Down > Controls				
Temporo-parietal junction	6.7	37 –42 12	5.9	5.9
Correlations with FA				
Semantic fluency in DS				
R frontal lobe	148.7*	27 48 4	4.4 (0.6)	4.2 (0.6)
L frontal lobe	*	–14 24 33	4.9 (0.6)	4.6 (0.5)
Corpus callosum	*	13 27 3	3.3 (0.5)	3.3 (0.5)
R semioval center	*	12 2 36	3.5 (0.5)	3.3 (0.5)
L semioval center	*	–11 –2 43	4.5 (0.6)	4.3 (0.6)
L arcuate fasciculus	*	–30 13 14	5.4 (0.6)	5.2 (0.6)
R caudate nucleus	*	13 27 3	3.3 (0.5)	3.3 (0.5)
L caudate nucleus	*	–19 20 18	4.4 (0.6)	4.5 (0.6)
R external capsule	*	35 1 –2	4.4 (0.6)	4.2 (0.6)
L external capsule	*	–30 13 14	5.3 (0.6)	5.2 (0.6)
R thalamus	*	8 –23 8	3.4 (0.5)	3.8 (0.5)
L thalamus	*	–3 –21 10	4.0 (0.5)	4.0 (0.5)
Age in healthy controls				
R frontal lobe	704.1*	24 48 7	4.2 (–0.4)	4.2 (–0.4)
L frontal lobe	*	–15 46 12	4.4 (–0.4)	4.4 (–0.4)
Corpus callosum	*	5 30 4	4.0 (–0.4)	4.0 (–0.4)
Thalamus	*	–1 –20 7	3.8 (–0.4)	3.7 (–0.4)
R pyramidal tract	*	13 –20 –25	4.0 (–0.4)	4.0 (–0.4)
L pyramidal tract	*	–15 –26 –13	3.5 (–0.4)	3.5 (–0,4)
Age in DS patients				
R frontal lobe	4.0	19 42 17	3.8 (–0.4)	3.3 (–0.3)
L arcuate fasciculus	2.4	–31 6 30	3.5 (–0.4)	3.2 (–0.3)
R external capsule	5.5	35 11 –2	3.0 (–0.3)	3.0 (–0.3)
Hypothalamus region	1.9	0 6 –2	3.4 (–0.3)	3.4 (–0.4)

DS, Down syndrome; *Same cluster; **without 3 patients with mild cognitive impairment- MCI. x y z coordinates given in Montreal Neurological Institute (MNI) space. Statistics at corrected threshold $P_{FWE} < 0.05$ according to Monte Carlo simulations.

controls involving parts of the frontal lobes, semioval centers, corpus callosum, external capsule, internal capsule, putamen, thalamus, pyramidal tracts, and brainstem (Table 2). Therefore, the major brain pathways were affected, although the alterations were more severe in the frontal-subcortical circuits (Fig. 1). For example, 21 out of 25 sub-clusters showing the largest between-group differences ($t > 5$) involved the frontal-subcortical circuits and only 4 did not ($\chi^2 = 11.5$, $p < 0.001$). In the opposite contrast, a region of significantly larger FA was found in Down syndrome at the temporo-parietal junction (Fig. 1).

Correlations with cognitive performance in Down syndrome

No significant correlations were found between FA measurements and both performance IQ (K-BIT matrices) and working memory scores (WAIS digit span). By contrast, FA showed significant positive correlation with semantic fluency (i.e., lower FA values, poorer performance) in a variety of regions involving the frontal lobes, corpus callosum, semioval centers, arcuate fasciculus, caudate nucleus, external capsule, thalamus, and hippocampus (Fig. 2 and Table 2).

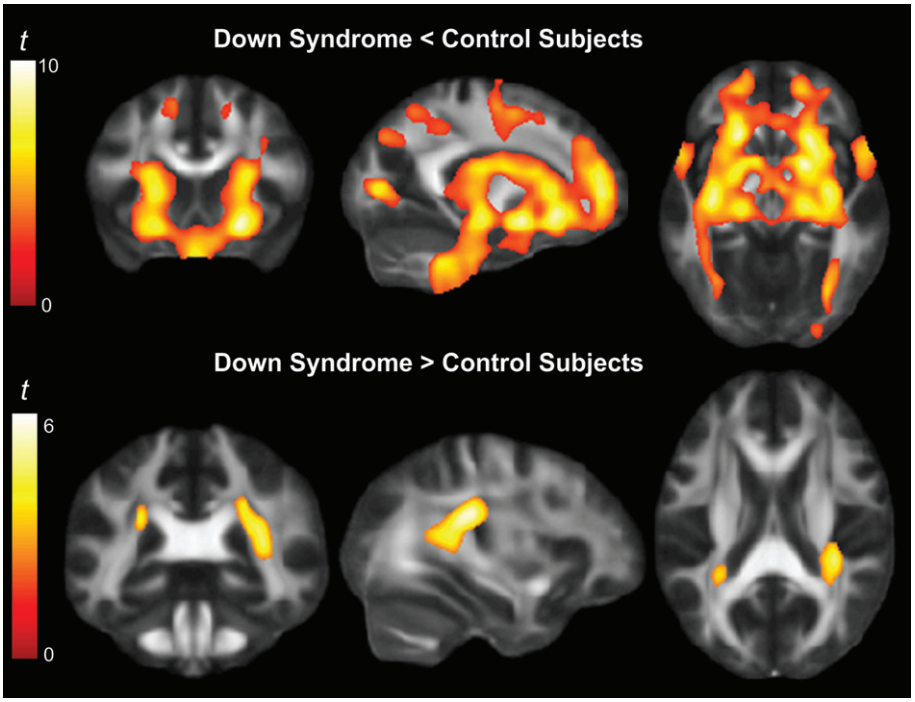

Fig. 1. Fractional anisotropy (FA) differences between Down syndrome and control subjects. Down syndrome patients showed a general pattern of lower FA in white matter, although the changes were more severe in the frontal-subcortical circuits (Top). By contrast, regions with significantly higher FA in Down syndrome patients than controls were limited to the temporo-parietal junction (Bottom). The right hemisphere corresponds to the right side of axial and coronal images.

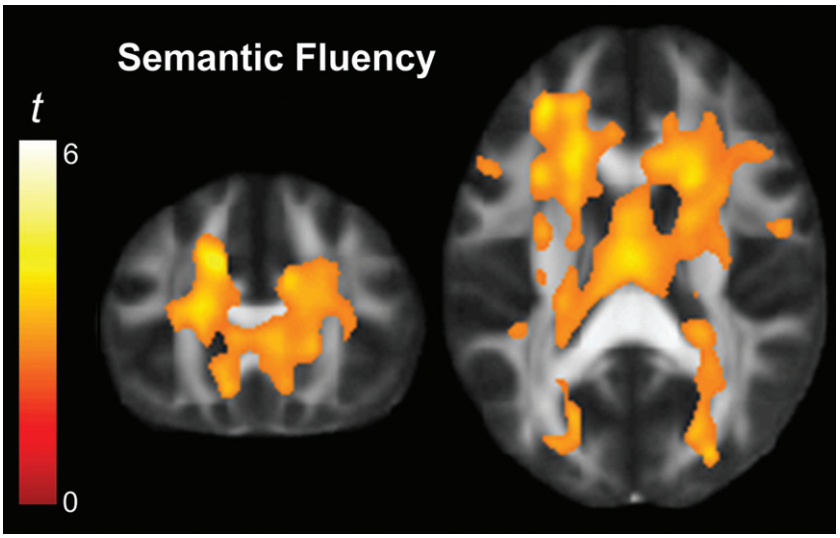

Fig. 2. Significant positive correlation between semantic fluency and fractional anisotropy (FA) measurements in the direction of lower FA values, the poorer performance. The right hemisphere corresponds to the right side of the images.

Age-related effect on fractional anisotropy

In both groups, FA decreased as a function of age. Healthy controls showed FA age-related changes in the frontal lobes, corpus callosum, basal ganglia (caudate), thalamus, semioval centers, and pyramidal tracts (Fig. 3 and Table 2). In Down syndrome, significant correlations with age were found in the frontal lobes, left arcuate fasciculus, right external capsule, and hypothalamus (Fig. 3 and Table 2). We found

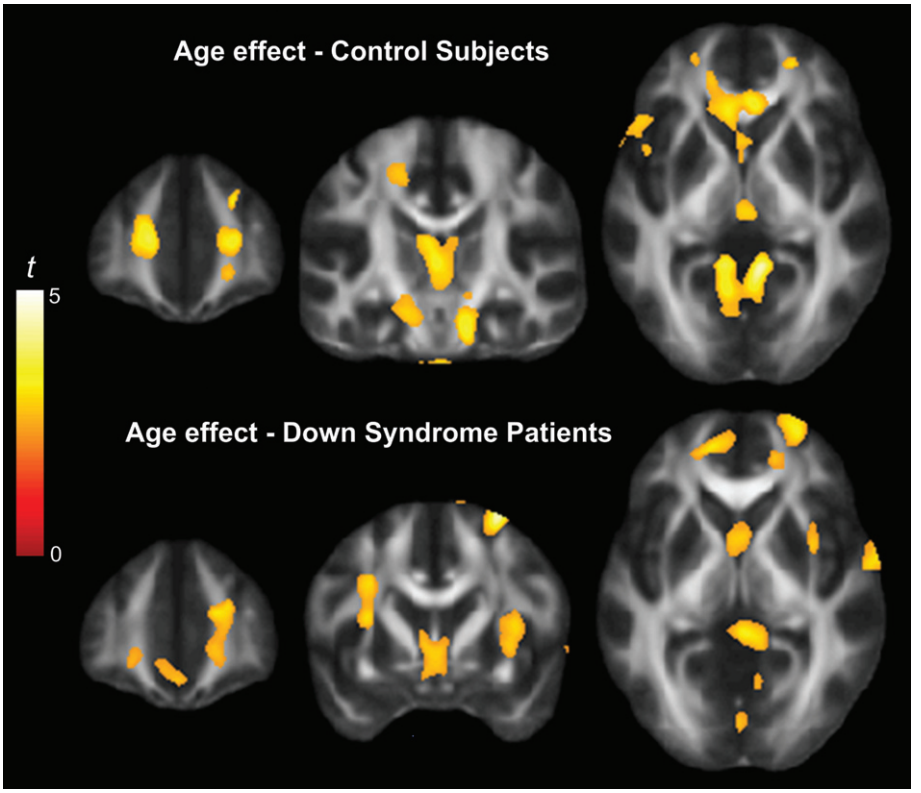

Fig. 3. Age-related effect on fractional anisotropy (FA). FA decreased as a function of age in both control subjects and Down syndrome patients. No significant between-group differences were identified.

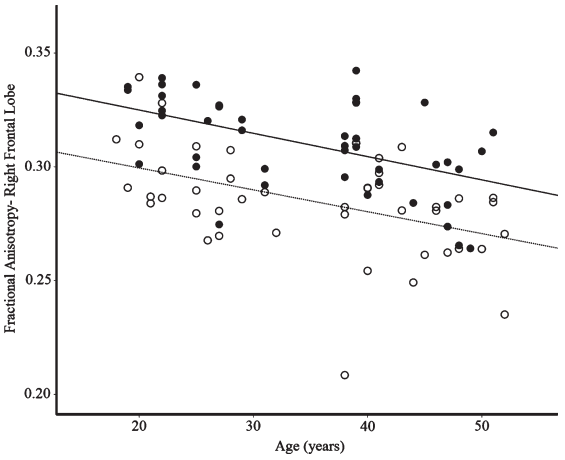

Fig. 4. Correlation between age and fractional anisotropy at the right frontal lobe. Down syndrome patient data are represented by the dashed line and open circles, and control subject data by solid line and solid circles.

no significant between-group differences relating to the strength of the correlations (i.e., no significant correlation interaction), which is illustrated in Fig. 4.

DISCUSSION

Our results indicate that white matter in Down syndrome patients showed generally lower FA compared with healthy participants. The most affected structures were the frontal lobes, subcortical white matter and some parts of the brainstem. Lower FA in Down syndrome was associated with poorer semantic fluency, which illustrates a degree of correspondence between white matter integrity and performance in patients. White matter FA did indeed decrease with age in both study groups, but we did not find the expected accelerated age effect in the Down syndrome group.

FA is a tissue measurement primarily independent of tissue volume that may generally express the extent to which an anatomical structure is composed of white matter tracts showing one dominant direction. In brain regions containing tracts with a single direction, FA increases as a result of brain maturation [4, 34]. In this context, our results indicate that Down syndrome subjects have a less developed white matter structure than controls in many white matter

tracts. This is a remarkable finding due to the few studies based on DTI in non-demented Down syndrome patients. Our results are consistent with studies of brain anatomy showing generally reduced white matter volumes in Down syndrome compared with healthy controls [13, 16]. However, our data may further contribute to characterizing white matter alterations in Down syndrome in that they would indicate that the changes are not limited to general volume reductions, but may also implicate a less developed structural connectivity pattern.

Although FA abnormalities involved the major brain pathways, the frontal-subcortical circuits showed more severe alterations. As a general trend, the results are consistent with the profile of cognitive deficits in Down syndrome typically progressing with deep impairment in language production and executive functions, which are cognitive domains notably dependent on the frontal lobes [35–37].

We also observed that Down syndrome individuals showed higher FA at the temporo-parietal junction. This observation is partly consistent with studies reporting relatively larger white matter volume in temporal and parietal regions [16, 20, 21], which may reflect a particular abnormality in white matter maturation. Indeed, in complex structures with tracts crossing in different directions (as in the temporo-parietal junction), higher FA may paradoxically denote less mature or less structured tissue [4, 34]. The multimodal temporo-parietal junction is certainly a complex area in terms of white matter connectivity. In Down syndrome, the pattern of connectivity would seem to be incomplete at this level. This event appears in parallel with a more general FA reduction in several other brain structures. In this general effect, the alteration may denote poor development of white matter pathways showing a predominant direction or a simpler structure.

A relevant problem in evaluating cognitive abilities in Down syndrome is the notable lack of consistency and reproducibility of ratings in some neuropsychological tests [38]. We used the K-BIT matrices subtest to estimate general intelligence, the digit span to evaluate working memory and semantic verbal fluency to test verbal output. Only verbal fluency was associated with FA alterations in Down syndrome in a rather general manner, thus indicating a certain parallelism between the identified pattern of white matter alterations and cognitive performance. Nevertheless, we failed to find similar associations with performance IQ and working memory. We now, *a posteriori*, consider that these tests are not perhaps the most suitable to reliably predict brain alterations in Down syndrome. The development of more specific and sensitive tools to evaluate cognition in Down syndrome, as recently proposed [39], could be helpful in future studies.

Our study did not find significant between-group differences in age-related white matter changes. That is to say, although both groups suffered a variation of white matter structure with age, there were no between-group differences. In our Down syndrome group, none of the participants were diagnosed with Alzheimer's disease and only 3 patients had MCI according to clinical criteria. Therefore, we were unable to demonstrate the anticipated premature aging effects on white matter using FA measurements, which contrast with positive findings in studies on familial Alzheimer's disease (summarized in a recent report [40]). This brings us to the conclusion that DTI FA measurements are perhaps not sufficiently sensitive to capture brain pathology related to the acceleration of aging in subclinical populations. Alternatively, age-related white matter neurodegeneration may be a later event, which is not obvious prior to overt clinical dementia. In the study by Powell et al. [22], FA alterations were indeed more evident when dementia was clinically evident in Down syndrome patients.

It is important to mention, however, that the identified FA decrease with age in the control group is not the expression of the white matter structure involution or degeneration occurring in the senile brain (also expressed in the form of additional FA decrease [41]), as age in the control group showed a mean of 34.6 years and range 19–51 years. Age-related FA changes may better reflect the normal active evolution of white matter tracts in the adult brain. Our findings are consistent with previous studies in normal populations showing FA peaks from early 20 s to late 30 s and subsequent subtle FA decreases starting around mid-adulthood with notably different timings across different tracts [42]. FA studies in normal populations further emphasize early proposals that white matter remodeling is a biological process active over the entire lifespan [43, 44].

One challenge in the assessment of DTI is the control of head-motion effects on the measurement, which may be relevant in low-performance populations. We have considered this issue carefully and adopted several means to rigorously control such effects. We decided to exclude cases with detectable image degradation, as no correction procedure is

wholly efficient once the images have been acquired. The regular use of MRI practice sessions with mock scanners may minimize the problem in future studies. A *post-hoc* analysis on DTI using less rigorous exclusion criteria ($n = 54$) showed similar but weakened DTI results, indicating that the data obtained in the more selective sample ($n = 45$) was most probably not due to motion effects. Although accurate control of head motion effects may be a strength of the study, it is important to mention that strict participant selection is also a limitation. In this context, our findings cannot generalize to all Down syndrome population, but conclusions should be limited to relatively highly performing individuals. A final limitation relates to using a 1.5-T system, as opposed to a 3-T system with higher MRI signal.

Conclusions

Results from our imaging approach indicate that the brain in relatively high-functioning Down syndrome patients shows generally lower FA, suggesting underdevelopment of white matter tracts. The altered white matter structure was associated with poorer performance at neuropsychological assessment. Finally, age-related reduction of FA did not significantly differ between the control group and our non-demented Down syndrome patients. Probably, the adopted DTI approach was not sufficiently sensitive to detect alterations related to the dementia process in subclinical stages of Alzheimer-like pathology. Further studies should focus on the temporal evolution of white matter structure involution and the development of dementia in Down syndrome adults and provide biomarkers for detecting early signs of premature aging.

ACKNOWLEDGMENTS

This study was supported in part by the Spanish Government (Grants SAF2010-19434, PI11/00744 and PI/120219) and the Jérôme Lejeune Foundation, Paris.

We thank the Fundació Catalana Síndrome de Down (FCSD, Spain) for their assistance with the recruitment of participants and the TESDAT Study Group members for their contribution (Lancet Neurology, May 12, 2016 http://dx.doi.org/10.1016/S1474-4422(16)30034-5). We thank the Agency of University and Research Funding Management of the Catalonia Government for their participation in the context of Research Groups SGR 2009/1450 and SGR 2009/718.

Authors' disclosures available online (http://j-alz.com/manuscript-disclosures/161112r1).

REFERENCES

[1] Wiseman FK, Al-Janabi T, Hardy J, Karmiloff-Smith A, Nizetic D, Tybulewicz VL, Fisher EM, Strydom A (2015) A genetic cause of Alzheimer disease: Mechanistic insights from Down syndrome. *Nat Rev Neurosci* **16**, 564-574.

[2] Ballard C, Mobley W, Hardy J, Williams G, Corbett A (2016) Dementia in Down's syndrome. *Lancet Neurol* **15**, 622-636.

[3] Mori S, Zhang J (2006) Principles of diffusion tensor imaging and its applications to basic neuroscience research. *Neuron* **51**, 527-539.

[4] Jones DK, Knösche TR, Turner R (2013) White matter integrity, fiber count, and other fallacies: The do's and don'ts of diffusion MRI. *Neuroimage* **73**, 239-254.

[5] Madden DJ, Bennett IJ, Song AW (2009) Cerebral white matter integrity and cognitive aging: Contributions from diffusion tensor imaging. *Neuropsychol Rev* **19**, 415-435.

[6] Gens S, Steward CE, Malpas CB, Velakoulis D, O'Brien TJ, Desmond PM (2016) Short-term white matter alterations in Alzheimer's disease characterized by diffusion tensor imaging. *J Magn Reson Imaging* **43**, 627-634.

[7] Langley J, Huddleston DE, Merritt M, Chen X, McMurray R, Silver M, Factor SA, Hu X (2016) Diffusion tensor imaging of the substantia nigra in Parkinson's disease revisited. *Hum Brain Mapp* **37**, 2547-2556.

[8] Adluru N, Destiche DJ, Lu SY, Doran ST, Birdsill AC, Melah KE, Okonkwo OC, Alexander AL, Dowling NM, Johnson SC, Sager MA, Bendlin BB (2014) White matter microstructure in late middle-age: Effects of apoliporotein E4 and parental family history of Alzheimer's disease. *Neuroimage Clin* **2**, 730-742.

[9] Marner L, Nyengaard JR, Tang Y, Pakkenberg B (2003) Marked loss of myelinated nerve fibers in the human brain with age. *J Comp Neurol* **462**, 144-152.

[10] Peters A (2002) The effects of normal aging on myelin and nerve fibers: A review. *J Neurocytol* **31**, 581-593.

[11] Tang Y, Nyengaard JR, Pakkenberg B, Gundersen HJ (1997) Age-induced white matter changes in the human brain: A stereological investigation. *Neurobiol Aging* **18**, 609-615.

[12] Schapiro MB, Luxenberg JS, Kaye JA, Haxby JV, Friendland RP, Rapoport SI (1989) Serial quantitative CT analysis of brain morphometrics in adult Down's syndrome at different ages. *Neurology* **39**, 1349-1353.

[13] Weis S, Weber G, Neuhold A, Rett A (1991) Down syndrome: MR quantification of brain structures and comparison with normal control subjects. *Am J Neuroradiol* **12**, 1207-1211.

[14] Kesslak JP, Nagata SF, Lott I, Nalcioglu O (1994) Magnetic resonance imaging analysis of age-related changes in the brains of individuals with Down's syndrome. *Neurology* **44**, 1039-1045.

[15] Raz N, Torres IJ, Briggs SD, Spencer WM, Thornton AE, Loken WJ, Gunning FM, McQuain JD, Driesen NR, Acker JD (1995) Selective neuroanatomic abnormalities in Down's syndrome and their cognitive correlates: Evidence from MRI morphometry. *Neurology* **45**, 356-366.

[16] White NS, Alkire MT, Haier RJ (2003) A voxel-based morphometric study of non demented adults with Down syndrome. *Neuroimage* **20**, 393-403.

[17] Teipel SJ, Alexander GE, Schapiro MC, Möller HJ, Papoport SI, Hampel H (2004) Age-related cortical grey matter reductions in non-demented Down's syndrome adults determined by MRI with voxel-based morphometry. *Brain* **127**, 811-824.

[18] Pujol J, Del Hoyo L, Blanco-Hinojo L, De Sola S, Macià D, Martínez-Vilavella G, Amor M, Deus J, Rodríguez J, Farré M, Dierssen M, de la Torre R (2015) Anomalous brain functional connectivity contributing to poor adaptative behavior in Down syndrome. *Cortex* **64**, 148-156.

[19] De la Torre R, de Sola S, Farré M, Pujol J, Dierssen M, the TESDAD, Study, Group (2016) Safety and efficacy of the combination of cognitive training and epigallocatechin-3-gallate for cognitive improvement in young adults with Down syndrome: A double-blind randomised controlled trial. *Lancet Neurol* **15**, 801-810.

[20] Carducci F, Onorati P, Di Gennaro G, Quarato PP, Pierallini A, Sarà M, Miano S, Cornia R, Albertini G (2013) Whole-brain voxel-based morphometry study of children and adolescents with Down syndrome. *Funct Neurol* **28**, 19-28.

[21] Pinter JD, Eliez S, Schmitt JE, Capone GT, Reiss AL (2001) Neuroanatomy of Down's syndrome: A high-resolution MRI study. *Am J Psychiatry* **158**, 1659-1665.

[22] Powell D, Caban-Holt A, Jicha G, Robertson W, Davis R, Gold BT, Schmitt FA, Head E (2014) Frontal white matter integrity in adults with Down syndrome with and without dementia. *Neurobiol Aging* **35**, 1562-1569.

[23] Kaufman A, Kaufman N (2004) *Kaufman Brief Intelligence Test*, Second Edition (KBIT-2), Pearson, Bloomington.

[24] Lanfranchi S, Jerman O, Vianello R (2009) Working memory and cognitive skills in individuals with Down syndrome. *Child Neuropsychol* **15**, 397-416.

[25] Hoyo LD, Xicota L, Sánchez-Benavides G, Cuenca-Royo A, de Sola S, Langohr K, Fagundo AB, Farré M, Dierssen M, de la Torre R (2015) Semantic verbal fluency pattern, dementia rating scores and adaptive behavior correlate with plasma Aβ42 concentrations in Down syndrome young adults. *Front Behav Neurosci* **9**, 301.

[26] Sheehan R, Sinai A, Bass N, Blatchford P, Bohnen I, Bonell S, Courtenay K, Hassiotis A, Markar T, McCarthy J, Mukherji K, Naeem A, Paschos D (2015) Dementia diagnostic criteria in Down syndrome. *Int J Geriatr Psychiatry* **30**, 857-863.

[27] World Health, Organisation (1992) ICD-10: *International Statistical Classification of Diseases and Related Health Problems*. World Health Organization; Geneva **20**, 3-9.

[28] American Psychiatric Association (2000) *Diagnostic and Statistical Manual-Text Revision (DSM-IV-TR)*. American Psychiatric Association, Washington, DC.

[29] Petersen RC (2011) Mild cognitive impairment. *N Engl J Med* **364**, 2227-2234.

[30] Krinsky-McHale SJ, Silverman W (2013) Dementia and mild cognitive impairment in adults with intellectual disability: Issues of diagnosis. *Dev Disabil Res Rev* **18**, 31-42.

[31] Smith SM, Jenkinson M, Woolrich MW, Beckmann CF, Behrens TEJ, Johansen-Berg H, Banniser PR, De Luca M, Drobnjak I, Flitney DE, Niazy R, Saunders J, Vickers J (2004) Advances in functional and structural MR image analysis and implementation as FSL. *Neuroimage* **23**(Suppl 1), 208-219.

[32] Smith SM, Jenkinson M, Johansen-Berg H, Rueckert D, Nichols TE, Mackay CE, Watkins KE, Ciccarelli O, Cader MZ, Matthews PM, Behrens TEJ (2006) Tract-based spatial statistics: Voxelwise analysis of multi-subject diffusion data. *Neuroimage* **31**, 1487-1505.

[33] Pujol J, Macià D, Garcia-Fontanals A, Blanco-Hinojo L, López-Solà M, Garcia-Blanco S, Poca-Dias V, Harrison BJ, Contreras-Rodríguez O, Monfort J, Garcia-Fructuoso F, Deus J (2014) The contribution of sensory system functional connectivity reduction to clinical pain in fibromyalgia. *Pain* **155**, 1492-1503.

[34] Douaud G, Jbabdi S, Behrens TE, Menke RA, Gass A, Monsch AU, Rao A, Whitcher B, Kindlmann G, Matthews PM, Smith S (2011) DTI measures in crossing-fibre areas: Increased diffusion anisotropy reveals early white matter alteration in MCI and mild Alzheimer's disease. *Neuroimage* **55**, 880-890.

[35] Chapman RS, Hesketh LJ (2000) Behavioral phenotype of individuals with Down syndrome. *Ment Retard Dev Disabil Res Rev* **6**, 84-95.

[36] Lott IT, Dierssen M (2010) Cognitive deficits and associated neurological complications in individuals with Down's syndrome. *Lancet Neurol* **9**, 623-633.

[37] Grieco J, Pulsifer M, Seligsohn K, Skotko B, Schwartz A (2015) Down syndrome: Cognitive and behavioral functioning across the lifespan. *Am J Med Genet C Semin Med Genet* **169**, 135-149.

[38] Silverman W, Miezejecki C, Ryan R, Zigman W, Krinsky-McHale S, Urv T (2010) Standford-Binet & WAIS IQ differences and their implications for adults with intellectual disability (aka mental retardation). *Intelligence* **38**, 242-248.

[39] De Sola S, de la Torre R, Sánchez-Benavides G, Benejam B, Cuenca-Royo A, Del Hoyo L, Rodríaguez J, Catuara-Solarz S, Sánchez-Gutiérrez J, Dueñas-Espin I, Hernández G, Peña-Casanova J, Langohr K, Videla S (2015) A new cognitive evaluation battery for Down syndrome and its relevance for clinical trials. *Front Psychology* **6**, 708.

[40] Sánchez-Valle R, Monté GC, Sala-Llonch R, Bosch B, Fortea J, Lladó A, Antonell A, Balasa M, Bargalló N, Molinuevo JL (2016) White matter abnormalities track disease progression in PSEN1 autosomal dominant Alzheimer's disease. *J Alzheimers Dis* **51**, 827-835.

[41] Madden DJ, Bennett IJ, Burzynska A, Potter GG, Chen NK, Song AW (2012) Diffusion tensor imaging of cerebral white matter integrity in cognitive aging. *Biochim Biophys Acta* **1822**, 386-400.

[42] Yap QJ, Teh I, Fusar-Poli P, Sum MY, Kuswanto C, Sim K (2013) Tracking cerebral white matter changes across the lifespan: Insights from diffusion tensor imaging studies. *J Neural Transm* **120**, 1369-1395.

[43] Yakovlev PI, Lecours AR (1961) The myelogenetic cycles of regional maturation of the brain. In *Regional development of the brain in early life*, Minkowski A, ed. Blackwell Scientific, Oxford, pp. 3-10.

[44] Pujol J, Vendrell P, Junqué C, Martí-Vilalta JL, Capdevila A (1993) When does human brain development end? Evidence of corpus callosum growth up to adulthood. *Ann Neurol* **34**, 71-75.